Nanoscale Advances

ROYAL SOCIETY OF CHEMISTRY

REVIEW

View Article Online
View Journal | View Issue

Check for updates

Cite this: *Nanoscale Adv.*, 2022, **4**, 697

Metal–organic frameworks for advanced transducer based gas sensors: review and perspectives†

Sanjit Manohar Majhi, [a] Ashraf Ali,[a] Prabhakar Rai, [b] Yaser E. Greish,[c] Ahmed Alzamly,[c] Sandeep G. Surya, [de] Naser Qamhieh[a] and Saleh T. Mahmoud*[a]

The development of gas sensing devices to detect environmentally toxic, hazardous, and volatile organic compounds (VOCs) has witnessed a surge of immense interest over the past few decades, motivated mainly by the significant progress in technological advancements in the gas sensing field. A great deal of research has been dedicated to developing robust, cost-effective, and miniaturized gas sensing platforms with high efficiency. Compared to conventional metal-oxide based gas sensing materials, metal–organic frameworks (MOFs) have garnered tremendous attention in a variety of fields, including the gas sensing field, due to their fascinating features such as high adsorption sites for gas molecules, high porosity, tunable morphologies, structural diversities, and ability of room temperature (RT) sensing. This review summarizes the current advancement in various pristine MOF materials and their composites for different electrical transducer-based gas sensing applications. The review begins with a discussion on the overview of gas sensors, the significance of MOFs, and their scope in the gas sensing field. Next, gas sensing applications are divided into four categories based on different advanced transducers: chemiresistive, capacitive, quartz crystal microbalance (QCM), and organic field-effect transistor (OFET) based gas sensors. Their fundamental concepts, gas sensing ability towards various gases, sensing mechanisms, and their advantages and disadvantages are discussed. Finally, this review is concluded with a summary, existing challenges, and future perspectives.

Received 9th November 2021
Accepted 11th December 2021

DOI: 10.1039/d1na00798j

rsc.li/nanoscale-advances

[a]*Department of Physics, College of Science, United Arab Emirates University, Al-Ain 15551, United Arab Emirates. E-mail: saleh.thaker@uaeu.ac.ae*
[b]*Zoological Survey of India, Kolkata, 700053, India*
[c]*Department of Chemistry, College of Science, United Arab Emirates University, Al-Ain 15551, United Arab Emirates*
[d]*Sensors Lab, Advanced Membranes & Porous Materials Center (AMPMC), CEMSE, King Abdullah University of Science and Technology (KAUST), Thuwal 23955-6900, Saudi Arabia*
[e]*Sensor Group, R&D Section, Dyson Tech. Limited, Malmesbury, UK*

† Electronic supplementary information (ESI) available. See DOI: 10.1039/d1na00798j

From Left to right : Dr Sanjit Manohar Majhi, Dr Ashraf Ali, Prof. Ahmed Alzamly, Prof. Saleh T. Mahmoud, and Prof. Yaser E. Greish

Sanjit Manohar Majhi obtained his PhD degree from Jeonbuk National University, South Korea. Currently, he is working as a Research Associate at United Arab Emirates University (UAEU), UAE. He is currently working on MXene based 2D materials for gas sensing applications. Ashraf Ali received his Master's in Physics at King's College, London, UK and PhD degree from Anna University, India. He is currently working as a Research Associate at UAEU. His research focuses on metal-oxide framework/conducting polymer composites for gas sensing applications. Yaser E Greish obtained his PhD degree from Pennsylvania State University (USA 2001). Currently, he is working as a professor of materials chemistry at UAEU. His research focuses on the design of various types of nanostructured materials for biomedical and environmental applications. Ahmed Alzamly obtained his PhD degree in inorganic chemistry from the University of Ottawa, Canada. Currently, he is an Associate Professor at the Dept. of Chemistry, UAEU. His research focuses on the design and synthesis of transition-metal catalysts for energy and environmental applications. Saleh T. Mahmoud obtained his PhD degree in Physics from IIT-Delhi, India. He is a full professor at the Dept. of Physics, UAEU. He is the PI and Co-PI of 20 research projects, and has vast experience in the synthesis of nanomaterials and sensors' fabrication for detecting hazardous gasses.

Open Access Article. Published on 13 december 2021. Downloaded on 11. 11. 2024 14:01:32.
This article is licensed under a Creative Commons Attribution-NonCommercial 3.0 Unported Licence.

© 2022 The Author(s). Published by the Royal Society of Chemistry

Open Access Article. Published on 13 december 2021. Downloaded on 11. 11. 2024 14:01:32.
This article is licensed under a Creative Commons Attribution-NonCommercial 3.0 Unported Licence.

1. Introduction

The significant development of high-performance gas sensors has witnessed a vast change in recent times owing to the growing awareness of increasing environmental pollution. Various types of pollutants such as toxic/hazardous gases and volatile organic compounds (VOC) are being released to the environment from different sources such as industrial wastes, household use, and human activities, thereby causing alarming damage to the environment and sustainability of human development.[1–5] Furthermore, some gases when exposed to even a very low concentration, such as parts per million (ppm), cause several health risks.[5,6] Therefore, gas sensors play a vital role in our daily lives including disease diagnosis, environmental monitoring and human safety, food quality monitoring, industrial safety, *etc.*7–9 In a typical gas sensor, the sensing materials are responsible for interacting with the chemical entities by changing their physical properties such as conductivity (σ)/resistivity (ρ), work function (φ), and dielectric constant (ε), as explained in Fig. 1.[10] The chemical interface between sensing materials and analytes plays a vital role in determining the sensing performance. The transduction unit of the gas sensor converts one of the physical quantity changes mentioned above to a change in one or more electrical parameters such as capacitance (C), inductance (L), or resistance (R).[11] The transducer transforms the analytical information into different types of readable signals such as current (I), voltage (V), impedance (Z), resistance (R), change of frequency (f), phase (ϕ), and electrical potential (E), as shown in Fig. 1a.[12,13] Therefore, based on the underlying different transduction mechanisms, gas sensors can be further categorized into various types.[13–21]

The current challenges in the gas sensing field are sensitivity, selectivity, response time, long-term stability, and cost of sensing devices. Over the years, several conventional analytical techniques such as gas chromatography (GC), mass spectrometry (GC-MS), optical spectroscopy, high-performance liquid chromatography (HPLC), and surface-enhanced Raman spectroscopy (SERS) have been utilized for the detection of gas/chemical species.[22–27] However, the use of the above techniques has some limitations, such as they are expensive and bulky in size, often require highly trained people to operate, and require complex and time-consuming sample preparation and analysis methods. To overcome the above issues, it is essential to develop inexpensive sensing techniques with high sensing performances for practical applications. Various strategies have been developed to improve the gas-sensing properties, including exploring new and novel sensing materials. Over the past few decades, metal-oxides semiconductors (MOXs)[19] have been widely used as promising chemiresistive sensing materials. However, their high working temperatures, poor selectivity, and low stability issues have hindered further practical applications. Thus, there is an urgent proposition to develop

Prabhakar Rai is currently serving as a Scientist (Chemist) in the Zoological Survey of India, Govt. of India. He has also worked at the Indian Institute of Technology Kanpur (INSPIRE Faculty), Korea University (Research Professor) and Chonbuk National University (Assistant Research Professor). He received his Doctoral degree (2012) in Materials Engineering from Jeonbuk National University, South Korea. He has visited the Research Center on Engineering of Materials and micro/nanoSystems (EMaS) at Universitat Rovira i Virgili, Spain as a visiting Scientist in 2018. His research is mainly focused on energy (electrochemical supercapacitors and dye-sensitized solar cells) and environmental (chemical sensors) applications of nanomaterials.

Sandeep G. Surya is currently working as a Research Scientist at the Sensor group of Dyson Tech. Limited, United Kingdom. Previously, he was a Post-doctoral Fellow at KAUST, Saudi Arabia and a Research Associate at Fondazione Bruno Kessler (FBK), Trento, Italy. He received his PhD degree from IIT Bombay and B.Tech. degree from JNTU, Hyderabad. His current research focusses on solid-state device based chemical and bio-sensors. He is an expert in CMOS compatible device fabrication of the MEMS and solid-state sensors. At present, leading a team working on a stand-off gas sensing prototype with a multi-sensor array.

Naser Qamhieh received his PhD degree in Physics in 1996 from the University of Leuven (Belgium). He is a full professor at the Department of Physics, UAEU. His research interest focused on the experimental study of the electronic properties and density of states of amorphous semiconductors and chalcogenide glasses. Among the materials of interest are phase change materials used in memory devices. His research involves fabrication and characterization of thin films and nanoclusters.

© 2022 The Author(s). Published by the Royal Society of Chemistry

Open Access Article. Published on 13 december 2021. Downloaded on 11. 11. 2024 14:01:32.
This article is licensed under a Creative Commons Attribution-NonCommercial 3.0 Unported Licence.

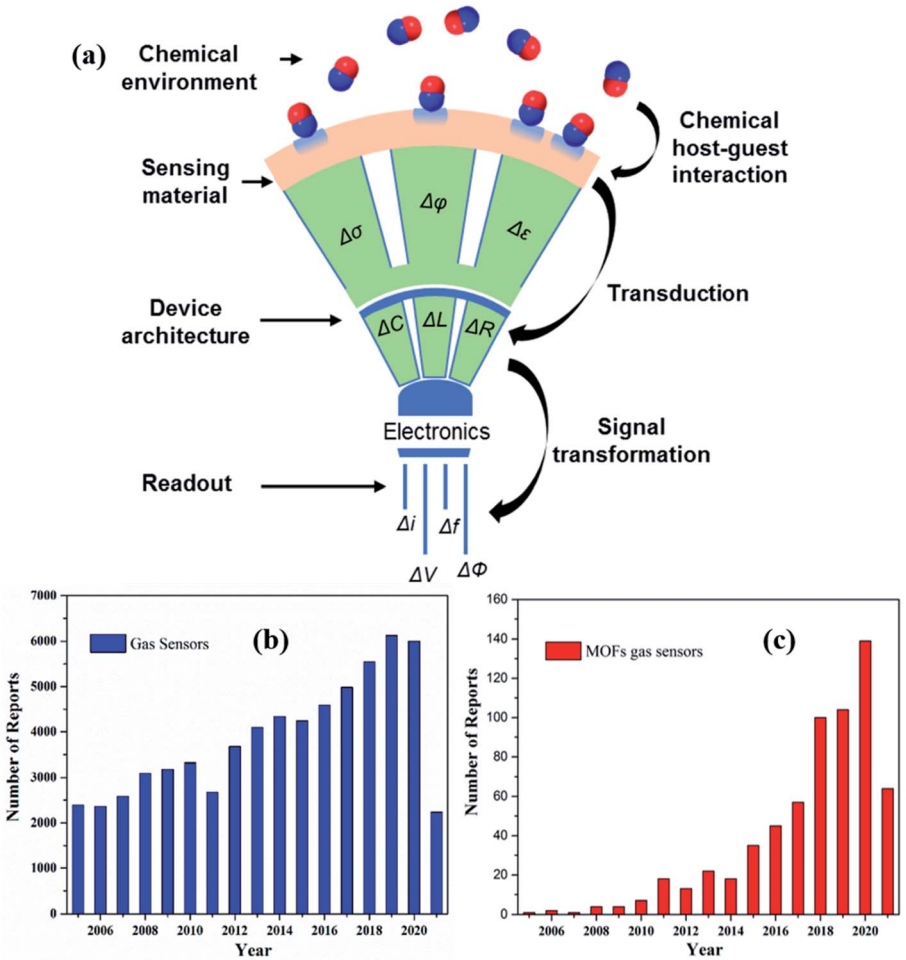

Fig. 1 (a) Schematic diagram of a function of a gas sensor with different principles of electrical transducers, where σ, φ, ε. C, L, R, I, V, E, f, and Φ are the conductivity, work function, permittivity capacitance, inductance, resistance, current, voltage, electrical potential, frequency, and phase, respectively. Reprinted from ref. 10 with permission from American Chemical Society, copyright 2021; (b and c) yearly publications in the field of gas sensors and MOF-based gas sensing materials from 2005–2021 (internet search of the Scopus on June 3rd, 2021) with sensor device fabrication and its integration. Keyword search: Gas sensors, MOF gas sensors, metal–organic framework-based gas sensors.

good sensing materials exhibiting a highly exposed surface and numerous active sites available for the analyte to bind and react with the surface, as well as with good mechanical properties and device flexibility.[9] In this context, metal–organic frameworks (MOFs) have garnered tremendous interest in exploring gas sensors.[28,29] The following section further discusses the significance of MOFs and their promising applications in gas sensing fields.

1.1 Metal–organic frameworks (MOFs): their significance and scope in gas sensing applications

MOFs have emerged as a class of materials with enormous academic research after the pioneering work led by Prof. Yaghi[30,31] by virtue of their superior features.[32] MOFs are endowed with exceptional properties, including diverse structures with tunable ultra-high porosity and pore size, high degree of crystallinity, ultrahigh surface area, abundant accessible active sites, high structural tunability, facile synthesis process, and high gas accessibility.[33–35] These features differentiate them from the conventional metal-oxides, thereby leading to MOF's application in a plethora of fields, including catalysis,[36–38] gas separation and adsorption,[39,40] energy storage and conversion,[41–43] and gas/chemical sensors.[17,44–46] Fig. 1b and c show the publications of gas sensors and MOF-based gas sensors and the number of times that they have been listed in the past 16 years based on a recent search in Scopus.

Upon adsorption of guest molecules, there would be a significant change in physicochemical and structural properties of MOFs as well as their selectivity, which may be due to the interaction with functional groups in the organic ligand and the active sites of the MOFs. Other interesting features, which make them highly sensitive and selective materials for many gases, are their ability to bind to different analytes through hydrogen bonds, electrostatic and van der Waals interactions. Additionally, MOFs can be utilized as versatile precursors to fabricate other forms of functional nanomaterials with hybrid structures, which showed superior properties compared to their counterparts when used as gas sensing materials.[47–50]

Open Access Article. Published on 13 december 2021. Downloaded on 11. 11. 2024 14:01:32.
This article is licensed under a Creative Commons Attribution-NonCommercial 3.0 Unported Licence.

Until now, various research-based and review articles on MOF-based gas and chemical sensing applications have been reported. For instance, Yi *et al.* reported a review article on chemical sensors based on MOFs.[51] However, they primarily focused on luminescence-based sensing towards ions, pH, humidity, biomolecules, and temperature. Vikrant *et al.* reported a review article on MOF-based luminescence and cataluminescence sensors for H_2S detection.[52] Kumar *et al.*[53] reported MOF-based optical, electrochemical and electroluminescence sensors for the detection of NOx. They also further reported a review article on MOF based sensing and sorptive/catalytic removal of nitroaromatic compounds.[54] Jing Li and coworkers published a review paper on MOF-based sensors that discusses sensing of fluorocarbons/chlorofluorocarbons and chemical warfare agents.[6] Fang *et al.*[55] reported MOF-based sensors for sensing environmental contaminants with a focus on the luminescence, electrochemical, and FET-based gas sensors in an aqueous solution. Wagner *et al.* reviewed MOF materials for the detection of pesticidal persistent organic pollutants (POPs).[56] Therefore, immense research attention has been focused on the investigation of sensing properties of MOF-based materials and their derivatives. This eventually opened the opportunity to explore other electrically transduced gas sensors such as capacitive, QCM, and organic field effect transistors (OFETs) in detail. However, there is no specific review article that exists to discuss the above advanced transducers for gas sensing applications utilizing the state-of-the-art MOF materials. As compared to MOX based chemiresistive sensors that operate at high temperatures, the above electrical transducers can operate under lower or RT conditions. Thus, it would be interesting to review the above three types of transducer gas sensors along with chemiresistive based gas sensors. The current review emphasizes to review recent advances in four types of the state-of-the-art MOF-based electrically transduced gas sensors based on chemiresistive, capacitive, QCM, and OFET principles. The first section covers recent advances in pristine MOF materials for chemiresistive gas sensors. It is further sub-grouped as MOF derived metal-oxides and their composite-based chemiresistive sensing materials. Secondly, we discuss capacitance-based transducers and their gas sensing applications. Thirdly, we discuss MOF-based QCM gas sensors and their sensing applications followed by organic field-effect transistor (OFET) based transducer gas sensors with some of their interesting sensing performances. The current review summarizes the design strategies of MOF materials, their integration into different transducers, sensing performances, and mechanisms. Finally, we discussed the present challenges and future perspectives of gas sensors.

The fundamental concepts and working principles of all the above electrically-transduced gas sensors have been discussed in the ESI.† Fig. 2 shows the overview of the MOF-based gas sensing materials with different transduction principles and the burgeoning field of MOFs in different gas sensing fields.[3]

2. Pristine metal–organic frameworks for chemiresistive gas sensors

Chemiresistive gas sensors detect gas molecules by changing the sensing material's electrical conductivity, resulting in a change in the resistance of the sensing layer as an output signal. In most of the chemiresistive gas sensors, the gas sensing materials are activated at some elevated temperature to

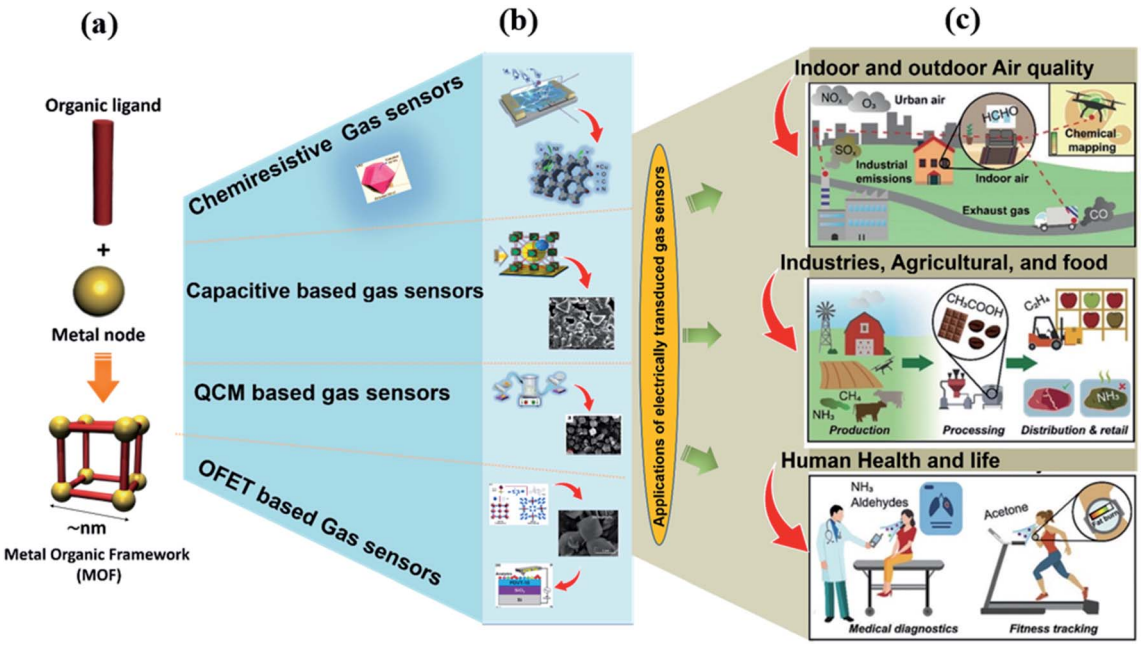

Fig. 2 Graphical representation of the formation of MOFs (a), MOF-based electrically transduced device fabrication (b), and the burgeoning field of MOFs in different sectors such as indoor and outdoor air quality monitoring, industries, agricultural and food sectors, and human health and security, (c), redrawn from ref. 3 under the Creative Commons Attribution-3.0 License, copyright 2021, Royal society of Chemistry.

© 2022 The Author(s). Published by the Royal Society of Chemistry

Open Access Article. Published on 13 december 2021. Downloaded on 11. 11. 2024 14:01:32.
This article is licensed under a Creative Commons Attribution-NonCommercial 3.0 Unported Licence.

acquire the desired electrical signal to detect target gases. In this regard, various materials such as metal-oxides and other conducting materials have been deployed for the sensing measurements. In addition, MOFs have been utilized in various applications, including gas sensing applications.[46] However, their insulating characteristics at RT limit the chemiresistive sensing application. Recently, there has been a surge in the development of various electrically conductive MOFs, which have opened the door for their application in chemiresistive-based gas sensors.[57,58] In these electrically conductive MOFs, the charge mobility can be increased with temperature. This section discusses recent advances in pristine MOFs and their chemiresistive-based gas sensing properties at moderate and RTs.[59] In addition, a few reports on pristine MOF based composites gas sensors are also discussed. The sensing performances of pristine MOF-based gas sensors are summarized in Table 1.

2.1 Application of pristine metal–organic frameworks in chemiresistive gas sensors

The pioneering work on chemiresistive-based gas sensors synthesized from pristine MOFs was studied for the first time by the Zhang group in 2014.[60] They used zeolitic imidazolate frameworks (ZIFs) with a remarkable surface area of 1832.2 $m^2 g^{-1}$ as the sensing materials for formaldehyde sensing. It was coated over the surface of interdigitated electrodes (IDEs) for formaldehyde sensing. The maximum response (13.9) of the ZIF-67 sensor with a low band gap ($E_g = 1.98$ eV) was recorded for 5 ppm formaldehyde at 150 °C with good selectivity. In another study they utilized a cobalt imidazolate framework material $[Co(im)_2]_n$ deposited on a Au-Pg IDE transducer for a trimethylamine (TEA) gas sensor.[61] The sensor exhibited excellent selectivity with a response of 14.1 at 75 °C towards 2 ppm TEA, among other VOCs. Due to the strong interaction between TEA molecules and the $[Co(im)_2]_n$ MOF sensing layer, a stronger adsorption of the target gas on the sensing layer caused a higher resistance change resulting in a higher response.

It has been reported that MOF-74, which is characterized by infinite $(–M–O–)_\infty$ chains, showed semiconductor properties with high charge mobility,[59] making it an ideal candidate for chemiresistive-based gas sensing materials. Accordingly, Phan and Kim *et al.* recently reported two kinds of conducting MOFs based on Mg-MOF-I and Mg-MOF-II, which are iso-reticular to the MOF-74 structure.[62] They used H_4ODA 4,4′-[oxalylbis(imino)] bis (2-hydroxybenzoic acid) and H_4TDA (4,4′-[1,4-phenylenebis-(carbonylimino)] bis (2-hydroxybenzoic acid) organic linkers with Mg^{2+} metal ions to synthesize Mg–MOF-I and II, respectively. When the above two sensors were tested at different temperatures ranging from 25–200 °C, it was revealed that Mg–MOF-II exhibited higher NO_2 response at 200 °C for 50 ppm NO_2 than Mg–MOF-I.

DMello *et al.*[63] reported a NH_2–UiO-66 (Zr) MOF towards the moderate temperature sensing. They have investigated the effect of modulation of the organic linkers (bdc (1,4 benzene dicarboxylic acid), bdc-NH_2, bdc-OH) on the sensing properties of different acidic gases (NO_2, SO_2 and CO_2). Their change in resistance was studied, and it was found that the NH_2 functionalized-UiO-66 (Zr) gas sensor exhibited a decrease in resistance (an increase of conductivity) in the presence of target gases. Among these three acidic gases, a sensor made from the NH_2–UiO-66 (Zr) MOF showed the highest response ($R = 21.6\%$) toward 10 ppm SO_2 at 150 °C. Also, basic groups such as $–NH_2$ facilitate the response to acidic gases in the order of $SO_2 > NO_2 > CO_2$. Hence, selecting organic ligands with appropriate functional groups plays a great role in the selectivity of MOF-based chemiresistive gas sensors.[64]

The emergence of highly conductive 2D MOFs resulting from redox-active organic linkers and metal nodes has provided an additional opportunity to utilize MOFs in chemiresistive

Table 1 Summary of the sensing performances of pristine MOF based gas sensors[a]

MOF materials	Target gas	Response ($S = R_a/R_g$) and $S\% = (R_a - R_g/R_a) \times 100$	Concentration	LOD	Working temp. (°C)	Ref.
ZIF-67	Formaldehyde	13.9	5 ppm	NA	150	50
$[Co(im)_2]_n$	TEA	14.1	2 ppm	NA	75	61
Mg–MOF-74 (Mg–MOF-II)	NO_2	1.35	50 ppm	NA	200	62
NH_2–UiO-66 (Zr)	SO_2	21.6%	10 ppm	NA	150	63
$Cu_3(HITP)_2$	NH_3	3.5 ($S\% = \Delta G/G_0$)	10 ppm	0.5 ppm	RT	66
$Ni_3(HITP)_2$	NH_3	0	10 ppm	NA	RT	65
Cu_3HHTP_2	Methanol	−9%	200 ppm	NA	RT	67
Cu_3HITP_2	Methanol	−1.8%	200 ppm	NA	RT	67
Cu_3HITP_2	Ethanol	−0.8%	200 ppm	NA	RT	67
Ni_3HITP_2	Ethanol	3.9%	200 ppm	NA	RT	67
Ni_3HITP_2	Methanol	3.9%	200 ppm	NA	RT	67
Cu_3HHTP_2	H_2S	0.5%	80 ppm	2	RT	67
Ni_3HHTP_2	H_2S	4.2%	80 ppm	2	RT	69
Cu_3HHTP_2	NO	−1.8%	80 ppm	2	RT	69
Ni_3HHTP_2	NO	1.7%	80 ppm	2	RT	69
Cu_3HHTP_2	Methanol	30%	100 ppm	NA	RT	70
Cu_3HHTP_2	NH_3	129%	100 ppm	0.5	RT	70

[a] NA: not available.

Open Access Article. Published on 13 december 2021. Downloaded on 11. 11. 2024 14:01:32.
This article is licensed under a Creative Commons Attribution-NonCommercial 3.0 Unported Licence.

sensing in RT sensing. Campbell *et al.* reported various Cu-based 2D conducting MOFs for chemiresistive gas sensing. They controlled the electronic conductivity of these MOFs by systematic variation in their metal centers.[65] Their structural effects on the gas sensing properties were investigated by replacing Ni atomic sites with Cu atoms in $Ni_3(HITP)_2$. The isostructural $Cu_3(HITP)_2$ (HITP: 2,3,6,7,10,11-hexaiminotriphenylene) MOFs showed a conductivity of 0.2 S cm^{-1} and were studied to detect ammonia. The $Cu_3(HITP)_2$ sensor fabricated by a simple drop-casting method on the IDE transducer showed a linear response ($S\% = \Delta G/G_0 = 3.5$) with p-type behavior towards ammonia starting from the sub-ppm level to the ppm level (0.5 ppm to 10 ppm). However a sensor made from a $Ni_3(HITP)_2$ MOF did not show any response towards ammonia. The possible higher response of $Cu_3(HITP)_2$ compared to $Ni_3(HITP)_2$ was attributed to the replacement of Ni^{2+} with Cu^{2+} with higher d-electrons increasing the energy of the Fermi level, thereby resulting in differences in the selectivity.[66] Thus, the functionality of chemiresistive sensors can be tuned by rational synthetic variation of conductive MOFs.

They further investigated the effect of chemical structures in MOFs on the chemiresistive response toward various analytes.[67] They constructed a few structurally analogous 2D MOFs such as $Cu_3(HHTP)_2$ (HHTP: 2,3,6,7,10,11-hexahydroxytriphenylene), $Cu_3(HITP)_2$, and $Ni_3(HITP)_2$, respectively and studied their array-based sensing properties towards the discrimination of many analytes, including aliphatic/aromatic hydrocarbons, ketones, amines, ethers, and alcohols. It is observed that the responses of the $Ni_3(HITP)_2$ MOF was found to be negative to $Cu_3(HHTP)_2$ and $Cu_3(HITP)_2$ MOFs when tested at 200 ppm of analytes. It has been found that the charge transfer as well as the hydrogen bonding are responsible for the observed sensing properties along with the charge density affected by the Ni(II) orbital (d8) *versus* the Cu(II) orbital (d9). However, the lack of good quality and the controlled thin film of such conductive MOFs have limited their application in high-performance devices. The deposition of MOFs into chemiresistive devices during fabrication often poses a challenge due to their high resistivity and poor solubility, which result in the ohmic contacts in the electrodes.[68] To overcome this, recently, Smith *et al.* described the technique for the miniaturized fabrication of MOF-based IDE chemiresistive devices.[69] Initially, graphite wires were drawn on shrinkable polymeric films using a commercial hard-black (HB) pencil for the fabrication of IDEs. The second step involved the growth of two MOF nanorods (Cu_3HHTP_2 and Ni_3HHTP_2) directly on the device chip from molecular precursors. The sensors made from the above materials were examined for NH_3, H_2S, and NO. Both MOFs displayed the lowest sensing response for NH_3. When the sensors were exposed to NO, a consistent decrease in resistivity was observed, whereas for H_2S, the resistivity was increased. This behavior corroborated the ability of Cu_3HHTP_2 and Ni_3HHTP_2 sensors to distinguish and monitor among these toxic gases NH_3, NO, and H_2S at the ppm-level.

Yao *et al.*[70] also demonstrated the fabrication of a $Cu_3(HHTP)_2$ thin film by a layer-by-layer (LBL) method using the liquid phase epitaxy (LPE) technique (Fig. 3a and b). The crystal structure of $Cu_3(HHTP)_2$ is shown in Fig. 3a. The thickness of the $Cu_3(HHTP)_2$ thin film was controlled by varying the growing cycles (the thickness of $Cu_3(HHTP)_2$–10C was ~20 nm, whereas for $Cu_3(HHTP)_2$–50C was ~100 nm). When the sensor was tested towards 100 ppm NH_3, a sensitivity ($S\%$) of 129% with a LOD of 0.5 ppm with an excellent selectivity among other interfering gases (Fig. 3c and d) was observed. The sensor also showed excellent long-term stability for three months. Fig. 3e shows the NH_3 gas sensing mechanism of the $Cu_3(HHTP)_2$ MOF. The strong interaction between the $Cu_3(HHTP)_2$ MOF and NH_3 is attributed to the high selectivity.

Recently, Surya and co-workers[71] studied zinc-based MOFs with three different organic ligands such as ZIF-8, isonicotinic acid (Zn–INA), and nicotinic acid (Zn–NA) and deployed them as a chemiresistive-based ammonia sensor at RT. The surface areas of the corresponding MOFs were found to be 160.6 $m^2\ g^{-1}$ (Zn (NA)), 525 $m^2\ g^{-1}$ (ZIF-8), and 103.6 $m^2\ g^{-1}$ (Zn (INA)), respectively. Among the three gas sensors, Zn (NA) displayed a high response ($R_a/R_g = 220$) towards ammonia at 100 ppm, 9 for ZIF-8, and 139 for Zn (INA). The sensors also showed good response and recovery times (46 s/200 s) and good stability with minimal response fluctuation for 15 days. This study revealed that isonicotinic acid and nicotinic acid-based MOF sensing materials showed good sensing ability towards ammonia compared to ZIF-8. The following sensing mechanism could be expected for the above sensor towards ammonia gas.

$$O_{2(g)} + e^- \rightarrow O_2^-(ads) \quad (1)$$

$$O_2^-(ads) + e^- \rightarrow 2O^-(ads) \quad (2)$$

$$2NH_3 + 3O^-(ads) \rightarrow 3H_2O + N_2 + 3e^- \quad (3)$$

Both high surface area and good efficiency of adsorption of test gas molecules are among the factors that led to the observed high sensing response towards ammonia for Zn–NA based MOF sensors.[72,73]

Utilizing pristine MOFs and to construct composite materials with tailored properties is at the forefront of novel technological exploration. Composites prepared from MOFs with polymers or organic materials can be used as potential sensing materials.[72,74] Our group has recently developed a flexible MOF–polymer-based composite gas sensing device based on a copper plate and stainless steel grid as top and bottom electrodes, respectively for ppb level H_2S gas sensing at RT. Ali *et al.*[75] reported MOF-5/Chitosan polymer (CS)/IL (ionic liquid)-based flexible membrane materials as gas sensing materials and examined their H_2S gas sensing at RT. A simple technique of grinding in a mortar and pestle was used to partially break the three dimensional (3D) structure of MOF-5 (as shown in Fig. 4a and b), which eventually provided high surface area (621 $m^2\ g^{-1}$ before grinding and 643 $m^2\ g^{-1}$ after grinding) and lowered the H_2S detection limit (1 ppm). The as-prepared MOF-5/CS/IL based sensor exhibited a response ($S\% = R_a/R_g \times 100$) of 91% at 100 ppm with a quick response time (<8 s) at RT. Selectivity is one of the important parameters of the gas sensor. Among other gases (H_2, C_2H_4, H_2S, and CO), the MOF-5/CS/IL gas sensor

© 2022 The Author(s). Published by the Royal Society of Chemistry

Open Access Article. Published on 13 december 2021. Downloaded on 11. 11. 2024 14:01:32.
This article is licensed under a Creative Commons Attribution-NonCommercial 3.0 Unported Licence.

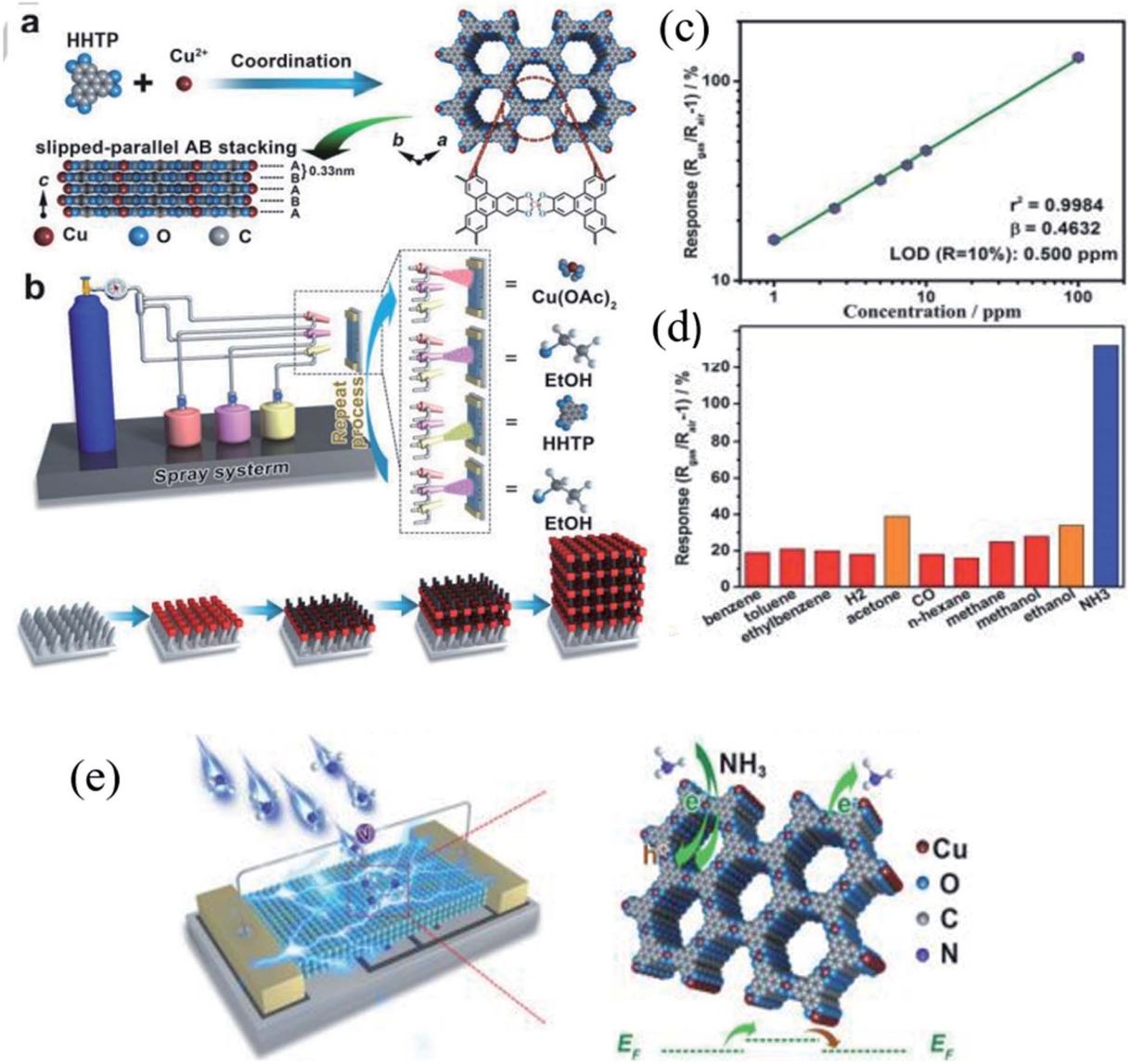

Fig. 3 (a) Illustration of the crystal structure of $Cu_3(HHTP)_2$. (b) Fabrication of the $Cu_3(HHTP)_2$ thin film by a spray layer-by-layer (LBL) method using the LPE technique, (c) LOD graph, (d) selectivity test of the $Cu_3(HHTP)_2$ thin-film sensor, and (e) NH_3 sensing mechanism of the $Cu_3(HHTP)_2$ thin film sensor at RT. Reproduced from ref. 70 with permission from Wiley Sons, copyright 2021.

exhibited high selectivity and response towards 100 ppm H_2S at RT (Fig. 4c). When the sensor was tested for long-term stability for 21 days, it showed excellent stability with minimal response fluctuation for 50 ppm H_2S at RT (Fig. 4d). Moreover, the sensor showed good repeatability for 5 consecutive cycles of 50 ppm H_2S (Fig. 4e). The high sensing performance is attributed to the geometry of MOF-5 having a number of oxygen atoms with nonbonding electrons, which facilitated the interaction of their active sites with an acidic proton of H_2S gas molecules. On the other hand, the CS-IL polymer matrix helps as an electron transport pathway throughout the membrane and leads to open porosity of the MOF-5 structure (Fig. 4f). Hence, the synergistic effect of the conducting polymer matrix and MOF-5 together with high porosity, the polarization of the MOF, controlled pore size and shape, and types of secondary components play a great role in deciding the sensitivity towards the gas sensing.[76]

2.2 Metal–organic framework derived metal–oxides and their composites for chemiresistive gas sensors

The previous section discussed the sensing properties of pristine MOF materials at room and moderate temperatures for different gas molecules and vapors. In addition to pristine MOFs as active sensing materials, researchers have also studied functional materials derived from pristine MOFs. Conventional MOX based gas sensors are often limited with low surface areas and high working temperatures.[60] On the other hand, MOFs endowed with the exceptional surface area are promising materials for sensing applications. The poor thermal stability of MOFs at high operating temperatures can be taken as an

Open Access Article. Published on 13 december 2021. Downloaded on 11. 11. 2024 14:01:32.
This article is licensed under a Creative Commons Attribution-NonCommercial 3.0 Unported Licence.

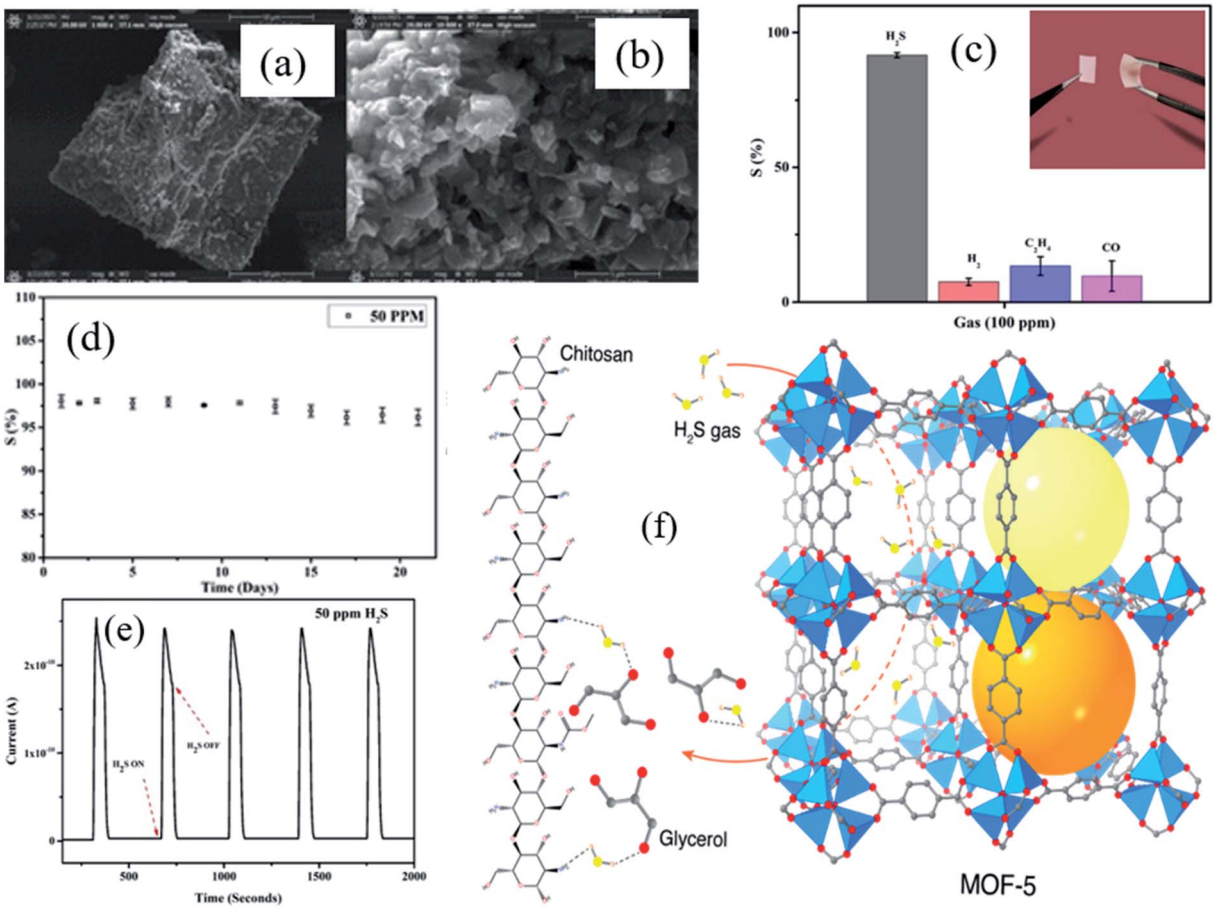

Fig. 4 (a and b) SEM images of MOF-5 before and after grinding, (c) the selectivity study of the MOF-5/CS/IL gas sensor towards various gases for 100 ppm at RT, (d and e) long-term stability and reproducibility test for MOF-5/CS/IL at RT for 21 days and four repeat cycles of 50 ppm H_2S at RT, and (f) schematic diagram of the H_2S sensing mechanism of MOF-chitosan-polymer based gas sensors. Reproduced from ref. 75 under the Creative Commons Attribution-4.0 License (https://creativecommons.org/licenses/by-nc-nd/4.0/), copyright 2021, American Chemical Society, copyright 2021.

advantage to prepare many interesting structures using the calcination method due to the easy decomposition of organic linkers. The newly formed porous MOXs/composites (Fig. 5) derived from pristine MOFs are endowed with high surface area with a controlled morphology and porosity, hollow architectures, and intrinsic open pores, which act as trapping centers for gas molecules.[77,78] Thus, MOF-derived MOXs and their composites can be further used as gas sensing materials.[50,79] In this section, different MOX materials derived from MOFs and their composites have been discussed along with their sensing applications towards many gases.[80] The sensing performances of MOF derived metal-oxides, and their composite-based gas sensors are summarized in Table 2.

2.2.1 Application of metal–organic framework derived materials in chemiresistive gas sensors. Among different MOFs, ZIF-67 has been extensively studied due to its simple fabrication to prepare p-type cobalt oxides (Co_3O_4). Zhang and co-workers[81] synthesized different kinds of porous hierarchical Co_3O_4 structures using ZIF-67 by a simple calcination method optimization. In this study, four kinds of Co_3O_4-based structures were developed such as core–shell (C–S) (350 °C for 3 h), porous core–shell (PC–S) (350 °C for 10 h), porous popcorn (PPC) (calcined in both air and N_2 atmospheres at 350 °C for 3 h and 500 °C for 1 h where the temperature was increased at a rate of 1°C min^{-1}), and Co_3O_4 nanoparticles (NPs) (calcined at 600 °C −3 h in air, where the temperature was increased at a rate of 10°C min^{-1}), with particle sizes ranging from 1.7 μm to 150 nm. Two sensors with sensor core–shell structures such as CS- and PCS–Co_3O_4 materials exhibited high sensing performance towards 200 ppm acetone with a response ($R_g/R_a = 13$) and ($R_g/R_a = 11$), respectively at 190 °C, and a quick response time (τ_{resp}) of 4 s. The repeatability and long-term stability test show excellent repeatability with minimal fluctuation of the response in long-term stability tests. Long-term stability was tested for 30 days, which showed excellent reproducibility with minor variations of responses. The high sensing performances of C–S and PC–S-Co_3O_4 core–shell materials were attributed to the open interior architectures derived from MOFs.

Kuang and co-workers[82] reported that Co_3O_4 nanoparticles were synthesized from ZIF-67 by the precipitation technique followed by annealing of ZIF-67 at 300–400 °C temperature. The obtained concave nanocubes of porous Co_3O_4-300 °C particles

© 2022 The Author(s). Published by the Royal Society of Chemistry

Open Access Article. Published on 13 december 2021. Downloaded on 11. 11. 2024 14:01:32.
This article is licensed under a Creative Commons Attribution-NonCommercial 3.0 Unported Licence.

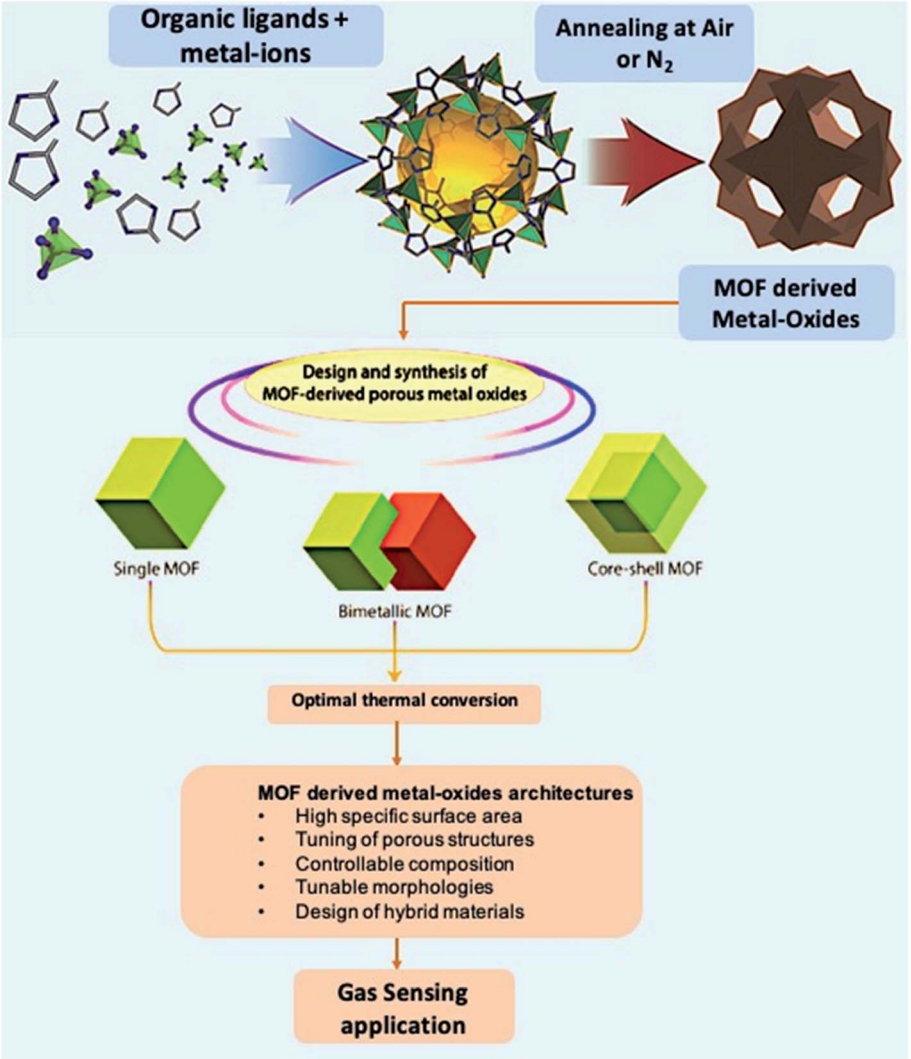

Fig. 5 Graphical representation of the preparation of MOFs and MOF-derived metal-oxide structures and their structural and morphological advantages for gas sensing applications. Adopted from ref. 77 with permission from American Chemical Society, copyright 2021.

showed a response of (R_g/R_a = 3.2) to ethanol (200 ppm) gas with a quick response time (τ_{res}) of 10 s and LOD of 10 ppm only. Such a performance of MOF derived Co_3O_4 concave nanocube particles was attributed to the excellent specific surface area (120.9 m^2 g^{-1}), high porosity, and abundant surface-adsorbed oxygen atoms. In 2017, Zhou *et al.*[83] prepared a hierarchical Co_3O_4 nanostructure by calcining Co_5–MOF ($Co_5(u3\text{-}OH)_2(1,4\text{-}NDC)_4(bix)_2]_n$) bar-shaped microcrystals for formaldehyde sensing at low operating temperatures. The Co_3O_4-350 spherical particles exhibited high formaldehyde sensing at 170 °C, a low detection limit of 10 ppm, and long-term stability (30 days) as compared to other calcination temperatures. Such extraordinarily efficient properties might have resulted from the hierarchical structures, larger surface area, and unique pore structure. Meanwhile, for high formaldehyde concentration sensing characteristics, the response (R_g/R_a) values of the Co_3O_4 NPs correspond to 11.7, 14.1, 15.1, 16, and 17 for 100, 200, 300, 400, and 500 ppm of formaldehyde vapor, respectively.

Recently, Wang *et al.*[84] synthesized a pristine Sn-based MOF aiming toward the formation of SnO_2 nanoparticles for formaldehyde sensing. A Sn-based MOF was synthesized from the H_3BTC (1,3,5-benzenetricarboxylic acid) and $SnCl_4$ precursors by a solvothermal method at 180 °C followed by calcination at 400 °C −2 h to obtain desired SnO_2 hollow hexagonal nanorods. The specific surface area of the pristine Sn–MOF was 1142.71 m^2 g^{-1} with a pore size of 3.0 nm. The obtained SnO_2 hollow hexagonal nanorod sensor displayed an ultrahigh response of 882, and τ_{res} of 19 s towards 2 ppm formaldehyde vapor at 120 °C. The high selectivity towards formaldehyde could be attributed to the low bond energy of formaldehyde (H–CHO = 368.4 kJ mol^{-1}),[85,86] where, formaldehyde gas molecules could be easily destroyed at such lower temperature to participate in the sensing reaction.[86]

Wu *et al.*[87] prepared various morphologies of CuO such as a pure octahedron, octahedron with a sponge like structure, and spheres from annealing of Cu(II)–MOF (HKAUST-1) at various

Open Access Article. Published on 13 december 2021. Downloaded on 11. 11. 2024 14:01:32.
This article is licensed under a Creative Commons Attribution-NonCommercial 3.0 Unported Licence.

Table 2 Summary of sensing performances of MOF derived metal-oxides and their composite based gas sensors

Materials	Target gas	Response [$S = R_a/R_g$ or R_g/R_a and $S\% = (R_a - R_g/R_a) \times 100$]	Concentration (ppm)	LOD	Working temp. (°C)	Response/ recovery time (sec)	Ref.
ZIF-67 (CS–Co_3O_4)	Acetone	13	200	NA	190	4 s/—	81
ZIF-67 (PCS–Co_3O_4)	Acetone	11	200	NA	190	4 s/—	81
2-Co_3O_4 rods-ZnO sheet	Acetone	29	5	NA	450	NA	91
PdO-loaded Co_3O_4/SnO_2 HNCs	Acetone	22.8	5	1.61 (5 ppb)	450	90 s/108.4 s	93
ZIF-8 (Au/ZnO NPs)	Acetone	17.1	1	600 ppb	275	247 s/209 s	108
Au–Co_3O_4 HNCs	Acetone	14.5	100	1 ppm	190	NA	103
PdO-loaded Co_3O_4–In_2O_3 hollow spheres	Acetone	146.9	5	N. A	225	NA	110
Porous Co_3O_4-300 °C	Ethanol	3.2	200	10 ppm	300	10 s	82
Co_3O_4/N-RGO-0.5	Ethanol	3.9%	200	NA	200	20 s/51 s	98
Co_3O_4-350 sphere	Formaldehyde	11.7	100	NA	170	NA	83
SnO_2 hollow hexagonal nanorods	Formaldehyde	882	2	NA	120	19 s/—	84
Pt@ZnO–TiO_2 NTs	Toluene	11.13	1	23 ppb	300	75 s/20.1 s	111
Pd/ZnO loaded WO_3 NFs	Toluene	22.22	1	NA	350	20	115
Co_3O_4 nanocages	*p*-xylene	78.6	5	NA	225	10 s/86 s	88
Pt/ZnO −1 wt% 3DIO NPs	H_2S	11.2	1	25 ppb	320	8.7 s/19.4 s	116
2% Pt NPs@ZnO polyhedra	CO	90	50	100 ppb	100	89 s/175 s	119
CuO-400 (HAKUST-1)	TEA	102	100	5 ppm	230	21 s/150 s	87
RGO/α-Fe_2O_3	TAE	24	50	NA	280	2 s/7 s	99
SWCNT/PdO–Co_3O_4 HNCs	NO_2	44.11%	20	1 ppm	100	NA	122
In_2O_3/MoS_2	NO_2	371.9	100	8.8 ppb	RT	152 s/179 s	123

temperatures (400–500 °C). The gas-sensing characteristics of the as-prepared CuO samples were investigated. The results revealed that the p-type CuO-400 sensor exhibited an excellent response ($R_g/R_a = 102$) towards 100 ppm triethylamine (TEA) with a LOD of 5 ppm at 230 °C. The sensor also displayed excellent long-term stability and reproducibility. The above sensing results of CuO-400 were attributed to its unique morphology having numerous active sites for sensing reactions, which facilitated the efficient adsorption of TEA molecules. The possible sensing mechanism of TEA sensing was reported as follows:

$$O_{2(g)} \rightarrow O_{2(ads)} \quad (4)$$

$$O_{2(ads)} \rightarrow {O_{2(ads)}}^- + {h_{(hole)}}^+ \quad (5)$$

$${O_{2(ads)}}^- \rightarrow 2O^{2-} + 3h^+ \quad (6)$$

$$N(C_2H_5)_3 + O^{2-} + 2h^+ \rightarrow N_2 + H_2O + CO_2 \quad (7)$$

It is essential to note that to achieve high sensing performance, the variation of sensing materials should be tailored by controlling the size of the nanostructures to be highly porous and gas-accessible. Controlling the morphology, size, porosity, and thickness of the shell wall of MOF-derived hollow nanostructures by one-pot hydrothermal/solvothermal is challenging.[88,89] Jo *et al.*[88] successfully synthesized Co_3O_4 nanocages derived from ZIF-67 with four different sizes. They were used as sacrificial templates to allow the growth of Co-layer double hydroxide (LDH) (schematically shown in Fig. 6A) followed by calcination to obtain Co_3O_4 hierarchical hollow nanocages (HHN). Fig. 6B–E show the TEM images of four different structures (30–40 μm) after calcination at 400 °C. Fig. 6F shows the response transients of the Co_3O_4 nanocage sensor tested at 225 °C. The as prepared sensor (size of ∼1.0 μm; 10-ZIF-67 derived 10-Co_3O_4) displayed high response ($R_a/R_g = 78.6$) to 5 ppm *p*-xylene with excellent selectivity to methylbenzene at 225 °C. Fig. 6G shows the repeatability of the Co_3O_4 nanocage sensor for 10 cycles towards 5 ppm xylene at 225 °C. The high sensing results are ascribed to the unique hierarchical hollow morphology, which facilitated abundant access of analyte molecules, high surface area, and the catalytic activity of Co_3O_4.

Construction of heterostructures is one of the best approaches towards increasing sensitivity and overall sensing performance.[90] Heterostructures possess high surface area, high porosity, and electronically sensitized multi-heterojunction structures.[91] Kim and co-workers[92] synthesized different morphologies of Co_3O_4 materials, including ZIF-67 with a rod shape, a sheet with a leaf shape (ZIF-L), a ZIF-67 polyhedron, and ZIF-67 belts, respectively, by simply controlling the mixing of solvents with cobalt precursors and 2-methylimidazole (HiM), as shown in Fig. 7A. Subsequently, daisy-flower like Co_3O_4–ZnO p–n heterojunction hybrid nanostructures were synthesized by mixing ZIF-67 rods (1.2 wt% to 7 wt%) in ZIF-L solution with Zinc precursors followed by annealing at 450 °C (as shown in Fig. 8B), which exhibited enhanced acetone sensitivity. Among three Co_3O_4–ZnO heteronanostructures, the 2 wt% Co_3O_4 rods-ZnO sensor exhibited the highest response ($S = R_a/R_g = 29$) for 5 ppm acetone at 450 °C in comparison to Co_3O_4 rod ($S = 1.06$) and ZnO sheet ($S = 10$) sensors. The possible sensing reaction for acetone gas sensors is as follows:

© 2022 The Author(s). Published by the Royal Society of Chemistry

Open Access Article. Published on 13 december 2021. Downloaded on 11. 11. 2024 14:01:32.
This article is licensed under a Creative Commons Attribution-NonCommercial 3.0 Unported Licence.

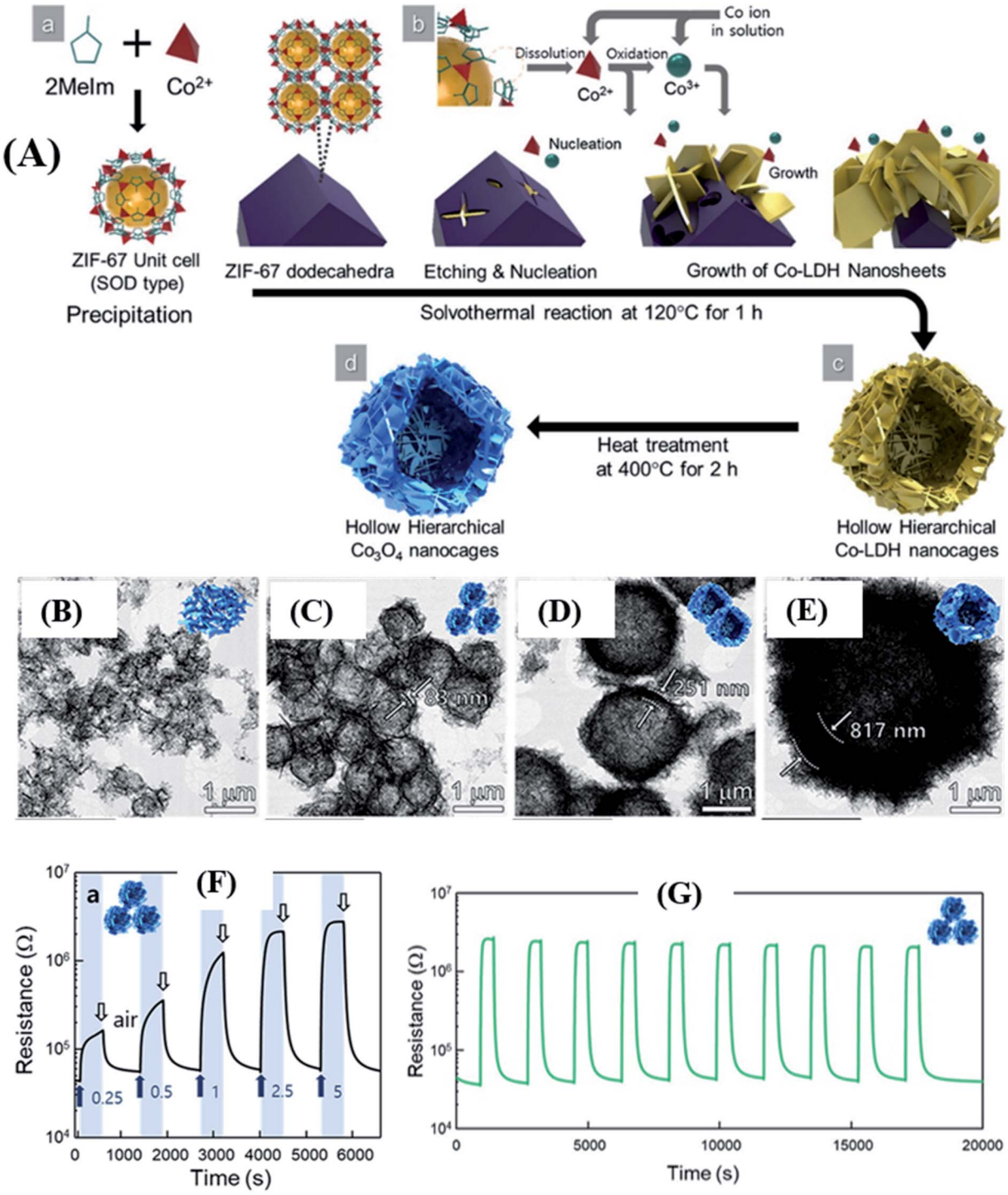

Fig. 6 (A) Synthesis protocol of hierarchical hollow Co_3O_4 nanocages using ZIF-67 as the template, (B–E) SEM images of Co_3O_4 hierarchical hollow nanocages (HHN) with different sizes, (F) response/recovery curves of the 10-Co_3O_4 sensor tested at 225 °C towards *p*-xylene (0.5–2.5 ppm), and (G) repeatability test at 225 °C. Reprinted from ref. 88 with permission from American Chemical Society, copyright 2021.

$$CH_3COCH_{3(g)} + 8O^- \rightarrow 3H_2O + 3CO_2 + 8e^- \quad (8)$$

The authors also studied the principal component analysis (PCA) as a pattern recognition tool to further study the selectivity of acetone.[93] The result showed that even at a high humidity level of 90 RH%, acetone and the other 6 interfering gas molecules were distinguished into regions (green and red dotted regions) (Fig. 7E). The enhanced acetone-sensing properties are attributed to the (i) formation of p–n heterojunctions, (ii) highly porous nanostructures, and (iii) chemical sensitization effect of Co_3O_4, respectively.[94,95]

Open Access Article. Published on 13 december 2021. Downloaded on 11. 11. 2024 14:01:32.
This article is licensed under a Creative Commons Attribution-NonCommercial 3.0 Unported Licence.

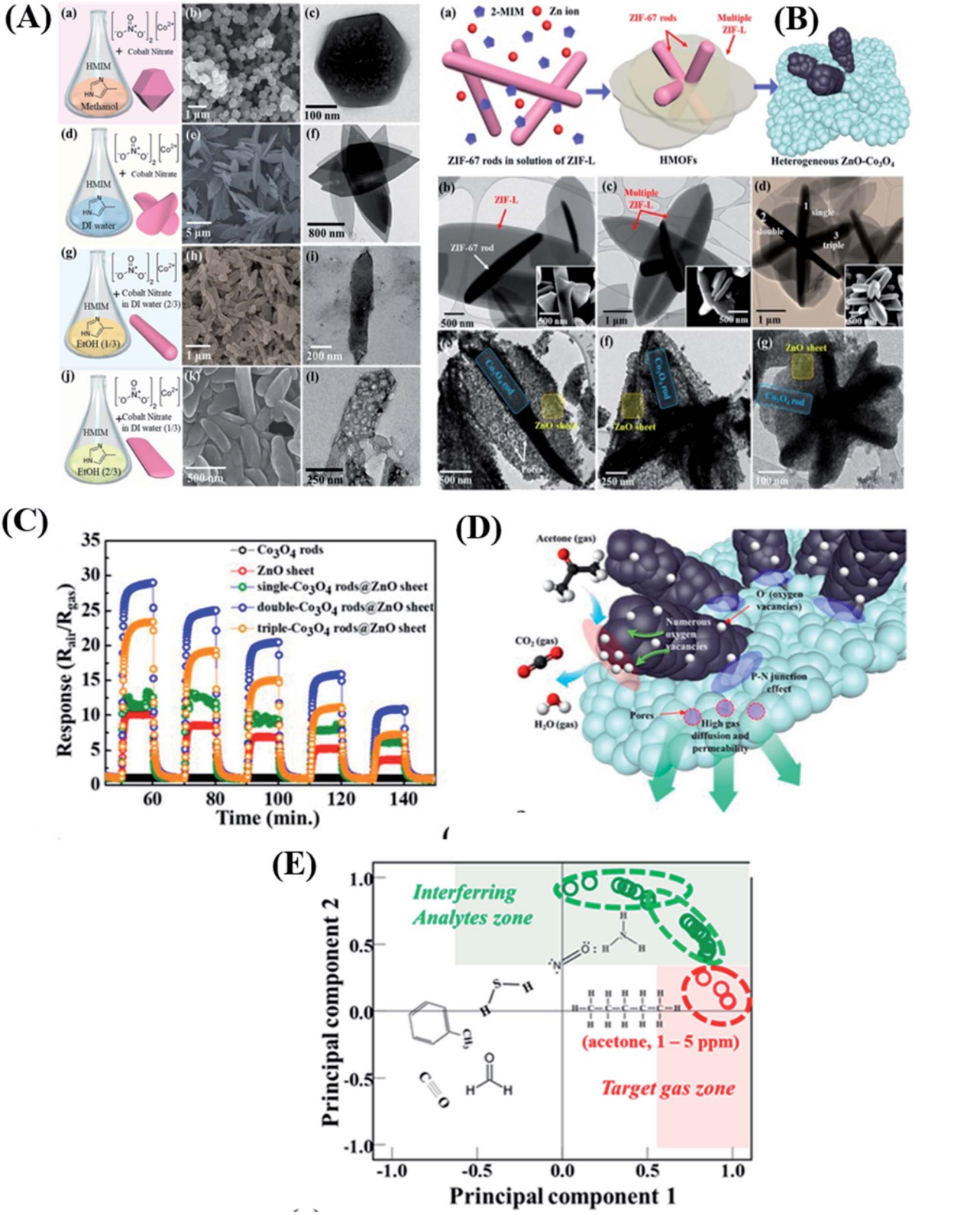

Fig. 7 ($A_{(a-j)}$) Schematic diagram of synthesis procedures of different morphologies of ZIF-67 based nanomaterials, ($B_{(a-g)}$) SEM and TEM images of different morphologies of single, double and triple ZIF-L/ZIF-67 rods and their Co_3O_4 composites, (C) response transients of all five sensor devices based on pristine ZnO sheets, Co_3O_4 rods, and single, double and triple Co_3O_4 rods-ZnO sheets, (D) sensing mechanism of the double Co_3O_4–ZnO sheet composite based sensor, and (E) PCA analysis to examine the pattern recognition of sensor arrays. Reproduced from ref. 92 under the ACS Author Choice License. Copyright 2021, American Chemical Society.

© 2022 The Author(s). Published by the Royal Society of Chemistry

Open Access Article. Published on 13 december 2021. Downloaded on 11. 11. 2024 14:01:32.
This article is licensed under a Creative Commons Attribution-NonCommercial 3.0 Unported Licence.

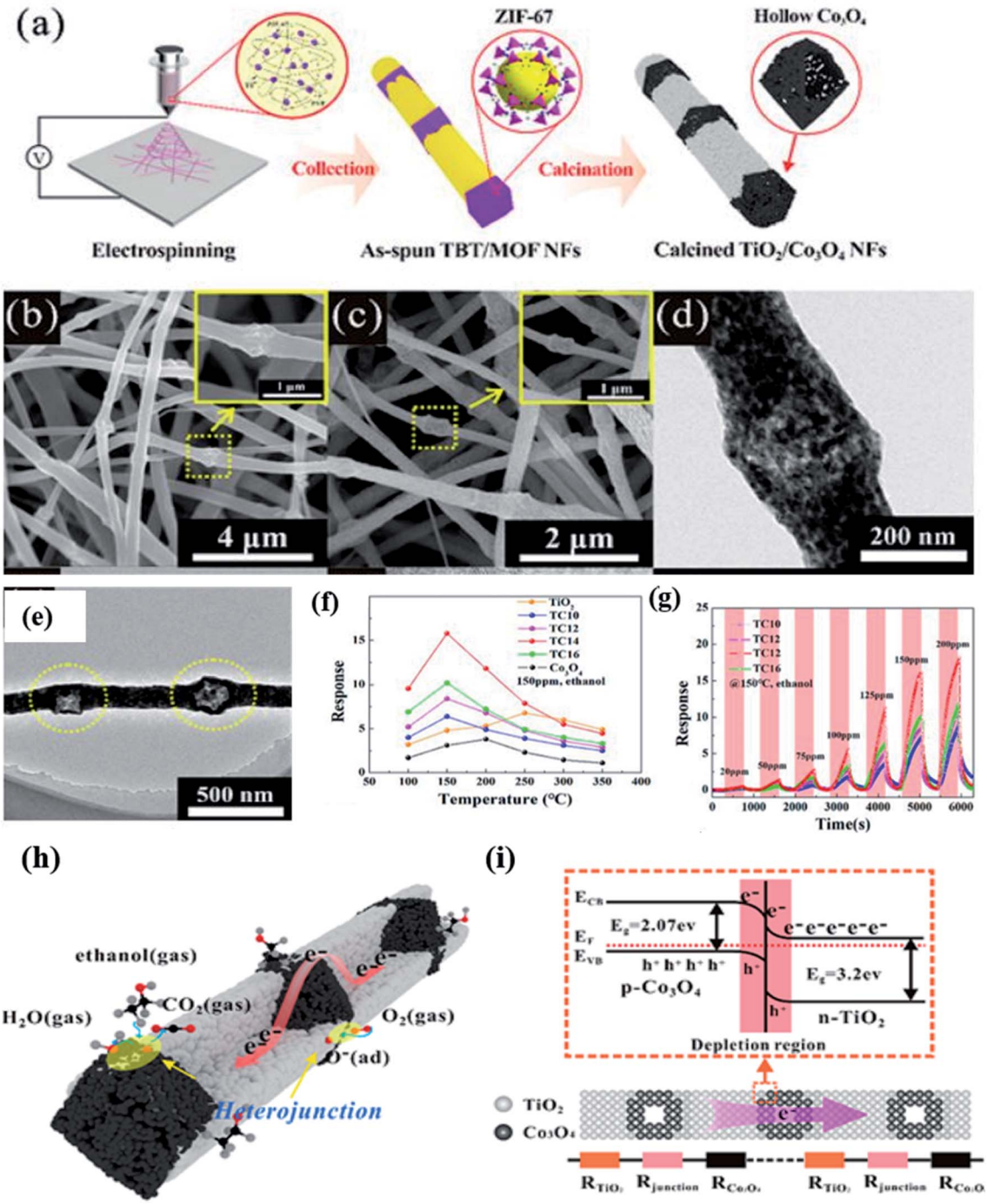

Fig. 8 (a) Schematic diagram of the fabrication procedure of MOF derived Co_3O_4–TiO_2 NFs, (b–e) SEM and TEM images of TiO_2–Co_3O_4 NFs, (f) response *versus* temperature study of TiO_2–Co_3O_4 NFs, (g) ethanol response transients of the TiO_2–Co_3O_4 NF sensor at 150 °C, (h and i) gas sensing mechanism of the TiO_2–Co_3O_4 NF sensor along with the corresponding energy band diagram of the TiO_2–Co_3O_4 NF sensor. Reproduced from ref. 96, copyright@2021, American Chemical Society.

Zeng and his co-workers[96] prepared a p–n junction-based heterostructure from 1D TiO_2 nanofibers coupled with a Co-MOF (Co_3O_4 nanoparticles) through the typical electrospinning method (as shown in Fig. 8a). As a gas sensing material, the obtained TiO_2/Co_3O_4 nanofiber heterostructures with ~240 nm size (as shown in the SEM and TEM images (Fig. 8b–e), exhibited enhanced ethanol sensing performance. Four types of TiO_2–Co_3O_4 p–n heterojunction structures were fabricated by controlling the content of ZIF-67 *i.e.*, TC_{10} (1800 nm), TC_{12} (1200 nm), TC_{14} (800 nm), and TC_{16} (400 nm), which corresponds to the internode distances. The highest ethanol response (R_a/R_g) of 16.7 at 150 ppm at a lower operating temperature of 150 °C was obtained for the TC_{14}-TiO_2–Co_3O_4 p–n heterojunction sensor (as shown in Fig. 8f). It was concluded that the p–n

Open Access Article. Published on 13 december 2021. Downloaded on 11. 11. 2024 14:01:32.
This article is licensed under a Creative Commons Attribution-NonCommercial 3.0 Unported Licence.

heterojunctions of TiO_2–Co_3O_4 were responsible for the improved sensitivity. The difference in the Fermi energy level of the p–n TiO_2–Co_3O_4 heterojunction sensor leads to the establishment of the space charge region on both sides of the interface (Fig. 8g). The effect of their individual contacts results in the electrical transfer, which made the TiO_2–Co_3O_4 p–n heterojunction sensor more sensitive towards ethanol gas. This phenomenon also increases the number of oxygen ion species, which facilitated a faster electron transfer compared to the individual junctions.[97] In addition, the Co_3O_4 NPs is well known for their excellent catalytic promotion of the gas sensing reaction and in this study, it further enhanced the ethanol gas sensing reaction.

Lin *et al.*[98] further worked on Co_3O_4 materials to enhance the sensitivity by synthesizing a ZIF-67-derived Co_3O_4/N-doped RGO nanocomposite. In this regard, ZIF-67 was used as a template and precursor to design the Co_3O_4/N-doped RGO nanocomposite. The effect of the amount of RGO plays a significant role in the sensing properties of the Co_3O_4/N-doped reduced graphene oxide (RGO) nanocomposite sensor. The as-prepared Co_3O_4/N-RGO-$_{0.5}$ based sensor exhibited high response (24.5), fast response/recovery time (20/51 s) towards 100 ppm ethanol at 200 °C.

Wei *et al.*[99] synthesized α-Fe_2O_3 porous spindle materials derived from MIL-88 (Fe) MOFs followed by mixing of 1 wt% RGO with it to form rGO/α-Fe_2O_3 composites. The sensor based on such materials exhibited high sensitivity ($R_a/R_g = 24$) for 50 ppm TEA at 280 °C with a very short response/recovery time of 2 s/7 s. The high response towards TEA was attributed to the differences in the molecular bonds of the target gases. TEA having a low C–N bond energy displayed an enhanced response.[100] Dmello *et al.*[101] reported a MOXs@MOF-based structure by synthesizing SnO_2 nanoparticles encapsulated in the ZIF-67 MOF (as shown in Fig. 9A). The ZIF-67 MOF was selected here due to its strong CO_2 capture characteristics.[102] Initially, SnO_2 nanoparticles with ~6.5 nm size (Fig. 9B) were

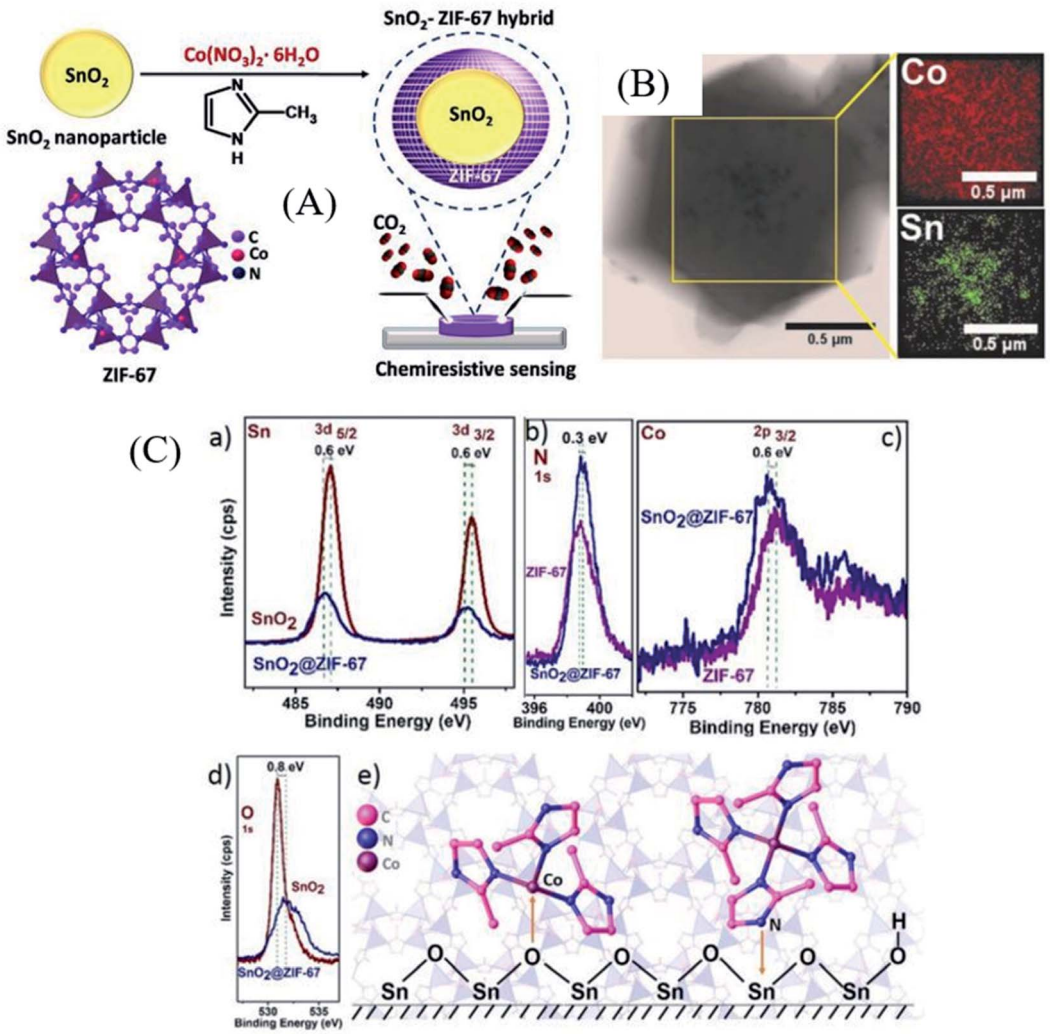

Fig. 9 (A) Schematic illustration of SnO_2@ZIF-67 architecture formation, (B) TEM image of the core–shell SnO_2@ZIF-67 material with its corresponding EDX-elemental analysis, and (C) XPS analysis to examine the synergistic effect of SnO_2 and the ZIIF-67 MOF. Reproduced from ref. 101 with permission from Wiley-VCH GmbH, copyright 2021.

© 2022 The Author(s). Published by the Royal Society of Chemistry

Open Access Article. Published on 13 december 2021. Downloaded on 11. 11. 2024 14:01:32.
This article is licensed under a Creative Commons Attribution-NonCommercial 3.0 Unported Licence.

prepared using a precipitation method followed by coating of ZIF-67 on it to form a core–shell SnO_2@ZIF-67 nanocomposite. Their CO_2 gas sensing was studied and showed a response of 80% at an optimal temperature of 205 °C, whereas a response of 16.5% was obtained for 5000 ppm CO_2. The improved senstivity is ascribed to the synergistic effect of the core–shell morphology of the SnO_2@ZIF-67 sensor, as shown in its XPS studies (Fig. 9C). The shift towards lower energy can be observed for the binding energies of Sn and Co peaks from Fig. 9C. On the other hand, the O1s and N1s peaks were shifted to a higher binding energy position, suggesting the partial electron transfer from the imidazole ligand to Sn and O_2 of SnO_2 to Co of ZIF-67. This study further assisted the synergistic effect of ZIF-67 and the SnO_2 interface.

Among different strategies to enhance the gas sensing performance, the use of noble-metal NPs as catalysts is one of the promising approaches. Loading of noble metal nanoparticles is an ideal choice for improving the gas sensing performances by designing a pristine sensor in the form of a hybrid nanostructure, which comparatively shows enhanced response properties.[103–105] Recently, many researchers have utilized MOFs as sensing layers to encapsulate or functionalize these noble metal NPs onto the surfaces of MOFs.[106] Gold nanoparticles (Au NPs) have been used as catalysts to encapsulate in MOF derived MOXs for high-performance sensing performances. Li *et al.*[107] prepared Au@ZnO core–shell NPs synthesized from Au@MOF-5 core–shell structure-based sensors, which exhibited significantly enhanced gas-sensing performance towards acetone ($R_a/R_g = 20.65$@5 ppm at 300 °C). Similarly, Xia *et al.*[108] presented a facile strategy to synthesize porous Au/ZnO composites from ZIF-8. The results showed that porous Au/ZnO NPs exhibited high response ($R_a/R_g = 17.1$) at 275 °C towards 1 ppm acetone with a response/recovery time of 247 s/209 s for 600 ppb acetone. Recently, Li *et al.*[109] reported Au metal decoration on MOF-derived Co_3O_4 hollow nano-cages by using the $NaBH_4$ (2–4 ml) reduction method for acetone detection. According to their results, the 4 ml $NaBH_4$ reduced Au loaded Co_3O_4 (Au–Co_3O_4-4) based sensor showed a high response of 14.5 towards 100 ppm of acetone at 190 °C with a LOD of 1 ppm. A sensor array was prepared from the two sensors, such as pristine Co_3O_4 and Au/Co_3O_4-4 sensors and with the help of principal component analysis (PCA), acetone was clearly distinguished from other interfering gases. The spillover effect and chemical sensitization effect of Au nanoparticles with excellent gas accessibility of nanocages were the main reasons for the high sensing performance of such sensors.[110]

Pt@ZnO NP-TiO_2 nanotubes (NTs) were prepared using Pt@ZIF-8 derived materials on TiO_2 nanotubes.[111] Pt@ZIF-8 was initially prepared, and then dropped onto the poly-styrene (PS) fibers to prepare Pt@ZIF-8-PS NFs. This was followed by dropping a solution of tetra butyl orthotitanate (TBOT) on the Pt@ZIF-8-PS NFs followed by their calcination to obtain the composite structure of Pt@ZnO–TiO_2 nanotubes (NTs). The results showed that the surface oxygen vacancy amount was increased by the addition of Pt NPs and Pt@ZIF-8 NPs into Pt@ZnO–TiO_2 NT materials.[112] The response of the as-prepared Pt@ZnO–TiO_2 NT sensor ($R_a/R_g = 11.13$) towards 1 ppm toluene was improved compared to Pt@TiO_2 NTs and TiO_2 NTs at 300 °C with a τ_{res}/τ_{recv} of 7.5 s/20.1 s. The improved sensing performances are ascribed to the high concentration of oxygen vacancies, the change of resistance of the heterostructure introduced by the unique NT structure, and highly dispersed and small-sized Pt NPs in TiO_2 NTs.

Lee and co-workers[113] reported In_2O_3 hollow spheres synthesized through the spray pyrolysis method followed by the coating of an ultrathin layer of Co-ZIF-L by a dip coating method with varied dipping times of 1, 2, 4, and 6 min (Fig. 10a–c). Accordingly, the Co-ZIF-L coated In_2O_3 hollow spheres were referred to as 1-, 2-, 4-, and 6-ZIF-L-In_2O_3. After that Pd NPs were loaded on the surfaces of these ZIF-L-In_2O_3 materials followed by calcination at 500 °C to convert them to PdO/Co_3O_4–In_2O_3 hollow nanostructures. The highest response (R_a/R_g) of the 2-PdO loaded Co_3O_4–In_2O_3 hollow sphere (Fig. 10(d and e)) sensor was found to be 146.9 at 225 °C towards 5 ppm acetone under 80% humidity conditions, whereas the 4-PdO loaded Co_3O_4–In_2O_3 hollow sphere-based materials showed a slightly decreased response ($R_a/R_g = 145.9$). Fig. 10f and g show the response transients and repeatability (20 repeat cycles, 5 ppm) of the 4-PdO/Co_3O_4–In_2O_3 sensor toward acetone (1–5 ppm) at RH = 80% and a working temperature of 225 °C. The enhanced response of the 4-PdO/Co_3O_4–In_2O_3 sensor is ascribed to the chemical and electronic sensitization of the presence of both Co_3O_4 and PdO.[114]

Exploring heterostructures with highly selective and sensitive detection under high humidity condition is highly needed to overcome the selectivity and sensitivity issues. Koo *et al.*[115] developed a heterostructure based on Pd-loaded ZIF-8-derived ZnO nanocubes (Pd/ZnO) sensitized on WO_3 nanofibers (NFs) (Fig. 11a). Fig. 11b–d show the TEM images of Pd-loaded ZIF-8. This study showed an improved toluene sensing performance as compared to the previous work.[111] The obtained Pd/ZnO loaded WO_3 NF sensor displayed a remarkable response toward toluene ($R_a/R_g = 22.22$ to 1 ppm) (as shown in Fig. 11h) with fast gas response speed (~20 s) at 350 °C, which demonstrated the improved sensing properties achieved by the functionalization of the catalyst onto WO_3 NFs. The improved sensing performance towards toluene gas by the Pd@ZnO–WO_3 NF sensor was attributed to the formation of heterojunction structures, and mesoporous structures. In addition, additional electron donation due to the transition from PdO to Pd after the reaction with toluene gas is attributed to the enhanced sensing performances. The above reports indicate that metal oxide sensors resulting from encapsulated or metal NP loaded ZIF-8 materials show excellent sensing performance.

Zhou *et al.*[116] reported ZnO NPs with a three-dimensional inverse opal (3DIO) structure-derived from ZIF-8 followed by Pt NPs for H_2S detection. As compared to conventional metal-oxides, MOFs possess high surface area and ordered pore sizes which facilitate an easy access to analyte molecules and fasten electron transport.[117] The response of the Pt/ZnO 3DIO NPs was found to be 11.2 for 1 ppm H_2S with a LOD of 25 ppb, excellent selectivity, and stability. The improved sensitivity of the sensor is ascribed to the spillover effect of the small Pt NPs and the

Open Access Article. Published on 13 december 2021. Downloaded on 11. 11. 2024 14:01:32.
This article is licensed under a Creative Commons Attribution-NonCommercial 3.0 Unported Licence.

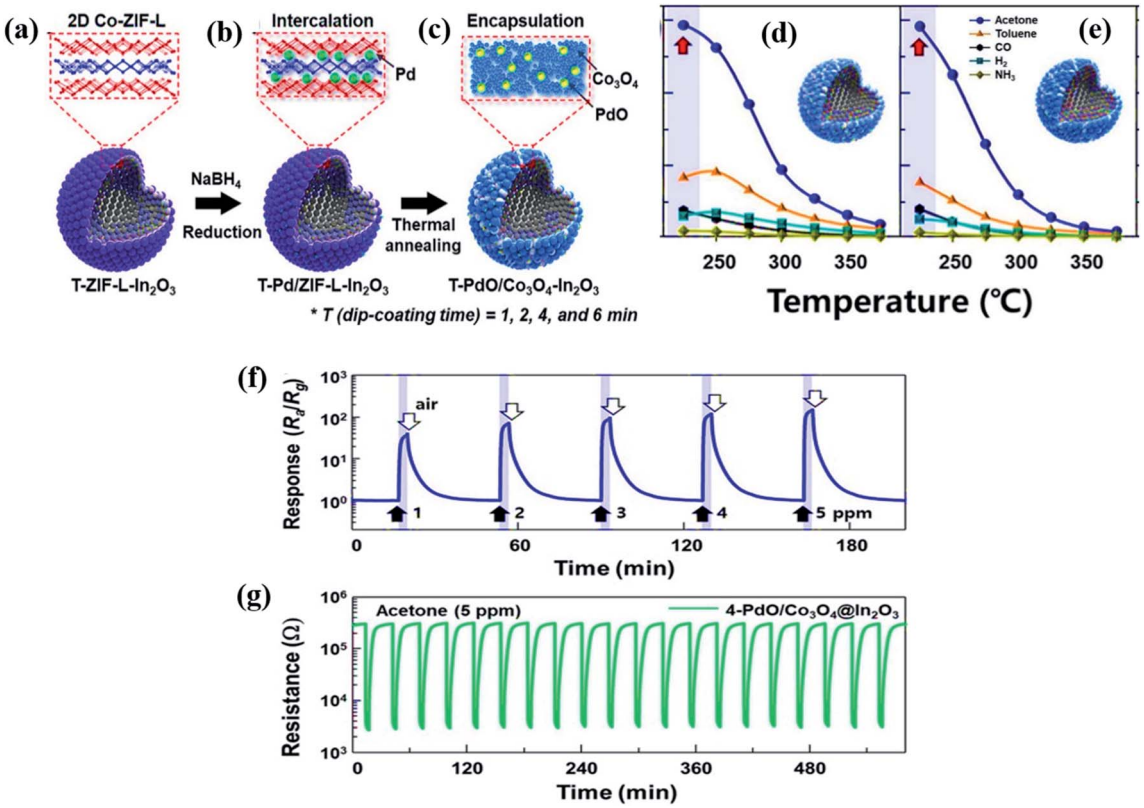

Fig. 10 (a–c) Schematic illustration of the synthesis procedures of the ultrathin Co-ZIF-L layer onto In_2O_3 hollow surfaces followed by Pd loading onto Co-ZIF-L-In_2O_3 hollow spheres with thermal annealing to prepare PdO/Co_3O_4–In_2O_3 hollow spheres, (d and e) responses of 2-and 4-PdO/Co_3O_4–In_2O_3 hollow sphere based sensors at different operating temperatures, and (f and g) response transients of the 4-PdO/Co_3O_4–In_2O_3 sensor for 20 repeat cycles toward acetone (1–5 ppm) at RH = 80% and repeatability test (5 ppm) at the working temperature of 225 °C. Reproduced from ref. 114 with permission from Elsevier, copyright 2021.

unique 3DIO structure of Pt/ZnO NPs. The above results indicate that the strategy to synthesize noble-metal NP loading onto a 3DIO structure shows great potential for ppb level H_2S detection.

Until now, conventional techniques such as gas chromatography or quantum cascade laser[118,119] have been utilized to detect CO at the ppb-level. Recently, Wang and co-workers[120] proposed Pt loaded ZIF-8-derived ZnO NP polyhedra (Pt NPs@ZnO polyhedra) for CO gas detection. The Pt NPs@ZnO polyhedra were prepared by depositing different wt% of Pt (1, 2 and, 3%) followed by calcination. The as-prepared 2% Pt NPs@ZnO polyhedron (SEM image shown in Fig. 12A) sensor displayed a response (R_S) of 65% at 50 ppm (as shown in Fig. 12C) and 9% at ~500 ppb with a LOD of 100 ppb for CO gas. The sensor showed good selectivity in the presence of other interfering gases (Fig. 12B). Fig. 12F and G show the stability test of the sensor for 1 ppm CO at 300 °C, and the humidity effect, which shows that after 50% humidity the response decreased because water vapors occupied the active sites of the sensor's surface interfering the CO response. The enhancement of the response of the as prepared Pt loaded/ZnO polyhedron sensors was due to the porous structures, catalytic effect and electron sensitization effect of Pt nanoparticles, and the establishment of p–n heterojunction of PtO and ZnO (Fig. 12D) structures.[93]

Since noble metal functionalization of MOF-based sensors was realized with enhanced sensing performance, a great amount of research studies has been carried out. However, low or RT operation of the gas sensor is highly necessary to reduce the energy consumption and deploy in real-time practical applications. Kim and co-workers[121] studied Pd incorporated on ZIF-67 MOFs for acetone gas sensing. However, its sensing performance was obtained at 450 °C operating temperature. The same group further studied and synthesized a flexible gas sensor made from PdO loaded Co_3O_4 hollow nanocubes (HNCs) derived from Pd-ZIF-67 MOFs functionalized with single wall carbon-nanotubes (SWCNTs) (Fig. 13) and then finally fabricated them on a Ni/Au mesh-based polyimide (PI) electrode as a flexible heating substrate.[122] PdO–Co_3O_4 HCNs derived from Pd/ZIF-67 MOFs were prepared according to their original work.[121] The conductivity of the PdO–Co_3O_4 HCN sensor on the flexible substrate was controlled by adding SWCNTs. The BET surface area was increased to 92.79 $m^2\ g^{-1}$ after the incorporation of SWCNTs. As shown in Fig. 13a and b, different voltages (C_H) (0–2.1 V) were applied to the Ni/Au mesh heater under the conducting PI film with the SWCNT-PdO–Co_3O_4 HNC sensor on the top. The fabricated sensor exhibited a response of 44.11%

© 2022 The Author(s). Published by the Royal Society of Chemistry

Open Access Article. Published on 13 december 2021. Downloaded on 11. 11. 2024 14:01:32.
This article is licensed under a Creative Commons Attribution-NonCommercial 3.0 Unported Licence.

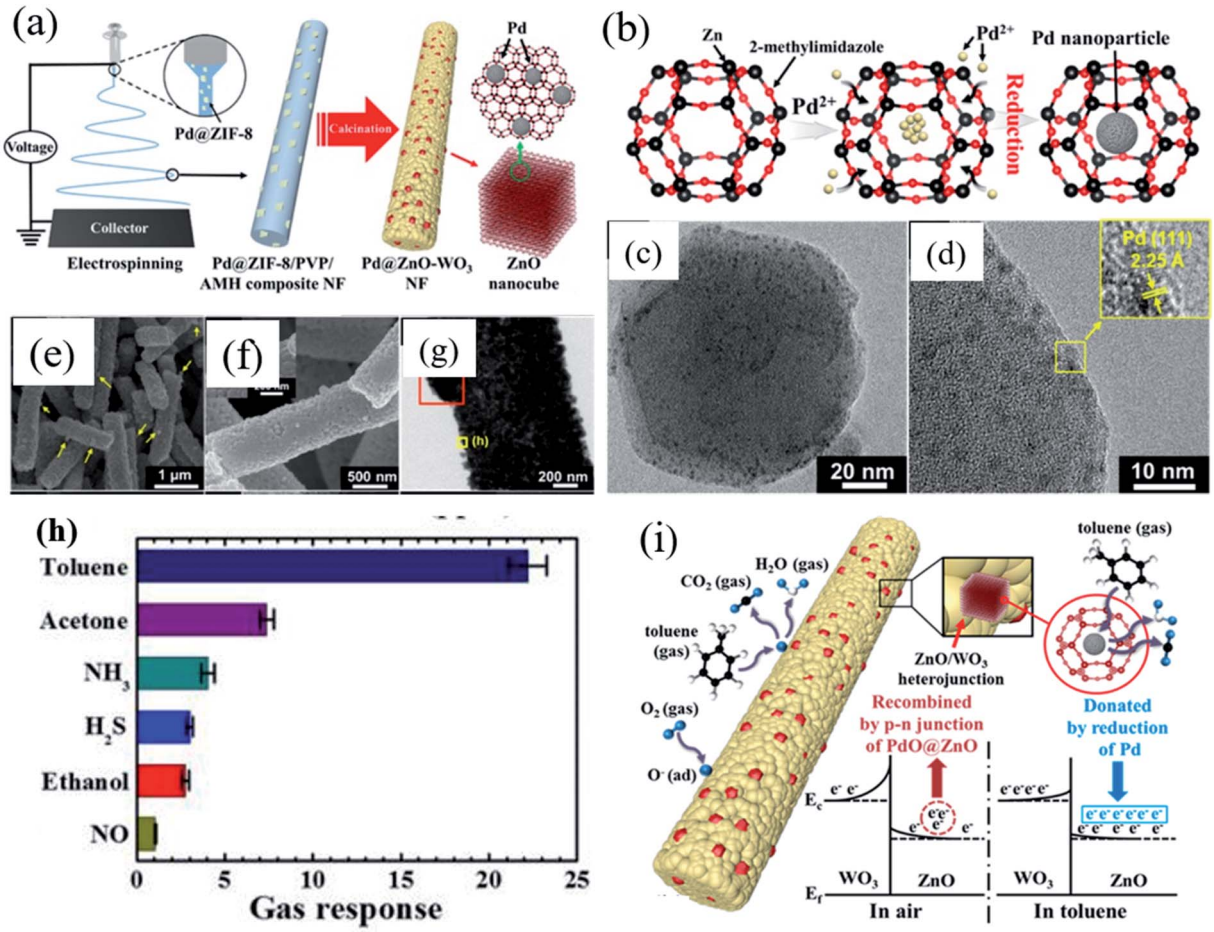

Fig. 11 (a) Schematic diagram showing the synthesis of Pd-loaded ZIF-8-derived ZnO nanocubes by electrospinning, (b) schematic diagram of Pd nanoparticle incorporation onto ZIF-8 molecules, (c and d) TEM images of Pd loaded ZIF-8, (e–g) SEM and TEM images of Pd/ZnO-WO_3 NFs, (h) selectivity test of the Pd/ZnO–WO_3 NF sensor in the presence of other gases, and (i) toluene sensing mechanism of Pd@ZnO–WO_3 NFs. Reproduced from ref. 115 with permission from American Chemical Society, copyright 2021.

towards 20 ppm NO_2 gas at 100 °C (2.1 V) with a LOD of 1 ppm. In addition, the sensor showed a minimal baseline change and an excellent bending over 4000 cycles. The improved NO_2 sensing properties are attributed to the synergistic effect of p-type SWCNTs and Co_3O_4 by the formation of charge transfer and hole accumulation layers as well as the electronic sensitization effect of PdO nanoparticles. The possible sensing reactions can be expressed as follows:

$$O_{2(g)} + e^- \rightarrow O_{2(ads)}^- \quad (9)$$

$$O_2^-(ads) + e^- \rightarrow 2O^-(ads) \quad (10)$$

$$O^-(ads) + e^- \rightarrow O^{2-}(ads) \quad (11)$$

$$NO_{2(g)} + O^-(ads) \rightarrow NO_3^-(ads) \quad (12)$$

$$NO_{2(g)} + O^{2-}(ads) \rightarrow NO_3^{2-}(ads) \quad (13)$$

To further progress in the development of gas sensors that can operate at RT, Zhang and co-workers[123] investigated a composite sensor based on In–MOFs with MoS_2 for NO_2 gas sensing at 25 °C. Initially, In_2O_3 hollow microcubes (HMCs) were prepared from MIL-68 (In) followed by annealing at 600 °C. After that, a sensor device fabrication was carried out *via* a layer-by-layer assembly[124,125] of poly (diallyl dimethylammonium chloride (PDDA)/poly (sodium 4-styrene sulfonate (PSS) (first bilayer) and In_2O_3/MoS_2 (five layers) on an epoxy substrate with Cu/Ni interdigitated electrodes. The In_2O_3/MoS_2 composite sensor exhibited a response value of 371.9 toward 100 ppm NO_2, as compared to pristine MoS_2 and In_2O_3, with an excellent LOD of 8.8 ppb. In addition to a consistent reproducibility, the response/recovery of the In_2O_3/MoS_2 sensor was found to be 152 s/179 s, respectively. The increase in the ambient relative humidity has affected the sensor responses. The sensing performance was attributed to the synergistic effect of the hollow structure of In_2O_3 microrods and MoS_2 NPs, the formation of n–n heterojunctions, and the high specific surface area. The sensor device prepared from this work shows great promise in RT-based gas sensing.

2.2.2 Application of metal-oxides/MOF based composites as sieving materials in chemiresistive gas sensors. In the

Open Access Article. Published on 13 december 2021. Downloaded on 11. 11. 2024 14:01:32.
This article is licensed under a Creative Commons Attribution-NonCommercial 3.0 Unported Licence.

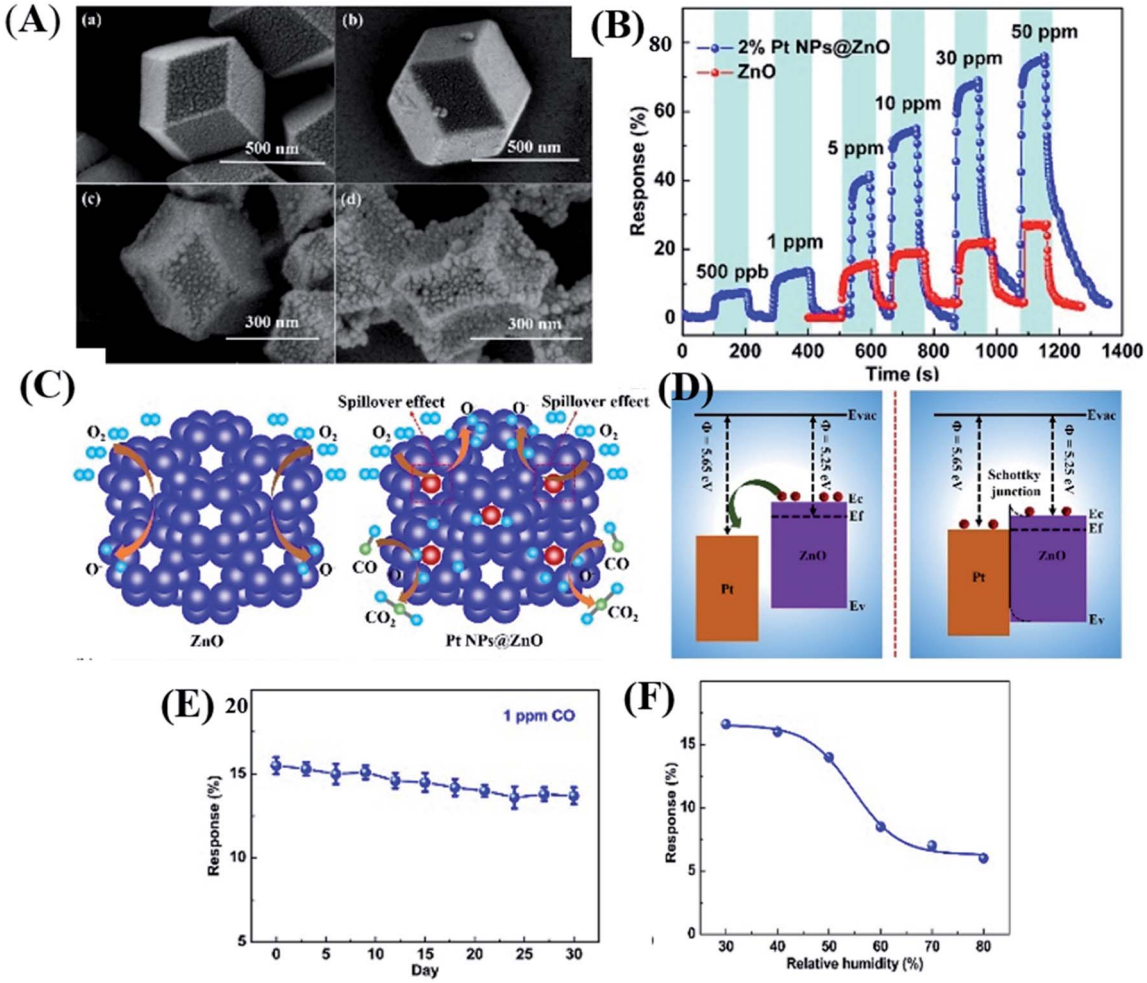

Fig. 12 (A) SEM image of the as prepared Pt@ZnO nanostructures, (B) selectivity test against other gases, (C and D) sensing mechanism depicting the energy band diagram of Pt/ZnO nanostructures, and (E and F) long-term stability and humidity tests of the 2% Pt NPs@ZnO polyhedron sensor. Reprinted from ref. 120, copyright@2021, Elsevier.

previous section, extensive studies on MOFs and metal-oxide materials with composites derived from the MOFs for detection of various gases were discussed. The effect of various architectures, morphologies, and functionalization strategies on the sensitivity, selectivity, and stability is demonstrated. One of the drawbacks of these MOF-derived metal oxides is their high working temperature and moderate selectivity towards specific gases, which further limits their practical applications. To overcome the above issues, recent research on MOF-based filter or sieving materials has been employed in gas sensing applications to achieve the specific desired selectivity properties. It would be interesting to describe some of the reports on MOFs that were utilized for the achievement of high-performance sieving materials.[126–129]

It was reported that the kinetic diameter (D_k) of gas molecules having similar sensing behavior is different, which would pave the way to design highly selective materials using a MOS@MOF core–shell structure by controlling the channel traffic of gas molecules due to their difference in D_k. Based on this, Tian *et al.*[126] reported a highly selective formaldehyde gas sensor using ZIF-8 as the sieving material on ZnO nanorods (NRs) (Fig. 14a). Fig. 14b shows the schematic diagram of ZIFs. Different D_k values of various gases are given in Fig. 14c, among which the response of formaldehyde is the highest. Fig. 14d shows the selectivity of gases based on their D_k. The D_k value of formaldehyde and that of ZIF-8 are comparable, which allows the gas molecules to selectively absorb and enter into the pores of the ZIF-8 MOF towards ZnO for enhanced gas sensing reactions.

Yao *et al.*[130] designed ZnO NWs@ZIF-CoZn MOF core@shell structures (as shown in Fig. 14e) for the selective detection of acetone. ZIF-Co Zn thin films with different thicknesses (5–15 nm) were prepared. Fig. 14f shows the SEM image of ZnO@5 nm ZIF-CoZn materials, while Fig. 14g and h show the performance of a ZnO NWs@ZIF-CoZn MOF sensor tested towards acetone. The results indicated that the selectivity towards acetone was improved due to the sieve membrane of ZIF and ZnO@5 nm-ZIF-CoZn NW arrays showed the maximum response towards 100 ppm acetone at 260 °C. In another study, the effect of pore sizes of MOFs and D_k values of gas molecules

© 2022 The Author(s). Published by the Royal Society of Chemistry

Open Access Article. Published on 13 december 2021. Downloaded on 11. 11. 2024 14:01:32.
This article is licensed under a Creative Commons Attribution-NonCommercial 3.0 Unported Licence.

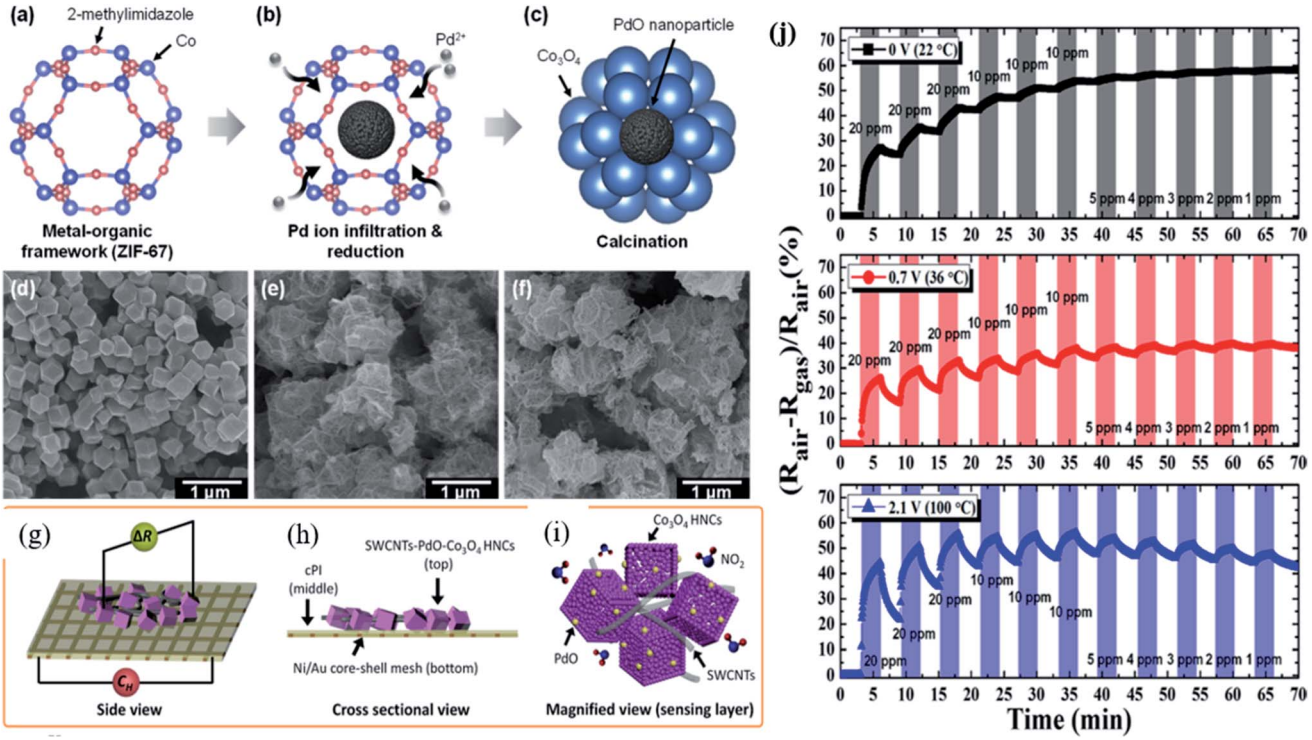

Fig. 13 (a–c) Schematic diagram of PdO loaded Co_3O_4 Pd/ZIF-67 after annealing at 400 °C, (d–f) SEM image of ZIF-67, PdO-loaded Co_3O_4 HNCs after calcination, and SWCNT-loaded PdO Co_3O_4 HNCs, (g–i) schematic illustration of the fabrication of the SWCNT-loaded PdO–Co_3O_4 HNC sensor device on a flexible conducting PI film (cPI) with a Ni/Au mesh heater based substrate, and (j) response transients of the SWCNT-loaded PdO–Co_3O_4 HNC sensor towards NO_2 at different applied voltages (0–2.1 V). Reprinted from ref. 122, copyright@2021, American Chemical Society.

was studied by Zheng and co-workers.[131] Two types of MOFs, including ZIF-8 with a pore size of ~3.4 Å and ZIF-71 with a pore size of ~4.8 Å, respectively (Fig. 14i) were evaluated. The gas selectivity of a specific gas among different gases (H_2, NH_3, ethanol, acetone, and benzene) could be modulated through the sieving effect of these ZIFs. Although ethanol and acetone have similar D_k values, the highest sensitivity and selectivity were shown by ethanol molecules, whereas ZIF-8 impeded both ethanol and acetone gases due to its lower pore size of 3.4 Å.[132]

Luo *et al.*[127] further advanced their studies to design noble metal nanoparticles (Au and Pd) loaded on MOX@MOF C–S architectures to enhance the selectivity of gas molecules. The latter one reported Pd loaded ZnO@ZIF-8 core–shell NPs for the selectivity of CH_4 in the presence of NO_2. The sensor showed a response ($R_a - R_g/R_g = 16.9\%$) toward 0.1% CH_4 under visible light illumination (470 nm) at a lower operating temperature of 80 °C with excellent selectivity against NO_2 ($S\% = 13.1\%$). Due to the lower aperture size of ZIF-8 (4.0–4.2 Å), the diffusion of NO_2 was reduced owing to its large D_k (4.5 Å), while CH_4 with a D_k value of 3.8 Å was easily diffused through it. The above strategies to improve the selectivity of specific gases would pave the way for other types of MOX and MOF-based gas sensors.

3. Metal–organic frameworks for capacitive based gas sensors

In addition to the chemiresistive gas sensors, another electrically transduced gas sensor based on the capacitive principle has been deployed for various gas analyte detection. A large number of materials have been reported in recent years for capacitive-based gas sensor applications. One of the drawbacks of MOF derived metal-oxides and their composite-based gas sensor is high working temperature, which limits their practical applications.[133] On the other hand, MOF-based capacitive gas sensing materials have been explored at RT only,[71,134–139] which have a high significance in recent days compared to the high-temperature-based chemiresistive gas sensors. The following section discusses the working principle of capacitive sensors followed by capacitive sensing results for VOCs and toxic/hazardous detection. The sensing performances of MOF-based capacitive-based gas sensors are summarized in Table 3.

3.1 Applications of metal–organic framework based capacitive gas sensors

In 2015, Salama and co-workers studied the capacitive-based gas sensor using Cu (bdc)·xH_2O as MOF thin film layers for the first time. They investigated VOCs and humidity sensing properties using the IDE capacitive electrode.[134] The as-prepared Cu-MOF based gas sensors were tested for different VOC gases at RT, and among them, it displayed a high sensing response (4.5 pF@500 ppm) to toluene at 22 °C. The sensor showed a linear sensing behavior to all gases at the corresponding concentrations. The high sensitivity to toluene gas was due to the π–π interaction in the benzene rings of the MOF.[137] In addition, humidity sensing was demonstrated and revealed that until 65% RH the sensors displayed linear behavior. This was

Open Access Article. Published on 13 december 2021. Downloaded on 11. 11. 2024 14:01:32.
This article is licensed under a Creative Commons Attribution-NonCommercial 3.0 Unported Licence.

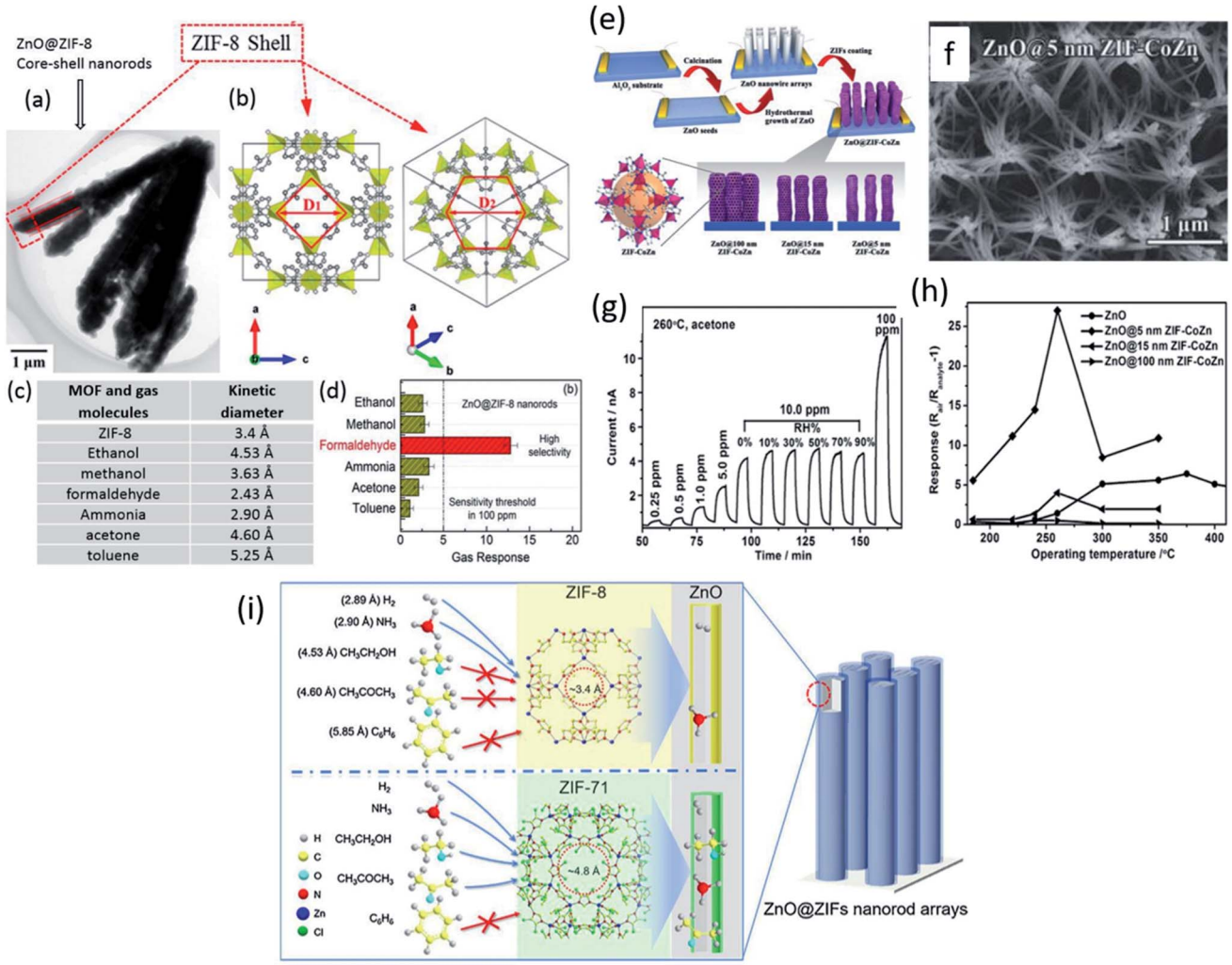

Fig. 14 (a and b) Morphology of ZnO@ZiF-8 core–shell NRs and schematic of the structure of ZIF-8, (c) comparison of MOFs and gas molecules and their kinetic diameters, and (d) selectivity test of the ZnO@ZIF-8 sensor for various gases for 100 ppm. Reprinted from ref. 126 with permission from American Chemical Society, copyright 2021; (e) schematic of the synthesis protocol of ZnO@ZIF-CoZn gas sensing devices, (f) SEM image of ZnO@5 nm ZIF-CoZn core–shell NW arrays, (g) response–recovery transients of ZnO@5 nm ZIF-CoZn core–shell NW arrays to acetone at 260 °C, and (h) temperature dependent sensing for 10 ppm acetone from 200 to 400 °C. Reproduced from ref. 130 with permission, copyright 206@Wiley and Sons; (i) schematic illustration of the effect of pore sizes of ZnO@ZIF-8 MOFs and kinetic diameter of gas molecules. Reproduced from ref. 131 with permission from Elsevier, copyright@2021.

Table 3 Summary of the sensing performances of capacitive based gas sensors[a]

MOF materials	Target gas	Response (pF) or [$\Delta C/C$ (%)]	Concentration (ppm)	Response time	LOD	Types of interactions between MOFs and gases	Ref.
Cu (BDC)·xH$_2$O	Toluene	4.5 pF	500	NA	NA	π–π interaction	134
MIL-96 (A)	Methanol	14.1 pF	2			NA	135
Fum-fcu-MOF	H_2S	40×10^{-4} ($\Delta C/C$%)	100	NA	5.4 ppb	NA	137
UiO-66 (Zr))	H_2S	9×10^{-1} ($\Delta C/C$%)	100	200 s	1 ppm	Interaction with Ag_2O to form Ag_2S	141
NDC-Y-fcu-MOF	NH_3	25×10^{-1} ($\Delta C/C$%)	100	250 s	92 ppb	lone pairs of NH_3 with the unsaturated metal sites	138
MFM-300	SO_2	16.5×10^{-4} ($\Delta C/C$%)	1	NA	5 ppb	O–H (ligand)–SO_2 (H_2 bonding)	138
Mg-MOF-74	Benzene	5.9×10^{-4} ($\Delta C/C$%)	100	NA	NA	Open metal sites (Mg(II) and S (SO_2)	134

[a] NA: not available.

© 2022 The Author(s). Published by the Royal Society of Chemistry

Open Access Article. Published on 13 december 2021. Downloaded on 11. 11. 2024 14:01:32.
This article is licensed under a Creative Commons Attribution-NonCommercial 3.0 Unported Licence.

followed by nonlinearity (increase of capacitance) as the response decreases with an increase in the humidity level up to 100% due to the adsorption of a greater amount of vapor in the porous MOF nature.

The same group[135] investigated another VOC gas sensor based on MIL-96 (Al) MOF materials. The novelty of this work lies in the fact that as compared to the conventional sensing layer fabrication such as by the drop casting method, this unique and novel technique of Langmuir–Blodgett (LB) provides homogeneous coverage of the surface and tunable thickness by judicious control of the parameters. They used the LB deposition technique to deposit the as prepared MIL-96 (Al) MOFs as a thin film layer on the sensor substrate for the investigation of capacitive-based sensing of methanol gas at RT (Fig. 15a). They performed sorption studies of the as-prepared MIL-96 (Al) MOFs for several organic vapors, including methanol. They revealed that the as-prepared MIL-96 (Al) displayed a high affinity for water and methanol vapor (Fig. 15b). At a higher concentration of methanol and water, the response (ΔC/C%) was linearly increased. In addition, they deposited another thin selective layer of parylene C with a thickness of ~250–300 nm over the LB based MOF films using a chemical vapor deposition (CVD) method, which eventually increased the sensitivity and selectivity of water vapor (Fig. 15d). In contrast, there was a severe decrease in methanol response.

Yassine *et al.*[137] synthesized a rare-earth-based MOF (fumarate-based yttrium MOF) (fum-fcu-MOF) by a solvothermal reaction at 105 °C for 36 h, which was directly grown on the IDE substrate (as shown in Fig. 16a). The capacitive sensors made from the fum-fcu-MOF exhibited high-sensitivity ($\Delta C/C = 40 \times 10^{-4}$) (Fig. 16b and c) for 100 ppm H_2S gas with a LOD of 8.4 ppb with high selectivity to H_2S at RT in the presence of other gases (as shown in Fig. 16d). Compared to MOFs such as Cu(bdc)·$x$$H_2O$, and ZIF-8, the as-prepared fum-fcu-MOF displayed excellent stability with the least variation in responses. The low stabilities of the above devices are due to the degradation of structures during the prolonged exposure to H_2S, which eventually results in the formation of metal sulfide.[140]

The effect of noble metal NPs on MOF materials for gas sensing performances was studied by Surya *et al.*[141] for H_2S gas sensing. The authors reported a zirconium-based MOF (UiO-66 (Zr)) followed by the anchoring of Ag NPs on the surface of the MOF for the investigation of H_2S. Three kinds of MOFs, including UiO-66(Zr) BDC, UiO-66(Zr) BDC-N_3, and UiO-66(Zr) BDC-NO_2, were prepared by tuning the different functional groups and their gas sensing properties were studied. The impregnation method was employed to anchor Ag NPs on the surfaces of all the prepared MOF structures. It was found that the Ag NPs were converted to silver oxide (Ag_2O) NPs. Among all three sensors, the Ag_2O loaded UiO-66(Zr) BDC-NO_2 loaded sensor displayed the highest response ($\Delta C/C = 9 \times 10^{-1}$) toward 100 ppm H_2S with a response time of 200 s and a LOD of 1 ppm at RT, which indicated that the sensor displays high affinity towards the chemical absorption of H_2S. The synergistic effect of Ag_2O and UiO-66 (Zr) MOFs and their sensitivity towards H_2S was attributed to the formation of metal sulfide (Ag_2S) as

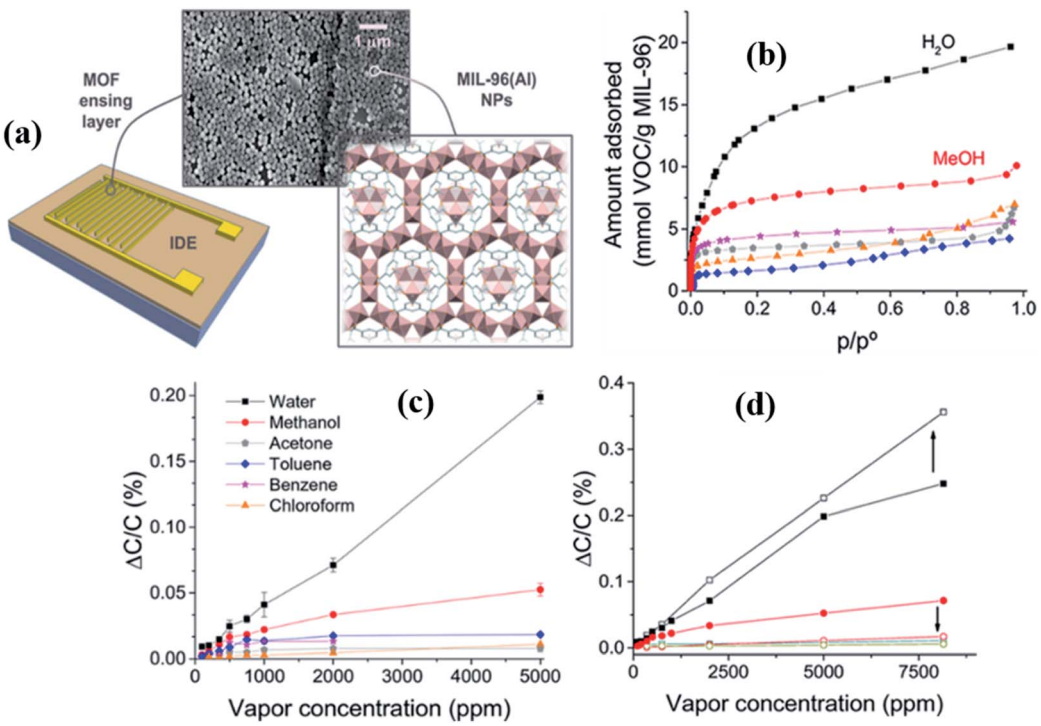

Fig. 15 (a) Schematic diagram of the MIL-96(Al) MOF structure and IDE substrate along with the SEM image of the MIL-96(Al) MOF thin film, (b) sorption study of MIL-96(Al) NPs for water and gas vapors (methanol, ethanol, acetone, chloroform, and toluene), (c) selectivity study of the LB film MIL-96(Al) MOF based sensor towards different gases including water, and (d) capacitive responses ($\Delta C/C$ (%)) of the MIL-96(Al) MOF IDE device to water and methanol using the parylene C film showing the effect of parylene C film layer on the LB deposited MIL-96(Al) MOF sensor. Reproduced from ref. 135 with permission from American Chemical Society, copyright 2021.

Open Access Article. Published on 13 december 2021. Downloaded on 11. 11. 2024 14:01:32.
This article is licensed under a Creative Commons Attribution-NonCommercial 3.0 Unported Licence.

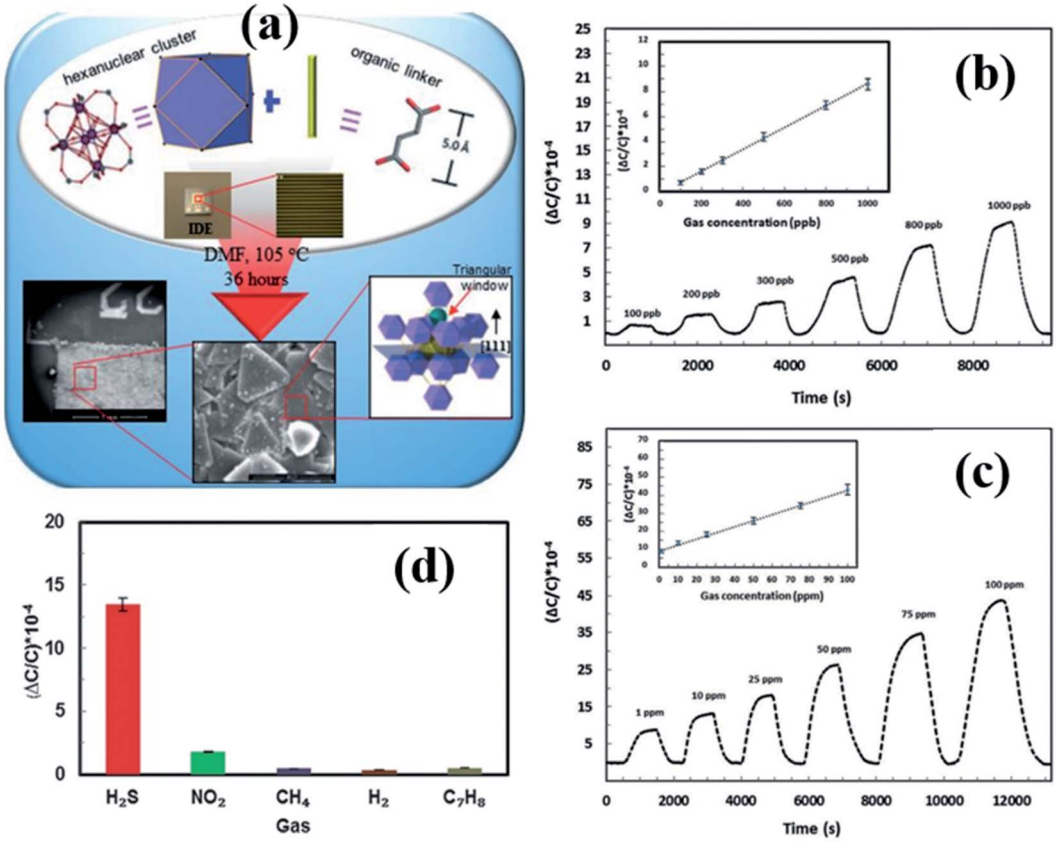

Fig. 16 (a) The schematic diagram of the preparation of the fum-fcu-MOF by the solvothermal method and its integration onto the IDE, (b and c) capacitive response transients of the fum-fcu-MOF sensor for the ppb and ppm levels of H_2S detection, and (d) the selectivity test of the fum-fcu-MOF sensor towards different interfering gases. Reprinted from ref. 137, copyright@2021, Wiley and Sons.

a product of the reaction between silver oxide (Ag_2O) and H_2S gas molecules.

In 2017, Salama and co-workers further extended their previous work[137] by fabricating naphthalene-based ditopic ligand (1,4-naphthalene dicarboxylate (1,4-NDC)) rare earth MOFs with a fcu topology (NDC-Y-fcu-MOF), which is an isostructural MOF to UiO-66 (Zr) and was used in a capacitive based NH_3 gas-sensor.[142] The NDC-Y-fcu-MOF was grown on the IDE substrate directly by a solvothermal method at 120 °C synthesis temperature (inset of Fig. 17a). Fig. 17b shows the FESEM image of the as-synthesized NDC-Y-fcu-MOF film. Fig. 17c and d show the selectivity study of the NDC-Y-fcu-MOF sensor toward 1 ppm NH_3. A comparison of sensitivity was carried out with other MOF materials such as Cu(bdc)·$x$$H_2O$, HKUST-1, and ZIF-8, and showed that the NDC-Y-fcu-MOF sensor showed enhanced capacitance change. As shown in Fig. 17a, the NDC-Y-fcu-MOFs showed a linear response ($\Delta C/C$ (%)) toward NH_3 (1 to 100 ppm) at RT with a LOD of 92 ppb, and a response time of 250 s. The humidity effect on the sensing performance of the NDC-Y-fcu-MOF was studied (Fig. 17e) at different RH levels (5% to 85%) for 10 and 25 ppm of NH_3 and found that until the RH level of 30% the response was stable. However, with further increase in the RH level up to 85%, the sensitivity showed a slight increase due to the rise in the dissolution of NH_3 molecules onto the NDC-Y-fcu-MOF sensing layer.[51,143]

To the best of our knowledge, there are no reports on SO_2 gas sensing based on the capacitive principle except one by the Prof. Salama group.[138] In their work, they developed an indium-based MOF known as MFM-300, which consists of infinite cis $InO_4(OH)_2$ octahedral chains bridged by (biphenyl-3,3,5,5-tetracarboxylic acid) tetradentate ligands (as shown in Fig. 18a). The MFM-300 sensor exhibited good sensitivity ($\Delta C/C\% = 16.5 \times 10^{-4}$ for 1 ppm) and high selectivity towards SO_2 gas with a low detection limit of ~5 ppb at a humidity level up to 30 RH% (Fig. 18b–d). Due to the large number of OH groups in the MFM-300 (In) channels, the –OH and –CH groups on the benzene ring provide a favorable adsorption site for SO_2, increasing the SO_2 adsorption capacity. The response intensities of MFM-300 to other gases were compared at 1000 ppb, and the results showed that the sensor displayed high SO_2 selectivity (Fig. 18e).

Yuan *et al.*[139] integrated Mg–MOF-74 thin films on a capacitive sensor chip to investigate benzene and CO_2 gases (Fig. 19). Fig. 19a shows the SEM image of Mg–MOF-74 as grown on the IDE substrate. The obtained Mg–MOF-74 sensor displayed selective sensitivity for CO_2 gas and benzene at RT (Fig. 19b). On the other hand, the Mg–MOF-74 film modified with a film of ethylenediamine decreases the response sensitivity to benzene, while it increases the selectivity to CO_2 (Fig. 19c). Fig. 19d shows the repeatability study of the ethylenediamine-functionalized Mg–MOF-74 sensor for 5000 ppm showing good repeatability. Due to the amine coordination on the surface of Mg–MOF-74, there was a significant reduction of porosity and blocking pores, which caused the decrease of sensing performance for benzene.

© 2022 The Author(s). Published by the Royal Society of Chemistry

Open Access Article. Published on 13 december 2021. Downloaded on 11. 11. 2024 14:01:32.
This article is licensed under a Creative Commons Attribution-NonCommercial 3.0 Unported Licence.

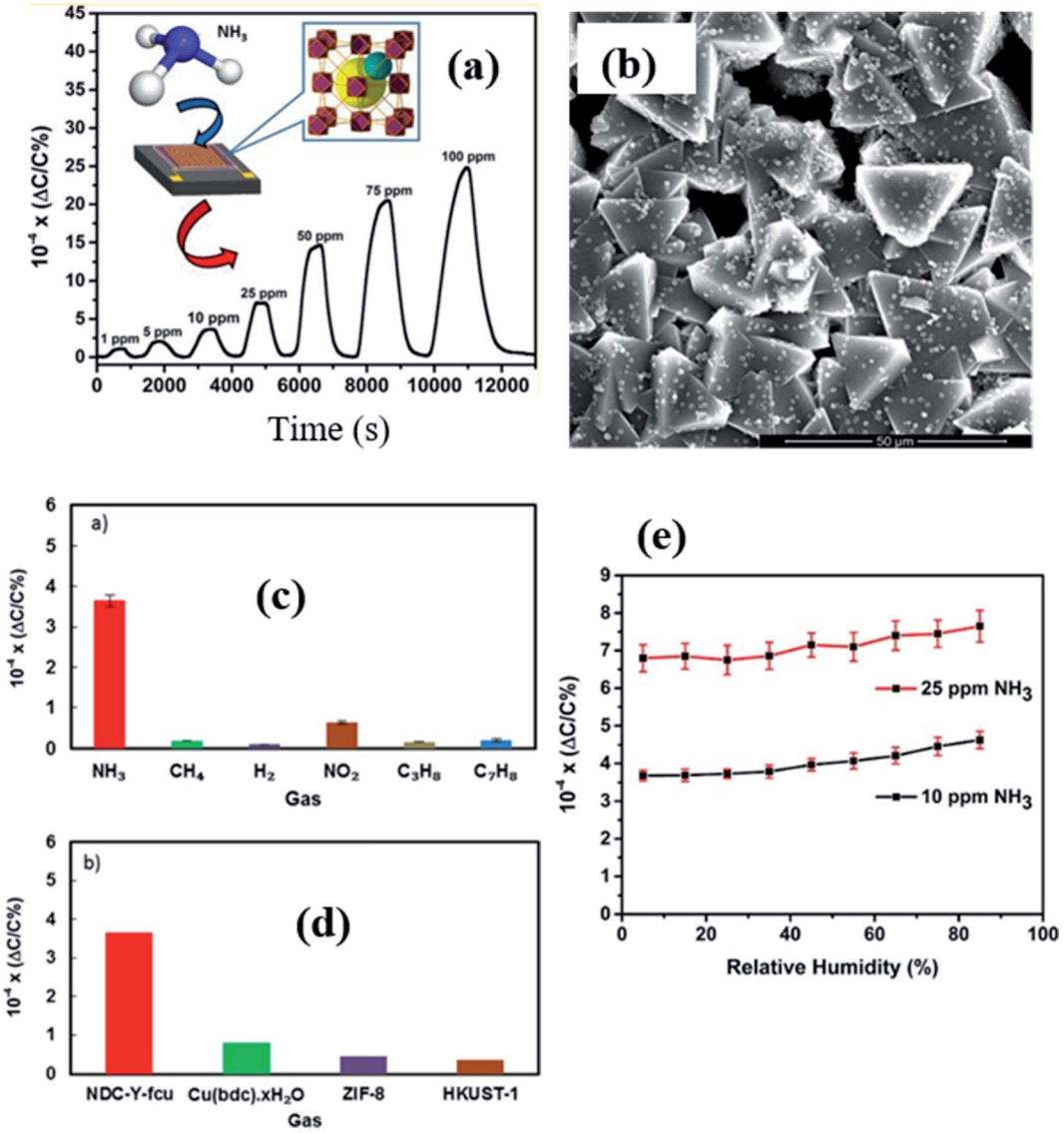

Fig. 17 (a) The NDC-Y-fcu-MOF based capacitive sensor and its response transient for (1–100 ppm). The inset shows the schematic diagram of the structure of the NDC-Y-fcu-MOF, (b) SEM image of the as grown NDC-Y-fcu-MOF film on the IDE substrate, (c and d) selectivity study toward 1 ppm NH_3 in different interfering gases and a comparison of sensitivity in the presence of other MOF materials, and (e) the effect on sensing properties of the NDC-Y-fcu-MOF sensor for 10–25 ppm NH_3 at different RH levels. Reprinted from ref. 142. Copyright@2021, American Chemical Society.

However, the enhanced sensing performance for CO_2 (by *ca.* 25%) resulted from the amine–CO_2 interaction (Fig. 19e). The above results indicate that with a feasible tuning of MOF–analyte interactions, high-performance MOF-based sensors can be developed.[139]

4. Metal–organic frameworks for quartz crystal microbalance based gas sensors

In the past few decades, the integration of different types of sensing materials into QCM based transducer devices has led to significant progress in investigating the gas sensing performance of various toxic and VOC analytes.[144–147] In QCM based gas sensors, the frequency change (Δf) is proportional to the change in mass adsorbed and/or sorbed (Δm) over the QCM electrode and is monitored for the target analyte. The interaction between target analyte molecules and sensing layers coated on the quartz crystal surface ("guest–host interaction") plays a great role in the sensing mechanism. However, due to the lack of good porosity and numerous sites for the absorption of target gases, the above materials show low sensing performance in QCM gas sensors. MOFs, as a typical class of materials with excellent porosity and numerous absorption sites, would be an ideal candidate for QCM based gas sensors. Due to their advantageous attributes such as cost-effectiveness, simple device structure, and the ability to operate at RT, QCM based transducers have gained a lot of attention.[148] In the following section, we discuss the fundamental principles of QCM gas

© 2022 The Author(s). Published by the Royal Society of Chemistry

Open Access Article. Published on 13 december 2021. Downloaded on 11. 11. 2024 14:01:32.
This article is licensed under a Creative Commons Attribution-NonCommercial 3.0 Unported Licence.

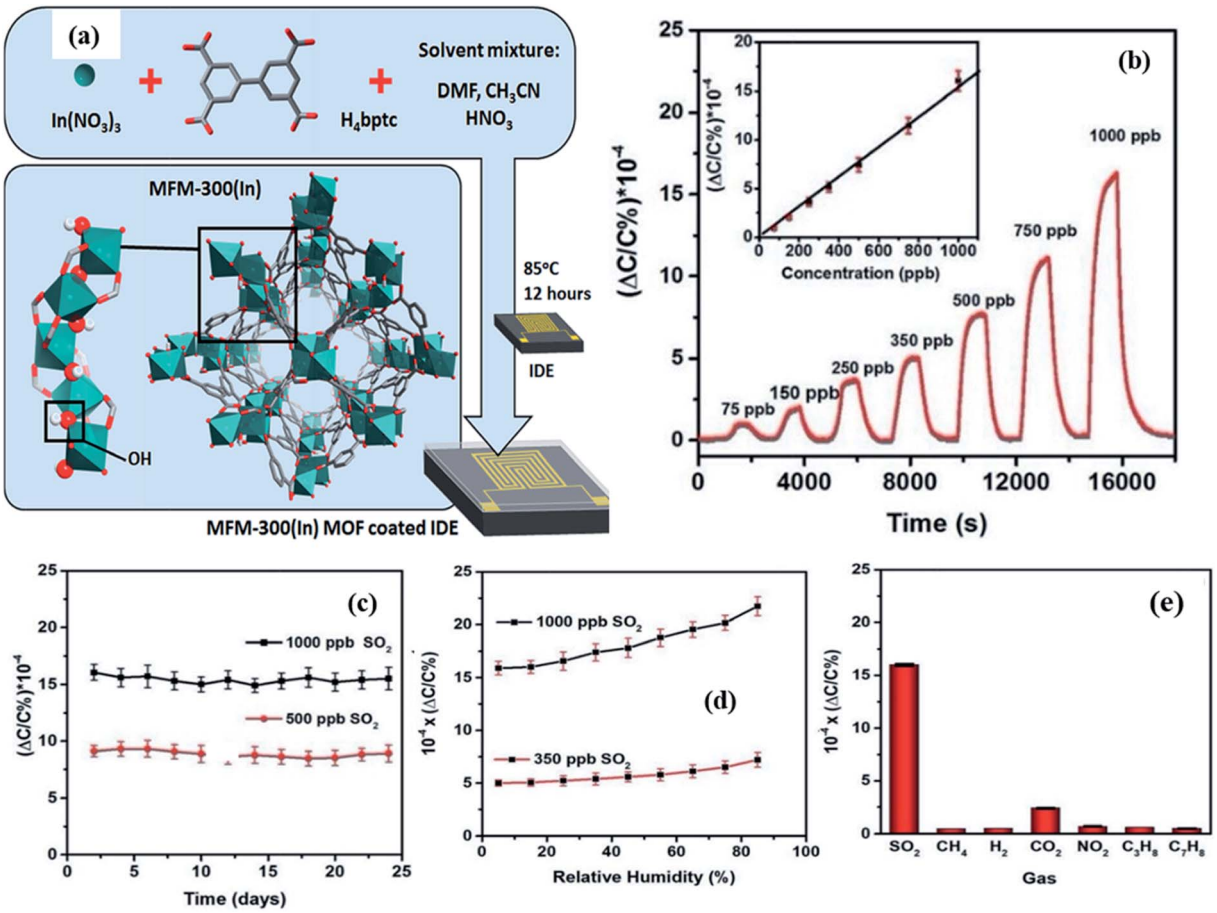

Fig. 18 (a) Schematic diagram of the structure of the MFM-300 (In) MOF grown on the IDE substrate, (b) capacitive sensing of SO_2 in different concentration ranges of SO_2 (75 to 1000 ppb), (c) long-term stability study of the MFM-300 (In) MOF-based sensor to 500 and 1000 ppb of SO_2 for 24 days, (d) effects of RH on the sensor performance of the MFM-300 (In) MOF, and (e) selectivity study of the MFM-300 (In) MOF sensor toward 1000 ppb of test gases. Reproduced from ref. 138 under the creative Commons Attribution-Non-Commercial 3.0 Unported Licence, copyright@2021, Royal Society of Chemistry.

sensors and the current advances of QCM-based electrical transducers for sensing properties towards the detection of environmentally hazardous and VOC gases. The sensing performances of MOF-based quartz crystal microbalance-based gas sensors are summarized in Table 4.

4.1 Applications of metal–organic framework quartz crystal microbalance based gas sensors

Zeolite-like imidazolate-based frameworks (ZIFs) have been widely used in many fields, including gas sensors, due to their high chemical and thermal stabilities.[149–151] For example, Salama and co-workers reported ZIF-8 materials and fabricated them as QCM based sensing platforms as a thin film.[152] They compared the sensing properties of ZIF-8 materials with IDE-based gas sensors for capacitive transduction. Different thicknesses and mass were varied in both electrodes. As compared to QCMs, the IDE capacitors showed higher sensitivity (1.3 and 1.4 $\times$ 10^{-5} per vol%) due to the larger change in the relative permittivity of acetone.[153] The effect of mass deposited on the IDE sand QCM substrates was studied. It was observed that the IDE capacitive substrates were highly sensitive towards acetone. The mass of adsorbed acetone on QCM substrates and the change in relative permittivity increased with increasing the amount of acetone vapor from 5.3 to 26.5 vol% with a nonlinear response. The stability of ZIF-8 materials in both transducers was favorable, with a stable response to acetone for 30 days.

In comparison to the above work, Zhang *et al.*[154] synthesized ZIF-8 (–CH_3 group) and ZIF-90 (–CHO group) polyhedron crystals by a facile biomimetic approach. The BET surface area of ZIF-8 was found to be 1020 m^2 g^{-1}, whereas, for ZIF-90, it was 730 m^2 g. The ZIF-90 based QCM sensor displayed excellent selectivity toward acetone gas compared to the ZIF-8 based QCM sensor with a stable baseline for all acetone concentrations, including fast response/recovery (12 s/17 s), good reversibility, and a frequency shift of 95 Hz/1 ppm. Also, the ZIF-90 based QCM sensors showed an increase of response with increasing the RH level up to 100%, including good stability of the sensor after 10 weeks. According to density functional theory (DFT) studies, the high acetone sensing properties could be ascribed to a greater number of hydrogen atoms in the –CHO group of ZIF-90 and a moderate adsorption enthalpy(ΔH^{θ}) between acetone molecules and ZIF-90.[155,156]

© 2022 The Author(s). Published by the Royal Society of Chemistry

Open Access Article. Published on 13 december 2021. Downloaded on 11. 11. 2024 14:01:32.
This article is licensed under a Creative Commons Attribution-NonCommercial 3.0 Unported Licence.

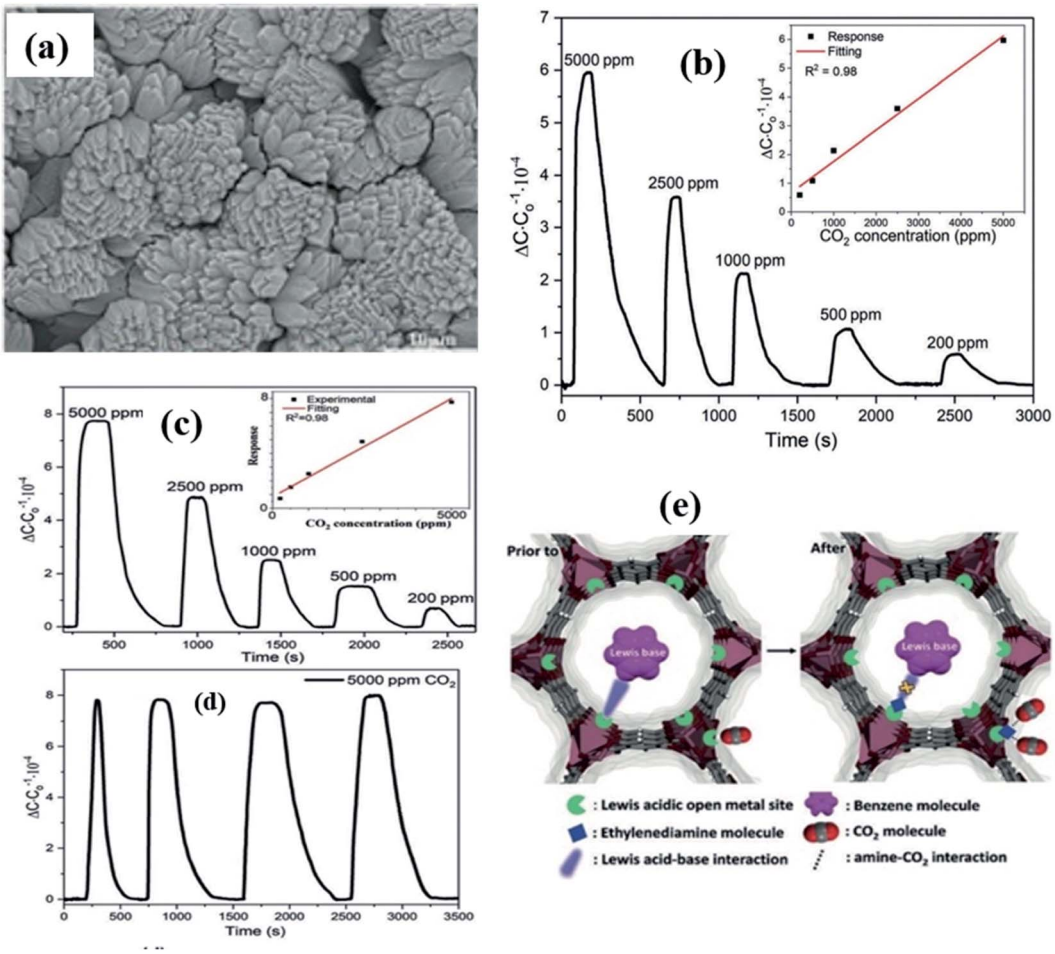

Fig. 19 (a) SEM image of the as grown Mg–MOF-74 on the IDE substrate, (b and c) capacitive response transients towards CO_2 at RT and after ethylenediamine-functionalization, (d) repeatability study of the ethylenediamine-functionalized Mg–MOF-74 sensor for 5000 ppm and (e) schematic diagram of the sensing mechanism of Mg–MOF-74. Reprinted from ref. 139, copyright@2021, John Wiley and Sons.

Zeinali *et al.*[157] reported a QCM gas sensor based on MIL-101(Cr) MOFs for formaldehyde gas sensing. MIL-101 (Cr) is built up with carboxylate ligands with numerous unsaturated Cr metal, which possess large surface area, giant pore volume, microporous windows (12 and 16 Å), and mesoporous cages (29 and 34 Å).[158] The synthesized MIL-101(Cr) MOF was fabricated as a gas sensing device by a drop-casting method. The response of the MIL-101(Cr) MOF sensor was found to be 6.3 Hz. The change of frequency can be defined as:

$$\Delta f = f - f_0 \quad (14)$$

Here, f is the frequency obtained in the test gas and f_0 is the frequency obtained in the presence of N_2 gas. The sensor demonstrates fast and short response/recovery time (15–69 s/58–170 s for 2–700 ppm of formaldehyde), a low detection limit of 1.79 ppm, excellent repeatability, high sensitivity of 1.67 Hz ppm^{-1} and selectivity towards formaldehyde, and LOD of 1.794 ppm. The sensing mechanism in this regard can be explained as follows. The sorption process, which is basically the interaction between the mass sensitive chemical sensor and analyte molecules, can take place in the form of hydrogen bonding (physisorption) or van-der-Waals interactions (chemisorption).[159] The MIL-101(Cr) MOF surface contains carboxylate groups which interact with formaldehyde gases through the weak C–H···O hydrogen bonding and O–H···O bond.[160] Due to the weak hydrogen bonding of the sensor, it shows a short recovery time, whereas the high diffusivity and faster molecular interactions through interconnected windows of the MIL-101(Cr) MOF sensor resulted in faster response time.

In contradiction to the above work, the same author has reported the use of the MIL-101 (Cr) MOF for QCM based gas sensing to detect different polar and non-polar VOCs with various functional groups except formaldehyde gas.[161] In this study, the highest response was found to be for pyridine with a LOD of 1.603 ppm and a high sensitivity of 2.793 Hz ppm^{-1} among other gases. For polar protic gas molecules, the sensitivity was in the order of 2-propanol > ethanol > methanol, which indicated that a larger molecular weight (MW) results in higher sensitivity,[162] whereas the sensitivity and frequency change for halomethanes were in the order of chloroform > dichloromethane due to the higher MW of chloroform despite the higher polarity of dichloromethane. On the other hand,

Open Access Article. Published on 13 december 2021. Downloaded on 11. 11. 2024 14:01:32.
This article is licensed under a Creative Commons Attribution-NonCommercial 3.0 Unported Licence.

Table 4 Summary of MOF materials for QCM and OFET based gas sensors

Gas sensing properties of MOF based QCM gas sensors

MOF materials	Target gas	Response (Hz)	Concentration (ppm)	Response time	LOD	Types of interactions between MOFs and gases	Ref.
ZIF-8	Acetone	1.4×10^{-5} ($\Delta f/f$%)	53 000 ppm	60 min	1300 ppm	NA	152
ZIF-8 (–CH_3 group)	Acetone	18 Hz	1 ppm	NA	NA	NA	154
ZIF-90 (–CHO group)	Acetone	95 Hz	1 ppm	12 s	13.7 ppb	Aldehyde group (–CHO) of ZIF-90 and acetone molecules	154
MIL-101(Cr) MOFs	Formaldehyde	6.3	2	15–69 s	1.794 ppm	C–H···O (hydrogen bond)–H···O	157
MIL-101(Cr) MOFs	Pyridine	17 Hz	5 ppm	7.67 s	1.603 ppm	Van der Waals interactions and π–π interaction with the MOF linker	161
MOF-14 (Cu (BTB	Benzene	1200 Hz	80	10 s	150 ppb	Steric hindrance effect and open metal sites	163

Gas sensing properties of MOF based OFET gas sensors

MOF materials	Target gas	Response (pF) or [$\Delta C/C$ (%)]	Concentration	Response time	LOD	Ref.
3D Ni (TiF_6) (TP_yP)]$_n$	NO_2	~18%	25 ppb	43 s	8.25 ppb	177
Diketopyrrolopyrrole (PDPP)	RDX	27.5 μA	NA	NA	NA	171

comparing 2-propanol and acetone, 2-propanol with a protic compound and –OH group forms a strong hydrogen bond with the sensing material, which resulted in high sensitivity. However, the highest sensitivity for pyridine among other gases was attributed to the lower vapor pressure and larger MW, and the strong π–π interaction between the aromatic rings.

A QCM platform-based sensor with a new type of MOF [MOF-14 (Cu (BTB)] was studied for benzene gas sensing properties.[163] The effects of the number of benzene rings in the ligands and changing the different types of central metal ions in the MOF were also evaluated to examine the sensing performance. The selectivity of benzene in a mixture of benzene, toluene and xylene (BTX) was achieved by controlling the pore size, which is dependent on the steric hindrance. Therefore, the authors compared their results with three other types of MOFs such as HKAUST-1 (Cu (BTC)), MOF-177 (Zn (BTB)), and MOF-74 [Mg (DOBDC)] (DOBDC; 2,5-dioxido-1,4-benzenedicarboxylate), respectively (as shown in Fig. 20a–d). The Langmuir surface areas of these synthesized materials were found to be in the range of 1521–1892 $m^3\ g^{-1}$. To evaluate their sensing properties, all the sensing materials were fabricated on QCM transducers. Among all the transducers, the MOF-14 modified QCM sensor exhibited the highest sensitivity (1200 Hz@80 ppm) (as shown in Fig. 20e) and high selectivity to benzene at RT with a low detection limit of 150 ppb in the presence of other various types of interfering gases (Fig. 20f). The sensor also showed reliable long-term stability and good cycling stability. It was found that the high selectivity and high response of MOF-14 towards benzene were attributed to the interaction between ligands and benzene molecules as well as the steric hindrance effect of the adsorption process. This work was based on the MOF-14 QCM sensor and showed the promising application and high-performance towards benzene sensing.

Tchalala *et al.*[164] reported a QCM based gas sensor by synthesizing isostructural fluorinated MOF KAUST-8 (AlFFIVE-1-Ni) and KAUST-7 (NbOFFIVE-1-Ni) with a pyrazine ligand solvothermal reaction for SO_2 sensing. The KAUST-7 MOF was prepared by mixing the Ni^{2+} salt with pyrazine ligands pillared with a square grid of $(AlF5(OH_2))^{2-}$, whereas the KAUST-8 MOF was obtained by pillaring Ni $(pyrazine)_2]^{2+}$ with a square grid $(NbOF_5)^{2-}$ pillar (as shown in Fig. 21a). Fig. 21d and e show the SEM images of the as-prepared AlFFIVE-1-Ni and NbOFFIVE-1-Ni MOFs and revealed that the morphologies of both samples were compact and uniform, and the particles were randomly oriented without any intergranular voids. The above prepared AlFFIVE-1-Ni and NbOFFIVE-1-Ni MOF materials were deposited onto QCM electrodes and unveiled the SO_2 sensing performance in the presence and absence of humidity. Fig. 21f shows the sensitivity of the as prepared MOFs tested towards SO_2 at 0–500 ppm. It can be seen that both sensors revealed a nonlinear response with increasing the SO_2 concentrations. Fig. 21g shows the frequency shifts of AlFFIVE-1-Ni and NbOFFIVE-1-Ni MOF sensors with respect to the 60% RH conditions. The results revealed that at 60% RH, the KAUST-7 sensor showed excellent sensitivity toward SO_2 as compared to KAUST-8 in the presence of humidity, which may be due to the affinity of SO_2 molecules to replace the water molecules.[165] Fig. 21h and i show the long-term stability and reproducibility studies towards SO_2 for 50, 100 and 157 ppm over 12 days.

5. Metal–organic frameworks for organic field-effect transistor-based gas sensors

Organic field-effect transistors (OFETs) are one of the types of electrical transducers with three-terminal electronic devices.

© 2022 The Author(s). Published by the Royal Society of Chemistry

Open Access Article. Published on 13 december 2021. Downloaded on 11. 11. 2024 14:01:32.
This article is licensed under a Creative Commons Attribution-NonCommercial 3.0 Unported Licence.

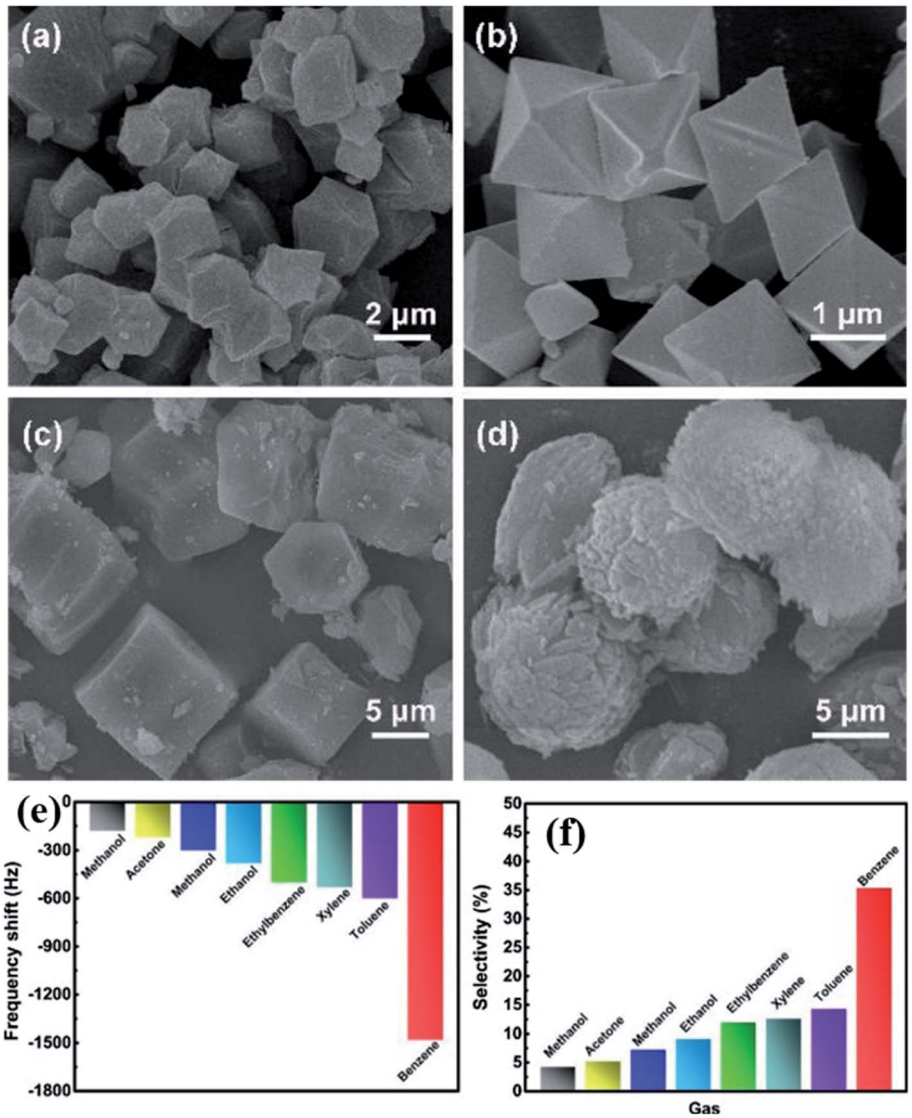

Fig. 20 FESEM images of the as prepared MOFs: (a) MOF-14, (b) HKAUST-1, (c) MOF-177, and (d) MOF-74, (e) response profile of the MOF-14-based QCM sensor towards different VOCs for 100 ppm benzene at 25C°C, and (f) selectivity study of the MOF-14-sensor in different interfering gases towards 100 ppm benzene at RT. Reproduced from ref. 163 with permission from Elsevier, copyright 2021.

Compared to their inorganic counterpart, OFET devices comprise organic semiconductors (OSCs) as active layers. FET-based gas sensors' major disadvantages are their high cost related to the materials fabrication and manufacturing process.[166] OFETs are currently one of the promising platforms for gas sensing applications due to their inherent advantageous attributes such as facile fabrication process, tunable properties of OSCs, low cost, low-power consumption, ability of low-operating temperature, device flexibility, ease of large-scale manufacturing, and compatibility with modern nano-fabrication technologies.[167,168] OSC materials are endowed with superior characteristics in terms of the design of lightweight materials, mechanical and substrate flexibility, controllable molecular structure, tunable physicochemical properties *via* precise organic synthesis, and functionalization for the improvement of sensing performances. Over the past few decades, much research effort in the design of high performance OFET gas sensors has been carried out for various fields such as the detection of VOCs and toxic gases, detection of explosives, disease diagnostics, wearable sensors, *etc.*169–174 The sensing performances of MOF based organic field-effect transistor based gas sensors are summarized in Table 4.

5.1 Applications of metal–organic framework based organic field-effect transistor gas sensors

Until now, OFET based gas sensors have been used for detection of various gases and each gas molecules display unique response characteristics when exposed to OFET devices. However, limited research has been reported on MOF-based OFET gas sensors.[167,171,174–176] Recently, Yuvraj *et al.*[177] reported a novel and highly sensitive and selective OFET-based transducer for NO_2 gas sensing. They designed an OFET platform

Open Access Article. Published on 13 december 2021. Downloaded on 11. 11. 2024 14:01:32.
This article is licensed under a Creative Commons Attribution-NonCommercial 3.0 Unported Licence.

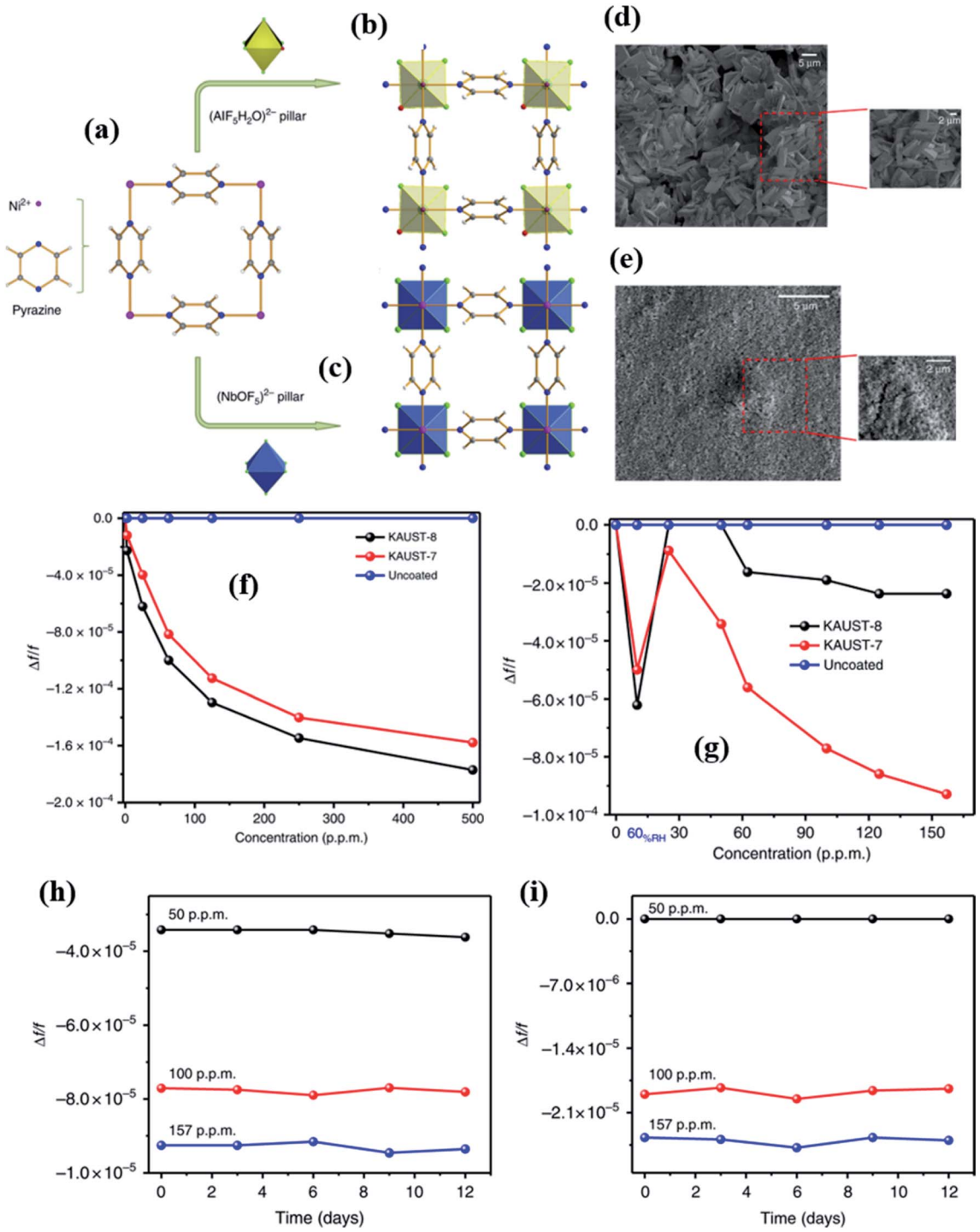

Fig. 21 (a) mixing of Ni^{2+} and pyrazine to form the Ni $(pyrazine)_2]^{2+}$ complex, (b and c) the schematic diagram of KAUST-8 and KAUST-7, (d and e) FESEM images of KAUST-7 and KAUST-8 thin films coated on the QCM electrode, (f) QCM based response study of both sensors towards SO_2 gas, (g) response study of both sensors towards SO_2 gas at 60% RH, and (h and i) long-term stability and reproducibility studies towards SO_2 for 50, 100 and 157 ppm over 12 days. Reproduced from ref. 164, copyright 2021@Nature, Creative Commons Attribution 4.0 International License.

utilizing a highly sensitive receptor layer of porous 3D MOF [Ni (TiF_6) (TPyP)]$_n$ an isostructural to fluorinated MOF combined with an organic semiconductor of PDVT-10 (as shown in Fig. 22a). It was unveiled that sensitivity toward the NO_2 analyte exhibited an unprecedented 700% increase (sensitivity of 680 nA/ppb) in contrast to the pristine PDVT-10 (Fig. 22b). It also showed an excellent detection limit with a remarkable LOD of 8.25 ppb (Fig. 22c and d), and high stability for a period of 6 months. Under humid conditions of 5%–90%, a negligible response of 4.232 nA was demonstrated. Moreover, the confined

© 2022 The Author(s). Published by the Royal Society of Chemistry

Open Access Article. Published on 13 december 2021. Downloaded on 11. 11. 2024 14:01:32.
This article is licensed under a Creative Commons Attribution-NonCommercial 3.0 Unported Licence.

space/pores in the [Ni (TPyP)(TiF_6)]$_n$ MOF led to stronger interaction of the NO_2 gas with the MOF (Fig. 22e) compared to other gases. The NO_2 molecules absorb electrons from the polymer due to its electrophilic nature, causing holes. The concentration of holes in PDVT-10 was also increased by the MOF as it attracts electrons due to the high electron affinity of the MOF material. As a result, the sensitivity to NO_2 was enhanced.

Yuvaraja *et al.* further approached a quantitative analysis with the help of an OFET-based integrated circuit to advance the NO_2 detection mechanism.[173] Initially, a spin coating method was applied to deposit the PDVT-10 OSC layer onto the sensor electrode followed by the drop casting of the porous 3D MOF layer to prepare the OFET device. Fig. 22a shows the schematic diagram of the preparation of the [Ni (TPyP)(TiF_6)]$_n$ MOF. Fig. 22b shows the SEM images of MOF-A [Ni(TPyP)(TiF_6)]$_n$. Both the pristine PDVT-10 sensor (device-1) and PDVT-10/MOF (device-2) OFET sensor were embedded into the integrated system. The as-prepared PDVT-10/MOF OFET sensor showed excellent sensitivity compared to pristine PDVT-10 alone.

Diketopyrrolopyrrole (DPP) based donor–acceptor OSCs have also shown great promise for various organic electronic device applications.[175,176,178,179] Surya *et al.*[171] demonstrated an explosive OFET-based gas sensor made from a composite of organic polymer-based material diketopyrrolopyrrole (PDPP) with thienylene–vinylene–thienylene (TVT), and MOF with a BGBC device structure. They studied their sensing characteristics towards the detection of 1,3,5-trinitro-1,3,5-triazacyclohexane (RDX) and 2,4,6-trinitrotoluene (TNT), which are nitro based explosive compounds. The role of the MOF was as a receptor

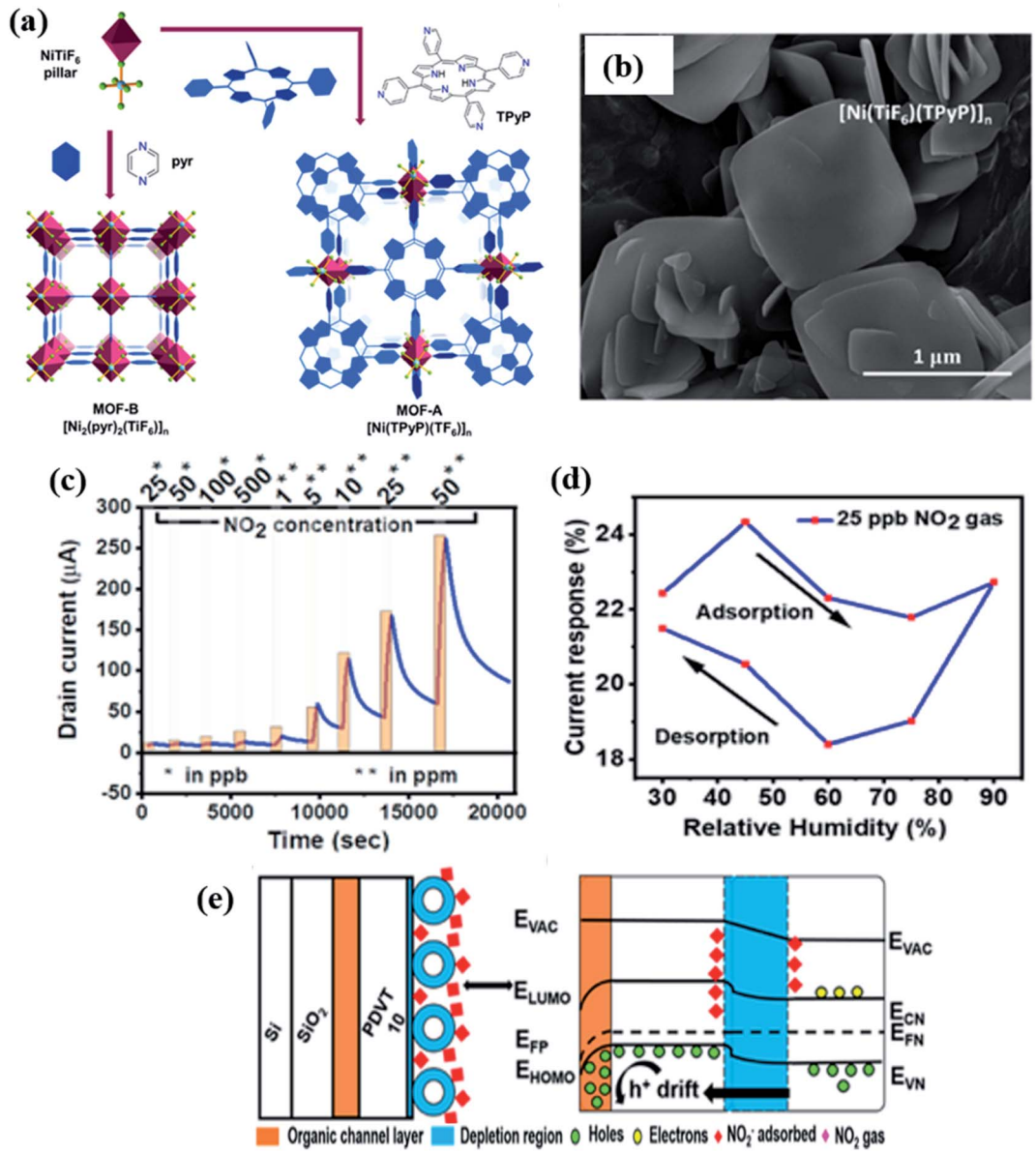

Fig. 22 (a) Schematic diagram of the preparation of the [Ni (TPyP)(TiF_6)]$_n$ MOF, (b) SEM images of MOF-A [Ni(TPyP)(TiF_6)]$_n$, (c) sensing properties towards NO_2 gas, (d) humidity effect of the OFET gas sensor, and (e) sensing mechanism of PVDT-10 and MOF based OFET sensors.[177]

© 2022 The Author(s). Published by the Royal Society of Chemistry

Open Access Article. Published on 13 december 2021. Downloaded on 11. 11. 2024 14:01:32.
This article is licensed under a Creative Commons Attribution-NonCommercial 3.0 Unported Licence.

layer. In contrast, PDPP-TVT used a conducting channel layer between the source and drain electrodes due to its better charge transporting properties. Also, the sensitivity of the sensor obtained was 1.7 μA for TNT, whereas it was 27.5 μA for RDX at RT. The OFET device made from PDPP-TVT and the MOF composite showed excellent stability over 35 days. The authors attributed the sensing mechanism to (1) the electrophilic nature of NO_2 molecules, (2) the drifting of the free holes (generated by NO_2 adsorption) towards the SiO_2 and DPP interface and subsequent channel current increase.

6. Summary

The growing demand for sensing materials with high sensitivity, selectivity, low power consumption, and robustness has propelled the active research in gas sensors. In this review article, we have thoroughly reviewed the recent advancements on MOF materials for various electrical transducers based on different principles. In particular, we have focused on various gas sensors based on chemiresistive, capacitive, QCM, and OFET based gas sensors. We systematically discussed MOF-based state-of-the-art materials and their different techniques to integrate with the aforementioned sensing devices to realize enhanced gas sensors. Their sensing mechanism is assessed based on different engineered materials derived from pristine MOFs and their composites for the detection of various toxic (H_2S, SO_2, NH_3, CO, NO_2, CO_2, trimethylamine, *etc.*) and VOCs (acetone, ethanol, methanol, formaldehyde, toluene, methyl benzenes, *etc.*). Also, the advantages and disadvantages of all the four types of electrically transduced gas sensors are summarized in Table 5.

Before the gas sensing measurement, the synthesis of MOFs and their fabrication of reliable gas sensing devices are important steps for gas sensing applications. Different types of MOFs (Cu–MOFs, Co–MOFs, Sn–MOFs, In–MOFs, Cu–BDC MOFs, ZIFs, Zn–MOFs, Al–MOFs, Ni–MOFs, Zr–MOFs, *etc.*) have been synthesized and integrated onto several transducers for the optimization of their sensing properties. Several synthetic methods have been employed to prepare high performance sensing materials. Pristine MOFs have been synthesized by the self-template method, which does not need a surfactant, a carbon source and other organic additives, and thus has advantages for large scale synthesis. The sacrificial template method and high-temperature solvothermal method have been used to synthesize MOFs. A direct calcination method is an easy approach to synthesize metal-oxide materials from the pristine MOFs. Also, self-pyrolysis methods using MOFs as a template have been employed to prepare MOF derived MOXs, which inherits the morphology and surface area of pristine MOFs. Several other techniques such as hydrothermal, solvothermal, electrospinning, spray-pyrolysis, *etc.* have been employed to prepare pristine and composite materials. The surfaces of MOFs were further catalytically functionalized *via* impregnation and chemical reduction methods. The growth of compact and homogeneous sensing films on the sensing device electrodes has remained a challenge. Different approaches have been carried out to fabricate sensing devices for different transducer gas sensors. Techniques such as drop casting and screen-

Table 5 Summary of advantages and disadvantages of different transducer gas sensors listed in the article

Transducers	Principle	Advantages	Disadvantages
MOX based chemiresistive sensors	Change of conductivity/resistance	High sensitivity quick response/recovery; portable; low cost; miniaturization; integration of integrated circuits (IC); sensor arrays/e-nose; commercially available sensors; ppb level detection limit	High operating temperature; require a heater; Complexity in device integration; high power consumption; sensitive to humidity; poor selectivity; limited sensing range; poor precision; sulfur and weak acid poisoning
Capacitive gas sensors	Change of capacitance	High sensitivity; low temperature operation; quick response/recovery; miniaturization; low power; portable; cheap; high precision; low detection limit; simple steps of modifying MOFs on the QCM	High cross sensitivity; sensitive to humidity and temperature; sensor life is limited
QCM gas sensors	Change of frequency	High sensitivity; low temperature operation; portable; low power consumption; short response time; LOD@ppb level; humidity sensing in an ultra-wide range; simple steps of modifying MOFs on the QCM	High device cost; instability; frequency dependent; poor precision; poor mechanical flexibility; sensitive to humidity and temperature; not commercially available; poor long-term stability, poor reproducibility
OFET gas sensors	Change of current/voltages	Device flexibility, low temperature operation; compatibility with CMOS technology, cost effective; low power consumption; simple electronic interface; real-time processability	Core semiconductor materials are yet to be made for high-speed switching; requires high mobility; subthreshold swing of lower values

© 2022 The Author(s). Published by the Royal Society of Chemistry

Open Access Article. Published on 13 december 2021. Downloaded on 11. 11. 2024 14:01:32.
This article is licensed under a Creative Commons Attribution-NonCommercial 3.0 Unported Licence.

printing method have been used by most of the researchers due to their simplicity in the fabrication of devices. The IDE substrate electrodes have been used both for chemirestive and capacitive gas sensing devices. On the other hand, QCM and FET based electrodes have been used for the preparation of QCM gas sensors and OFET based gas sensors. Liquid phase epitaxial growth techniques and the *in situ* solvothermal method have been used to grow sensing materials as thin films on the IDE substrate using carboxylic acid-self-assembled monolayers (SAMs). This approach simplifies the multistep synthesis of MOFs and subsequent construction of sensing devices. Another thin film technique named the Langmuir–Blodget technique has been used to deposit sensing materials on the sensing device directly without using any SAM layers. The problems associated with different deposition techniques have been discussed in the following section.

Chemiresistive gas sensors based on pristine MOFs with conductive behaviors have been researched due to their low conductivity or insulating behavior at RT. The metal active sites, pores, different functional and hydroxyl groups of MOF materials play a great role in adsorbing different gas molecules. MOFs display selectivity for different gases due to the varied diameters and chemical properties of the molecules towards different gases. The recent advances in conductive MOFs with excellent porosity and detection ability towards low concentration gas vapors at RT have triggered tremendous research attention in this area. In addition, the pristine MOFs have been used as a host material to design hybrid materials by combining them with conductive carbon materials. Chemiresistive gas sensors based on MOF–metal oxide materials have also been discussed. Further progress was made by combining MOF derived metal-oxide nanostructures with other secondary components such as 2D nanomaterials, organic polymers, noble metal NPs, and carbon materials (rGO) to design novel hybrid materials. Various factors such as humidity interference, effect of the construction of composite structures, and effect of noble metal NPs have been discussed. The poor conductivity of MOFs is taken as an advantage to synthesize highly porous diverse nanostructures for high sensing performance. The metal oxides derived from pristine MOFs have shown excellent sensing results without compromising any structural and morphological changes.

In comparison to MOF derived metal oxide-based gas sensors, capacitive, QCM and OFET based transducers have been used as gas sensors. One of the major advantages of these MOF-based transducers over the standard MOX sensors is the ability to detect gases at RT. Thanks to their remarkable porosity and unique functional groups, MOF-based capacitive and QCM sensors have been investigated in a variety of gas sensing applications. The high sensitivity, low response time, and low detection limit at the ppb level of MOF-based capacitive and QCM sensors make them superior sensing materials. Furthermore, MOF-based capacitive and QCM sensors can detect humidity across an extremely wide range. Organic semiconductors are currently emerging as a new generation of electronic devices due to their low power consumption and low cost since they operate at RT. OFET based sensors are endowed with excellent properties of flexibility and lightweight. Despite the outstanding detecting capability of these above MOF-based sensors, there are still challenges to overcome before these sensors are used in real-time applications.

One of the most important parameters of gas sensors is to improve the selectivity of a specific gas with similar sensing reactivity. The selection of functional groups in organic ligands during the design of MOFs plays a great role in the selectivity of MOF-based electrically transduced gas sensors. Basic functional groups (–OH and $–NH_2$) have shown high selectivity towards acidic gases. Also, the strong interactions between gas molecules and the framework of organic ligands result in the high selectivity. Other than the organic ligands and functional groups, the selectivity can be controlled by tuning the kinetic molecular diameter of the gas molecules. Generally, CuO based materials derived from the Cu-MOFs show high selectivity to H_2S gas due to the formation of CuS, which acts as a metal catalyst. Similarly, loading a small amount of Ag NP catalysts can enhance the selectivity for H_2S, although having different functional group-based MOFs (UiO-66 (Zr)–NO_2, and UiO-66 (Zr)–N_3). Also, electrostatic interaction, hydrogen bonding, open metal sites of MOFs, high dipole moment of gas molecules, steric hindrance, and π–π aromatic ring of ligands are responsible for the possible sensing mechanism and selectivity. In many studies, the selectivity to a specific gas among other interfering gases has been attributed to the bond energy differences in different gases. The lower the bond energy of a gas molecule, the easier it is to break and participate in the gas sensing reaction. MOFs have been utilized as filters to block the passage of other interfering gas molecules, thus designing and controlling the selectivity properties.

7. Challenges and perspectives

When compared to other sensing materials, pristine MOFs should show a higher response with greater stability and reproducibility. Furthermore, the selectivity of pristine MOF-based chemiresistors should be expanded to a variety of analytes. In our opinion, the use of catalysts in conductive MOFs can improve the sensitivity of pure-MOF-based sensors. Despite the outstanding contribution of metal oxide-based gas sensors towards sensing different VOCs and toxic gases, they show poor sensing performance at RT, limiting their practical applications. High operating temperature for gas sensing further complicates the sensing system and poses challenges with regard to stability and cross-selectivity as well as difficulty to use in highly flammable places. On the other hand, MOX-based sensors have a fast response/recovery time, but their selectivity and water stability are poor. Also, MOF-derived MOXs with carbon composites have some drawbacks such as poor response, stability, and low selectivity. Therefore, in MOF derived materials, the use of single-atom catalysts and bimetallic catalysts or construction of heterogeneous nanostructures are highly anticipated to improve their sensing properties. With careful optimization of the structure, morphology, composition, and controlled arrangement of metal-catalysts on MOFs, unique qualities are expected to boost their sensing performance.

© 2022 The Author(s). Published by the Royal Society of Chemistry

Open Access Article. Published on 13 december 2021. Downloaded on 11. 11. 2024 14:01:32.
This article is licensed under a Creative Commons Attribution-NonCommercial 3.0 Unported Licence.

For MOF as filters or sieving materials, simple and reliable deposition procedures should be devised to produce uniform and homogeneous coverage of different MOF layers on sensing materials with a controlled pore size and minimal disruption of active sites. The traditional drop-casting method is utilized to mix MOF materials with electrodes, which results in unsatisfactory sensor performance due to the uncontrolled film thickness.

OFETs with organic materials as the semiconducting layer have proved to be excellent sensors in gas detection. The use of functional groups to change OSCs is a successful technique for improving selectivity; however, mass production is still an issue. More gas analytes and OSC materials should be introduced to expand the sensing database, thereby understanding the sensing mechanism. As a result, greater efforts are needed to focus on cutting-edge solutions. The sensor array integration of the above transducers can assess complicated analytes and is a promising future area. Despite the wide variety of sensing properties of MOF-based gas sensors, they are yet to be commercially marketed. More research should be focused on the deployment of other thin film deposition techniques such as spin coating, the layer-by-layer assembly, and the Langmuir–Blodgett techniques, which are used to generate facile, well-ordered, homogeneous, and robust MOF films on the sensing electrodes to overcome the unsatisfactory sensor performance due to the uncontrolled film thickness. The integration of MOF materials with advanced flexible/wearable substrates, as well as device stability in the long-term test, should be the focus of future research. An e-nose is a powerful technique to detect and quantify a wide range of gases using gas-sensor arrays and pattern recognition. It is a portable and low-cost technique that outperforms chromatography and mass-spectrometry systems in terms of sensitivity, selectivity, and stability. E-noses with advanced MOF materials would be advantageous over metal-oxide sensing systems, which consume more power. The e-nose, which integrates sensing and signal-processing capabilities by utilizing appropriate pattern-recognition algorithms, can replace large arrays of individual MOF-based gas sensors in a single device. More sensitive, selective, and stable gas sensors based on innovative MOF-based materials are expected to be developed in the future, potentially opening up a new frontier in gas sensing technology.

Author contributions

S. M. Majhi: idea, review writing, editing; A. Ali, P. Rai, and S. Surya: review writing, editing; Y. E. Greish, N. Qamhieh, and S. T. Mahmoud: funding, supervision, concept; A. Alzamly: review writing, guidance, editing.

Conflicts of interest

There is no conflict of interest.

Acknowledgements

The authors gratefully acknowledge the financial support from the United Arab Emirates University through Grant Code-G00003453 with fund code: 12R003-ZCHS-3-2020 and Grant Code-USRP-G00003232 with fund code: 31R238/activity code R238M4.

References

1 G. F. Fine, L. M. Cavanagh, A. Afonja and R. Binions, *Sensors*, 2010, **10**(6), 5469–5502.
2 D. Kohl, *J. Phys. D: Appl. Phys.*, 2001, **34**(19), R125.
3 J. Van den Broek, I. C. Weber, A. T. Güntner and S. E. Pratsinis, *Mater. Horiz.*, 2020, **8**, 661–684.
4 S. S. Varghese, S. Lonkar, K. Singh, S. Swaminathan and A. Abdala, *Sens. Actuators, B*, 2015, **218**, 160–183.
5 J. Zhang, Z. Qin, D. Zeng and C. Xie, *Phys. Chem. Chem. Phys.*, 2017, **19**(9), 6313–6329.
6 H. Wang, W. P. Lustig and J. Li, *Chem. Soc. Rev.*, 2018, **47**(13), 4729–4756.
7 C. Zhang, Y. Luo, J. Xu and M. Debliquy, *Sens. Actuators, A*, 2019, **289**, 118–133.
8 S. Das and M. Pal, *J. Electrochem. Soc.*, 2020, **167**(3), 037562.
9 Y. Wang, L. Duan, Z. Deng and J. Liao, *Sensors*, 2020, **20**(23), 6781.
10 Z. Meng, R. M. Stolz, L. Mendecki and K. A. Mirica, *Chem. Rev.*, 2019, **119**(1), 478–598.
11 B. G. Yacobi, *Semiconductor materials: an introduction to basic principles*, Springer, 2003.
12 S. Marco and A. Gutierrez-Galvez, *IEEE Sens. J.*, 2012, **12**(11), 3189–3214.
13 S. M. Majhi, A. Mirzaei, H. W. Kim and S. S. Kim, *Sensors*, 2021, **21**(4), 1352.
14 S. Navale, M. Shahbaz, S. M. Majhi, A. Mirzaei, H.-W. Kim and S.-S. Kim, *Chemosensors*, 2021, **9**(6), 127.
15 B. Sowmya, A. John and P. Panda, *Sensors International*, 2021, **2**, 100085.
16 S. Yuvaraja, V. N. Bhyranalyar, S. A. Bhat, M. T. Vijjapu, S. G. Surya, C. V. Yelamaggad and K. N. Salama, *Adv. Electron. Mater.*, 2021, **7**, 2000853.
17 A. Kaushik, R. Kumar, S. K. Arya, M. Nair, B. Malhotra and S. Bhansali, *Chem. Rev.*, 2015, **115**(11), 4571–4606.
18 V. Balasubramani, S. Chandraleka, T. S. Rao, R. Sasikumar, M. Kuppusamy and T. Sridhar, *J. Electrochem. Soc.*, 2020, **167**(3), 037572.
19 N. Joshi, T. Hayasaka, Y. Liu, H. Liu, O. N. Oliveira Jr and L. Lin, *Microchim. Acta*, 2018, **185**, 213.
20 W. Yuan, K. Yang, H. Peng, F. Li and F. Yin, *J. Mater. Chem. A*, 2018, **6**(37), 18116–18124.
21 B. Sharma and J. S. Kim, *Sci. Rep.*, 2018, **8**, 5902.
22 N. B. Tiscione, D. T. Yeatman, X. Shan and J. H. Kahl, *J. Anal. Toxicol.*, 2013, **37**(8), 573–579.
23 S. Pang, T. Yang and L. He, *TrAC, Trends Anal. Chem.*, 2016, **85**, 73–82.
24 F. Biasioli, C. Yeretzian, T. D. Mark, J. Dewulf and H. V. Langenhove, *TrAC, Trends Anal. Chem.*, 2011, **30**(7), 1003–1017.
25 L. N. Plummer, E. Busenberg, S. M. Eberts, L. M. Bexfield, C. J. Brown, L. S. Fahlquist, B. G. Katz and M. K. Landon, *Journal of Hydrologic Engineering*, 2008, **13**(11), 1049–1068.

© 2022 The Author(s). Published by the Royal Society of Chemistry

Open Access Article. Published on 13 december 2021. Downloaded on 11. 11. 2024 14:01:32.
This article is licensed under a Creative Commons Attribution-NonCommercial 3.0 Unported Licence.

26 E. A. Hogendoorn, High-Performance Liquid Chromatography Methods in Pesticide Residue Analysis, in *Encyclopedia of Analytical Chemistry*, ed. R. A. Meyers and A. Di-Corcia, Wiley, 2006.
27 P. Kumar, A. Deep, K. H. Kim and R. J. Brown, *Prog. Polym. Sci.*, 2015, **45**, 102–118.
28 M.-S. Yao, W.-H. Li and G. Xu, *Coord. Chem. Rev.*, 2021, **426**, 213479.
29 W.-T. Koo, J.-S. Jang and I.-D. Kim, *Chem*, 2019, **5**(8), 1938–1963.
30 H. Li, M. Eddaoudi, M. O'Keeffe and O. M. Yaghi, *Nature*, 1999, **402**(6759), 276–279.
31 O. M. Yaghi, G. Li and H. Li, *Nature*, 1995, **378**(6558), 703–706.
32 H. Furukawa, K. E. Cordova, M. O'Keeffe and O. M. Yaghi, *Science*, 2013, **341**(6149), 1230444.
33 O. K. Farha, I. Eryazici, N. C. Jeong, B. G. Hauser, C. E. Wilmer, A. A. Sarjeant, R. Q. Snurr, S. T. Nguyen, A. O. z. r. Yazaydın and J. T. Hupp, *J. Am. Chem. Soc.*, 2012, **134**(36), 15016–15021.
34 P. Kumar, K.-H. Kim, P. K. Mehta, L. Ge and G. Lisak, *Crit. Rev. Environ. Sci. Technol.*, 20219, **49**(21), 2016–2048.
35 P. Kumar, E. Vejerano, A. Khan, G. Lisak, J. H. Ahn and K.-H. Kim, *Korean J. Chem. Eng.*, 2019, **36**(11), 1839–1853.
36 Y. Chen, J. Li, G. Yue and X. Luo, *Nano-Micro Lett.*, 2017, **9**(3), 32.
37 F. L. i Xamena, O. Casanova, R. G. Tailleur, H. Garcia and A. Corma, *J. Catal.*, 2008, **255**(2), 220–227.
38 L. Meng, Q. Cheng, C. Kim, W. Y. Gao, L. Wojtas, Y. S. Chen, M. J. Zaworotko, X. P. Zhang and S. Ma, *Angew. Chem.*, 2012, **124**(40), 10229–10232.
39 D. Alezi, Y. Belmabkhout, M. Suyetin, P. M. Bhatt, Ł. J. Weseliński, V. Solovyeva, K. Adil, I. Spanopoulos, P. N. Trikalitis and A.-H. Emwas, *J. Am. Chem. Soc.*, 2015, **137**(41), 13308–13318.
40 T. Rodenas, I. Luz, G. Prieto, B. Seoane, H. Miro, A. Corma, F. Kapteijn, F. X. L. i Xamena and J. Gascon, *Nat. Mater.*, 2015, **14**(1), 48–55.
41 C. Dong and L. Xu, *ACS Appl. Mater. Interfaces*, 2017, **9**(8), 7160–7168.
42 X. Zhang, A. Chen, M. Zhong, Z. Zhang, X. Zhang, Z. Zhou and X.-H. Bu, *Electrochem. Energy Rev.*, 2019, **2**(1), 29–104.
43 T. Qiu, Z. Liang, W. Guo, H. Tabassum, S. Gao and R. Zou, *ACS Energy Lett.*, 2020, **5**(2), 520–532.
44 Z. Hu, B. J. Deibert and J. Li, *Chem. Soc. Rev.*, 2014, **43**(16), 5815–5840.
45 L. E. Kreno, K. Leong, O. K. Farha, M. Allendorf, R. P. Van Duyne and J. T. Hupp, *Chem. Rev.*, 2012, **112**(2), 1105–1125.
46 M. Ma, Y. Bi, Z. Tong, Y. Liu, P. Lyu, R. Wang, Y. Ma, G. Wu, Z. Liao and Y. Chen, *RSC Adv.*, 2021, **11**(27), 16572–16591.
47 B. Yan, *J. Mater. Chem. C*, 2019, **7**(27), 8155–8175.
48 A. Karmakar, P. Samanta, A. V. Desai and S. K. Ghosh, *Acc. Chem. Res.*, 2017, **50**(10), 2457–2469.
49 J. V. Alegre-Requena, E. Marqués-López, R. P. Herrera and D. D. Díaz, *CrystEngComm*, 2016, **18**(22), 3985–3995.
50 C. Arul, K. Moulaee, N. Donato, D. Iannazzo, N. Lavanya, G. Neri and C. Sekar, *Sens. Actuators, B*, 2021, **329**, 129053.
51 F.-Y. Yi, D. Chen, M.-K. Wu, L. Han and H.-L. Jiang, *ChemPlusChem*, 2016, **81**, 675–690.
52 K. Vikrant, V. Kumar, Y. S. Ok, K.-H. Kim and A. Deep, *Trends Anal. Chem.*, 2018, **105**, 263–281.
53 P. kumar, K.-H. Kim, S. Rarotra, L. Ge and G. Lisak, *Trends Anal. Chem.*, 2020, **122**, 115730.
54 P. Kumar, K.-H. Kim, J. Lee, J. Shang, M. I. Khazi, N. Kumar and G. Lisak, *J. Ind. Eng. Chem.*, 2020, **84**, 87–95.
55 X. Fang, B. Zong and S. Mao, *Nano-Micro Lett.*, 2018, **10**(4), 1–19.
56 M. Wagner, K.-Y. Andrew Lin, W.-D. Oh and G. Lisak, *J. Hazard. Mater.*, 2021, **413**, 125325.
57 T. C. Narayan, T. Miyakai, S. Seki and M. Dincă, *J. Am. Chem. Soc.*, 2012, **134**(31), 12932–12935.
58 Y. Kobayashi, B. Jacobs, M. D. Allendorf and J. R. Long, *Chem. Mater.*, 2010, **22**(14), 4120–4122.
59 L. Sun, M. G. Campbell and M. Dincă, *Angew. Chem., Int. Ed.*, 2016, **55**(11), 3566–3579.
60 E.-X. Chen, H. Yang and J. Zhang, *Inorg. Chem.*, 2014, **53**(11), 5411–5413.
61 E.-X. Chen, H.-R. Fu, R. Lin, Y.-X. Tan and J. Zhang, *ACS Appl. Mater. Interfaces*, 2014, **6**(24), 22871–22875.
62 J.-H. Lee, T.-B. Nguyen, D.-K. Nguyen, J.-H. Kim, J.-Y. Kim, B. T. Phan and S. S. Kim, *Sensors*, 2019, **19**(15), 3323.
63 M. E. DMello, N. G. Sundaram, A. Singh, A. K. Singh and S. B. Kalidindi, *Chem. Commun.*, 2019, **55**(3), 349–352.
64 G.-Y. Lee, J. Lee, H. T. Vo, S. Kim, H. Lee and T. Park, *Sci. Rep.*, 2017, **7**(1), 1–10.
65 M. G. Campbell, D. Sheberla, S. F. Liu, T. M. Swager and M. Dincă, *Angew. Chem., Int. Ed.*, 2015, **54**(14), 4349–4352.
66 B. Zhao, J. Zhang, W. Feng, Y. Yao and Z. Yang, *Phys. Rev. B: Condens. Matter Mater. Phys.*, 2014, **90**(20), 201403.
67 M. G. Campbell, S. F. Liu, T. M. Swager and M. Dincă, *J. Am. Chem. Soc.*, 2015, **137**(43), 13780–13783.
68 U. Lange and V. M. Mirsky, *Anal. Chim. Acta*, 2011, **687**(2), 105–113.
69 M. K. Smith, K. E. Jensen, P. A. Pivak and K. A. Mirica, *Chem. Mater.*, 2016, **28**(15), 5264–5268.
70 M. S. Yao, X. J. Lv, Z. H. Fu, W. H. Li, W. H. Deng, G. D. Wu and G. Xu, *Angew. Chem.*, 2017, **129**(52), 16737–16741.
71 A. J. M. Reddy, N. Katari, P. Nagaraju and S. M. Surya, *Mater. Chem. Phys.*, 2020, **241**, 122357.
72 C. S. Rout, M. Hegde, A. Govindaraj and C. Rao, *Nanotechnology*, 2007, **18**(20), 205504.
73 M. Gomaa, G. RezaYazdi, M. Rodner, G. Greczynski, M. Boshta, M. Osman, V. Khranovskyy, J. Eriksson and R. Yakimova, *J. Mater. Sci.: Mater. Electron.*, 2018, **29**(14), 11870–11877.
74 A. A. Talin, A. Centrone, A. C. Ford, M. E. Foster, V. Stavila, P. Haney, R. A. Kinney, V. Szalai, F. El Gabaly and H. P. Yoon, *Science*, 2014, **343**(6166), 66–69.
75 A. Ali, A. Alzamly, Y. E. Greish, M. Bakiro, H. L. Nguyen and S. T. Mahmoud, *ACS Omega*, 2021, **6**(27), 17690–17697.
76 W. Kleist, M. Maciejewski and A. Baiker, *Thermochim. Acta*, 2010, **499**(1–2), 71–78.
77 R. R. Salunkhe, Y. V. Kaneti and Y. Yamauchi, *ACS Nano*, 2017, **11**(6), 5293–5308.

Open Access Article. Published on 13 december 2021. Downloaded on 11. 11. 2024 14:01:32.
This article is licensed under a Creative Commons Attribution-NonCommercial 3.0 Unported Licence.

78 Y. V. Kaneti, S. Dutta, M. S. Hossain, M. J. Shiddiky, K. L. Tung, F. K. Shieh, C. K. Tsung, K. C. W. Wu and Y. Yamauchi, *Adv. Mater.*, 2017, **29**(38), 1700213.
79 X. Wu, S. Xiong, Y. Gong, Y. Gong, W. Wu, Z. Mao, Q. Liu, S. Hu and X. Long, *Sens. Actuators, B*, 2019, **292**, 32–39.
80 H. He, R. Li, Z. Yang, L. Chai, L. Jin, S. I. Alhassan, L. Ren, H. Wang and L. Huang, *Catal. Today*, 2020, **375**, 10–29.
81 R. Zhang, T. Zhou, L. Wang and T. Zhang, *ACS Appl. Mater. Interfaces*, 2018, **10**(11), 9765–9773.
82 Y. Lü, W. Zhan, Y. He, Y. Wang, X. Kong, Q. Kuang, Z. Xie and L. Zheng, *ACS Appl. Mater. Interfaces*, 2014, **6**(6), 4186–4195.
83 W. Zhou, Y.-P. Wu, J. Zhao, W.-W. Dong, X.-Q. Qiao, D.-F. Hou, X. Bu and D.-S. Li, *Inorg. Chem.*, 2017, **56**(22), 14111–14117.
84 B. J. Wang, S. Y. Ma, S. T. Pei, X. L. Xu, P. F. Cao, J. L. Zhang, R. Zhang, X. H. Xu and T. Han, *Sens. Actuators, B*, 2020, **321**, 128560.
85 W. M. Haynes, *Handbook of Chemistry and Physics, Handbook of Chemistry and Physics*, CRC PRess, 2016, pp. 97–98.
86 Y. Li, N. Chen, D. Deng, X. Xing, X. Xiao and Y. Wang, *Sens. Actuators, B*, 2017, **238**, 264–273.
87 Y.-P. Wu, W. Zhou, W.-W. Dong, J. Zhao, X.-Q. Qiao, D.-F. Hou, D.-S. Li, Q. Zhang and P. Feng, *Cryst. Growth Des.*, 2017, **17**(4), 2158–2165.
88 Y.-M. Jo, T.-H. Kim, C.-S. Lee, K. Lim, C. W. Na, F. Abdel-Hady, A. A. Wazzan and J.-H. Lee, *ACS Appl. Mater. Interfaces*, 2018, **10**(10), 8860–8868.
89 J.-H. Lee, *Sens. Actuators, B*, 2009, **140**(1), 319–336.
90 C. Arul, K. Moulaee, N. Donato, D. Iannazzo, N. Lavanya, G. Neri and C. Sekar, *Sens. Actuators, B*, 2021, **329**, 129053.
91 M. M. Rahman, S. B. Khan, A. M. Asiri, K. A. Alamry, A. A. P. Khan, A. Khan, M. A. Rub and N. Azum, *Microchim. Acta*, 2013, **180**(7), 675–685.
92 J.-S. Jang, W.-T. Koo, D.-H. Kim and I.-D. Kim, *ACS Cent. Sci.*, 2018, **4**(7), 929–937.
93 J.-S. Jang, W.-T. Koo, S.-J. Choi and I.-D. Kim, *J. Am. Chem. Soc.*, 2017, **139**(34), 11868–11876.
94 F. Qu, J. Liu, Y. Wang, S. Wen, Y. Chen, X. Li and S. Ruan, *Sens. Actuators, B*, 2014, **199**, 346–353.
95 Z. Zhang, L. Zhu, Z. Wen and Z. Ye, *Sens. Actuators, B*, 2017, **238**, 1052–1059.
96 T. Zhang, X. Tang, J. Zhang, T. Zhou, H. Wang, C. Wu, X. Xia, C. Xie and D. Zeng, *Langmuir*, 2018, **34**(48), 14577–14585.
97 J. Zhang, P. Tang, T. Liu, Y. Feng, C. Blackman and D. Li, *J. Mater. Chem. A*, 2017, **5**(21), 10387–10397.
98 G. Lin, H. Wang, X. Lai, R. Yang, Y. Zou, J. Wan, D. Liu, H. Jiang and Y. Hu, *Sens. Actuators, B*, 2020, **303**, 127219.
99 Q. Wei, J. Sun, P. Song, J. Li, Z. Yang and Q. Wang, *Sens. Actuators, B*, 2020, **304**, 127306.
100 L. Zhang, J. Zhao, H. Lu, L. Li, J. Zheng, J. Zhang, H. Li and Z. Zhu, *Sens. Actuators, B*, 2012, **171**, 1101–1109.
101 M. E. DMello, N. G. Sundaram and S. B. Kalidindi, *Chem.–Eur. J.*, 2018, **24**(37), 9220–9223.
102 G. Zhong, D. Liu and J. Zhang, *J. Mater. Chem. A*, 2018, **6**(5), 1887–1899.
103 S. M. Majhi, P. Rai, S. Raj, B.-S. Chon, K.-K. Park and Y.-T. Yu, *ACS Appl. Mater. Interfaces*, 2014, **6**(10), 7491–7497.
104 Y.-T. Yu, S. M. Majhi and H.-G. Song, *Procedia Eng.*, 2016, **168**, 227–230.
105 S. M. Majhi, P. Rai and Y.-T. Yu, *ACS Appl. Mater. Interfaces*, 2015, **7**(18), 9462–9468.
106 G. Lu, S. Li, Z. Guo, O. K. Farha, B. G. Hauser, X. Qi, Y. Wang, X. Wang, S. Han and X. Liu, *Nat. Chem.*, 2012, **4**(4), 310–316.
107 W. Li, X. Wu, N. Han, J. Chen, W. Tang and Y. Chen, *Powder Technol.*, 2016, **304**, 241–247.
108 J. Xia, K. Diao, Z. Zheng and X. Cui, *RSC Adv.*, 2017, **7**(61), 38444–38451.
109 W. Li, X. Wu, N. Han, J. Chen, X. Qian, Y. Deng, W. Tang and Y. Chen, *Sens. Actuators, B*, 2016, **225**, 158–166.
110 C. Liu, Q. Kuang, Z. Xie and L. Zheng, *CrystEngComm*, 2015, **17**(33), 6308–6313.
111 W. Liu, L. Xu, K. Sheng, X. Zhou, X. Zhang, C. Chen, B. Dong, X. Bai, L. Geyu and H. Song, *Sens. Actuators, B*, 2018, **273**, 1676–1686.
112 X. Jiang, Y. Zhang, J. Jiang, Y. Rong, Y. Wang, Y. Wu and C. Pan, *J. Phys. Chem. C*, 2012, **116**(42), 22619–22624.
113 Y.-M. Jo, K. Lim, H. J. Choi, J. W. Yoon, S. Y. Kim and J.-H. Lee, *Sens. Actuators, B*, 2020, **325**, 128821.
114 Y. Zhao, B. Yang and J. Liu, *Sens. Actuators, B*, 2018, **271**, 256–263.
115 W.-T. Koo, S.-J. Choi, S.-J. Kim, J.-S. Jang, H. L. Tuller and I.-D. Kim, *J. Am. Chem. Soc.*, 2016, **138**(40), 13431–13437.
116 X. Zhou, X. Lin, S. Yang, S. Zhu, X. Chen, B. Dong, X. Bai, X. Wen, L. Geyu and H. Song, *Sens. Actuators, B*, 2020, **309**, 127802.
117 W.-T. Koo, S. Qiao, A. F. Ogata, G. Jha, J.-S. Jang, V. T. Chen, I.-D. Kim and R. M. Penner, *ACS Nano*, 2017, **11**(9), 9276–9285.
118 S. Mahajan and S. Jagtap, *Applied Materials Today*, 2020, **18**, 100483.
119 G. Konvalina and H. Haick, *Acc. Chem. Res.*, 2014, **47**(1), 66–76.
120 C. Qin, B. Wang, P. Li, L. Sun, C. Han, N. Wu and Y. Wang, *Sens. Actuators, B*, 2021, **331**, 129433.
121 W.-T. Koo, S. Yu, S.-J. Choi, J.-S. Jang, J. Y. Cheong and I.-D. Kim, *ACS Appl. Mater. Interfaces*, 2017, **9**(9), 8201–8210.
122 S.-J. Choi, H.-J. Choi, W.-T. Koo, D. Huh, H. Lee and I.-D. Kim, *ACS Appl. Mater. Interfaces*, 2017, **9**(46), 40593–40603.
123 Z. Yang, D. Zhang and H. Chen, *Sens. Actuators, B*, 2019, **300**, 127037.
124 D. Zhang and C. Jiang, *J. Alloys Compd.*, 2017, **698**, 476–483.
125 D. Zhang, C. Jiang and J. Wu, *Sens. Actuators, B*, 2018, **273**, 176–184.
126 H. Tian, H. Fan, M. Li and L. Ma, *ACS Sens.*, 2016, **1**(3), 243–250.
127 S. Luo, R. Chen, J. Wang, D. Xie and L. Xiang, *Sens. Actuators, B*, 2021, **344**, 130220.

© 2022 The Author(s). Published by the Royal Society of Chemistry

Open Access Article. Published on 13 december 2021. Downloaded on 11. 11. 2024 14:01:32.
This article is licensed under a Creative Commons Attribution-NonCommercial 3.0 Unported Licence.

128 K. Hwang, J. Ahn, I. Cho, K. Kang, K. Kim, J. Choi, K. Polychronopoulou and I. Park, *ACS Appl. Mater. Interfaces*, 2020, **12**(11), 13338–13347.
129 M. Drobek, J.-H. Kim, M. Bechelany, C. Vallicari, A. Julbe and S. S. Kim, *ACS Appl. Mater. Interfaces*, 2016, **8**(13), 8323–8328.
130 M. S. Yao, W. X. Tang, G. E. Wang, B. Nath and G. Xu, *Adv. Mater.*, 2016, **28**(26), 5229–5234.
131 T. Zhou, Y. Sang, X. Wang, C. Wu, D. Zeng and C. Xie, *Sens. Actuators, B*, 2018, **258**, 1099–1106.
132 S. Calero and P. Gómez-Álvarez, *J. Phys. Chem. C*, 2015, **119**(41), 23774–23780.
133 V. Kumar, S. M. Majhi, K.-H. Kim, H. W. Kim and E. E. Kwon, *Chem. Eng. J.*, 2020, **404**, 126472.
134 C. Sapsanis, H. Omran, V. Chernikova, O. Shekhah, Y. Belmabkhout, U. Buttner, M. Eddaoudi and K. N. Salama, *Sensors*, 2015, **15**(8), 18153–18166.
135 M. A. Andrés, M. T. Vijjapu, S. G. Surya, O. Shekhah, K. N. Salama, C. Serre, M. Eddaoudi, O. Roubeau and I. Gascón, *ACS Appl. Mater. Interfaces*, 2020, **12**(3), 4155–4162.
136 S. Zeinali, S. Homayoonnia and G. Homayoonnia, *Sens. Actuators, B*, 2019, **278**, 153–164.
137 O. Yassine, O. Shekhah, A. H. Assen, Y. Belmabkhout, K. N. Salama and M. Eddaoudi, *Angew. Chem.*, 2016, **128**(51), 16111–16115.
138 V. Chernikova, O. Yassine, O. Shekhah, M. Eddaoudi and K. N. Salama, *J. Mater. Chem. A*, 2018, **6**(14), 5550–5554.
139 H. Yuan, J. Tao, N. Li, A. Karmakar, C. Tang, H. Cai, S. J. Pennycook, N. Singh and D. Zhao, *Angew. Chem., Int. Ed.*, 2019, **58**(40), 14089–14094.
140 B. Van de Voorde, B. Bueken, J. Denayer and D. De Vos, *Chem. Soc. Rev.*, 2014, **43**(16), 5766–5788.
141 S. G. Surya, S. Bhanoth, S. M. Majhi, Y. D. More, V. M. Teja and K. N. Chappanda, *CrystEngComm*, 2019, **21**(47), 7303–7312.
142 A. H. Assen, O. Yassine, O. Shekhah, M. Eddaoudi and K. N. Salama, *ACS Sens.*, 2017, **2**(9), 1294–1301.
143 L. T. Duy, T. Q. Trung, V. Q. Dang, B. U. Hwang, S. Siddiqui, I. Y. Son, S. K. Yoon, D. J. Chung and N. E. Lee, *Adv. Funct. Mater.*, 2016, **26**(24), 4329–4338.
144 N. L. Torad, S. Zhang, W. A. Amer, M. M. Ayad, M. Kim, J. Kim, B. Ding, X. Zhang, T. Kimura and Y. Yamauchi, *Adv. Mater. Interfaces*, 2019, **6**(20), 1900849.
145 Y. Yao, X. Chen, X. Li, X. Chen and N. Li, *Sens. Actuators, B*, 2014, **191**, 779–783.
146 X. Fan and B. Du, *Sens. Actuators, B*, 2012, **166**, 753–760.
147 F. Yakuphanoglu, *Solid State Sci.*, 2012, **14**(6), 673–676.
148 A. Oprea and U. Weimar, *Anal. Bioanal. Chem.*, 2019, **411**(9), 1761–1787.
149 F. Wang, H.-R. Fu, Y. Kang and J. Zhang, *Chem. Commun.*, 2014, **50**(81), 12065–12068.
150 L. Wang, H. Zhu, Y. Shi, Y. Ge, X. Feng, R. Liu, Y. Li, Y. Ma and L. Wang, *Nanoscale*, 2018, **10**(24), 11384–11391.
151 B. Pattengale, S. Yang, J. Ludwig, Z. Huang, X. Zhang and J. Huang, *J. Am. Chem. Soc.*, 2016, **138**(26), 8072–8075.
152 K. N. Chappanda, M. R. Tchalala, O. Shekhah, S. G. Surya, M. Eddaoudi and K. N. Salama, *Sensors*, 2018, **18**(11), 3898.
153 M. Mohsen-Nia, H. Amiri and B. Jazi, *J. Solution Chem.*, 2010, **39**(5), 701–708.
154 D. Zhang, Y. Fan, G. Li, W. Du, R. Li, Y. Liu, Z. Cheng and J. Xu, *Sens. Actuators, B*, 2020, **302**, 127187.
155 P. Xu, H. Yu, S. Guo and X. Li, *Anal. Chem.*, 2014, **86**(9), 4178–4187.
156 P. Xu, X. Li and H. Yu, Transducers-2015 18th International Conference on Solid-State Sensors, Actuators and Microsystems (TRANSDUCERS), *IEEE*, 2015, 953–956.
157 E. Haghighi and S. Zeinali, *Microporous Mesoporous Mater.*, 2020, **300**, 110065.
158 C.-Y. Huang, M. Song, Z.-Y. Gu, H.-F. Wang and X.-P. Yan, *Environ. Sci. Technol.*, 2011, **45**(10), 4490–4496.
159 S. Öztürk, A. Kösemen, Z. A. Kösemen, N. Kılınç, Z. Z. Öztürk and M. Penza, *Sens. Actuators, B*, 2016, **222**, 280–289.
160 Q. Gou, L. B. Favero, S. S. Bahamyirou, Z. Xia and W. Caminati, *J. Phys. Chem. A*, 2014, **118**(45), 10738–10741.
161 E. Haghighi and S. Zeinali, *RSC Adv.*, 2019, **9**(42), 24460–24470.
162 P. Sun, Y. Jiang, G. Xie, J. Yu, X. Du and J. Hu, *J. Appl. Polym. Sci.*, 2010, **116**(1), 562–567.
163 Z. Ma, T. Yuan, Y. Fan, L. Wang, Z. Duan, W. Du, D. Zhang and J. Xu, *Sens. Actuators, B*, 2020, **311**, 127365.
164 M. Tchalala, P. Bhatt, K. Chappanda, S. Tavares, K. Adil, Y. Belmabkhout, A. Shkurenko, A. Cadiau, N. Heymans and G. De Weireld, *Nat. Commun.*, 2019, **10**(1), 1–10.
165 E. Martínez-Ahumada, A. López-Olvera, V. Jancik, J. E. Sánchez-Bautista, E. González-Zamora, V. Martis, D. R. Williams and I. A. Ibarra, *Organometallics*, 2020, **39**(7), 883–915.
166 S. G. Surya, H. N. Raval, R. Ahmad, P. Sonar, K. N. Salama and V. R. Rao, *Trends Anal. Chem.*, 2019, **111**, 27–36.
167 C. Zhang, P. Chen and W. Hu, *Chem. Soc. Rev.*, 2015, **44**(8), 2087–2107.
168 M. Wu, S. Hou, X. Yu and J. Yu, *J. Mater. Chem. C*, 2020, **8**(39), 13482–13500.
169 S. Yuvaraja, V. N. Bhyranalyar, S. A. Bhat, S. G. Surya, C. V. Yelamaggad and K. N. Salama, *Mater. Horiz.*, 2021, **8**(2), 525–537.
170 A. S. Sizov, A. A. Trul, V. Chekusova, O. V. Borshchev, A. A. Vasiliev, E. V. Agina and S. A. Ponomarenko, *ACS Appl. Mater. Interfaces*, 2018, **10**(50), 43831–43841.
171 S. G. Surya, S. S. Nagarkar, S. K. Ghosh, P. Sonar and V. R. Rao, *Sens. Actuators, B*, 2016, **223**, 114–122.
172 S. G. Surya, R. S. Dudhe, D. Saluru, B. K. Koora, D. K. Sharma and V. R. Rao, *Sens. Actuators, B*, 2013, **176**, 46–51.
173 S. Yuvaraja, S. G. Surya, M. T. Vijjapu, V. Chernikova, O. Shekhah, M. Eddaoudi and K. N. Salama, *Phys. Status Solidi RRL*, 2020, **14**(6), 2000086.
174 S. Yuvaraja, A. Nawaz, Q. Liu, D. Dubal, S. G. Surya, K. N. Salama and P. Sonar, *Chem. Soc. Rev.*, 2020, **49**(11), 3423–3460.

© 2022 The Author(s). Published by the Royal Society of Chemistry

Open Access Article. Published on 13 december 2021. Downloaded on 11. 11. 2024 14:01:32.
This article is licensed under a Creative Commons Attribution-NonCommercial 3.0 Unported Licence.

175 V. Rajeev, A. K. Paulose and K. N. Unni, *Vacuum*, 2018, **158**, 271–277.
176 P. Mougkogiannis, M. Turner and K. Persaud, *Sensors*, 2021, **21**(1), 13.
177 S. Yuvaraja, S. G. Surya, V. Chernikova, M. T. Vijjapu, O. Shekhah, P. M. Bhatt, S. Chandra, M. Eddaoudi and K. N. Salama, *ACS Appl. Mater. Interfaces*, 2020, **12**(16), 18748–18760.
178 J. D. Yuen and F. Wudl, *Energy Environ. Sci.*, 2013, **6**(2), 392–406.
179 Y. Li, P. Sonar, L. Murphy and W. Hong, *Energy Environ. Sci.*, 2013, **6**(6), 1684–1710.

© 2022 The Author(s). Published by the Royal Society of Chemistry